DESIGN OF AN EXPERIMENTAL FMCW WEATHER RADAR

A THESIS SUBMITTED TO
THE GRADUATE SCHOOL OF NATURAL AND APPLIED SCIENCES
OF
MIDDLE EAST TECHNICAL UNIVERSITY

BY

SALİH COŞKUN

IN PARTIAL FULFILLMENT OF THE REQUIREMENTS
FOR
THE DEGREE OF MASTER OF SCIENCE
IN
ELECTRICAL AND ELECTRONICS ENGINEERING

AUGUST 2015

Approval of the thesis:

DESIGN OF AN EXPERIMENTAL FMCW
WEATHER RADAR

submitted by **SALİH COŞKUN** in partial fulfillment of the requirements for the degree of **Master of Science in Electrical and Electronics Engineering Department, Middle East Technical University** by,

Prof. Dr. Gülbin Dural Ünver _____
Dean, Graduate School of **Natural and Applied Sciences**

Prof. Dr. Gönül Turhan Sayan _____
Head of Department, **Electrical and Electronics Engineering**

Prof. Dr. Ali Özgür Yılmaz _____
Supervisor, **Electrical and Electronics Eng. Dept., METU**

Prof. Dr. Sencer Koç _____
Co-Supervisor, **Electrical and Electronics Eng. Dept., METU**

Examining Committee Members:

Prof. Dr. Yalçın Tanık _____
Electrical and Electronics Engineering Dept., METU

Prof. Dr. Ali Özgür Yılmaz _____
Electrical and Electronics Engineering Dept., METU

Prof. Dr. Sencer Koç _____
Electrical and Electronics Engineering Dept., METU

Assoc. Prof. Dr. Çağatay Candan _____
Electrical and Electronics Engineering Dept., METU

Prof. Dr. Orhan Arıkan _____
Electrical and Electronics Engineering Dept., Bilkent Uni.

Date: _____

I hereby declare that all information in this document has been obtained and presented in accordance with academic rules and ethical conduct. I also declare that, as required by these rules and conduct, I have fully cited and referenced all material and results that are not original to this work.

Name, Last name: Salih COŞKUN

Signature:

ABSTRACT

DESIGN OF AN EXPERIMENTAL FMCW
WEATHER RADAR

Coşkun, Salih
M.S., Department of Electrical, and Electronics Engineering
Supervisor: Prof. Dr. Ali Özgür Yılmaz
Co-Supervisor: Prof. Dr. Sencer Koç

August 2015, 103 pages

FMCW Radars are used in many applications including weather surveillance. Transmitting during the entire observation interval makes them efficient in terms of required power. They are also cheap and easy to implement. This study which was conducted as a master's thesis, is a radar system working at X band. In this system, 0.8 Watts continuous electromagnetic wave which is modulated with a frequency ramp of 30 MHz bandwidth is generated and radiated through the transmit antenna. The scattered signal from the targets (buildings, cars, and hydrometeors) is multiplied with the being transmitted one and a beat signal is obtained. As a result of this deramping process, the range information of a target is converted into the frequency domain. Obtained signal data is processed in MATLAB® after passing through an analog to digital converter. The range and velocity information of the targets are obtained by signal processing. Verification of the system is performed in a controlled environment with buildings and cars whose range and velocities are

known. The system is finally used to calculate range of clouds and speed of wind while it is raining.

Keywords: Radar, FMCW, Meteorology, Weather, Range, Velocity, Doppler, Hydrometeors

ÖZ

FMCW DENEYSEL METEOROLOJİ

RADARI TASARIMI

Coşkun, Salih
Yüksek Lisans, Elektrik ve Elektronik Mühendisliği Bölümü
Tez Yöneticisi: Prof. Dr. Ali Özgür Yılmaz
Ortak Tez Yöneticisi: Prof. Dr. Sencer Koç

Ağustos 2015, 103 sayfa

FMCW Radarlar, hava gözetleme işlemi de dahil olmak üzere birçok alanda kullanılmaktadırlar. Gözlem yaptıkları tüm zaman diliminde elektromanyetik yayılım yaptıkları için, güç bakımından verimlidirler. Bunun yanında ucuz ve basit yapıdadırlar. Yüksek lisans tez çalışması olarak yürütülen bu çalışmada, X bandta çalışan bir radar sistemi kurulmuştur. Bu sistemde, 30 MHz bant genişliğine sahip frekans rampası ile modüle edilmiş, 0.8 Watt gücüne sahip, sürekli bir elektromanyetik dalga üretilir ve göndermeç anteninden basılır. Menzildeki hedefe (su parçacıkları, bina yada arabalar) çarparak, belli bir gecikme ile geri yansıyıp gelen sinyal, gönderilmekte olan sinyal ile çarpılarak vuru sinyali elde edilir. Yapılan bu "deramping" işlemi ile hedeflerin menzil bilgisi frekans tabanına taşınır. Analog/Sayısal çeviricilerle sayısal tabana geçirilen sinyal, MATLAB® programı ile işlenir. Uygulanan sinyal işleme teknikleriyle menzil ve hız bulma işlemleri yapılır. Sistemin doğrulanması menzili bilinen bina ve hızı bilinen araçlar ile kontollü

ortamda yapılmıştır. Sistem bulutların menzil ölçümü ile yağış anındaki rüzgar hızı hesaplamalarında kullanılmıştır.

Anahtar Kelimeler: Radar, FMCW, Meteoroloji, Hava, Menzil, Hız, Doppler, Hidrometeor

To my son, wife and parents

Oğlum, eşim ve anne-babama

ACKNOWLEDGEMENT

First of all, I want to express my deepest gratitude to mother of my son, my wife, Esna COŞKUN. She was the one encouraging me to complete this study. Thanks to her patience to spend my time on this project even at nights and weekends, I could able to finish. I feel both embarrassed and thankful to her.

I would like to express my deepest gratitude to also my supervisor Prof. Dr. Ali Özgür YILMAZ for his advice, criticism, and encouragement throughout development of this work. I would also like to express sincere thanks to my co-supervisor Prof. Dr. Sencer KOÇ for his valuable comments, suggestions, and support. The technical discussions with them are gratefully appreciated and contributed a lot to this study.

I am grateful to Mert Çelik who was the person if he does not contribute, this project will not progress. I learned a lot from him and his suggestion and solutions increased my motivation on this project. We fatigued together while doing experiments in the tower. I can't thank him enough for all that he has done for me.

I also wish to thank ASELSAN INC for the environment provided to me throughout the research. All my colleagues and friends at ASELSAN INC are appreciated for their support and encouragement.

I would like to thank my parents for bringing up and trusting in me.

Lastly, I would like to thank my son, Salim Ömer COŞKUN for being the greatest motivation to finish this study and giving a lot of energy with his wonderful scent.

TABLE OF CONTENTS

LIST OF TABLES

TABLES

LIST OF FIGURES

FIGURES

LIST OF ABBREVIATIONS

CTFT: Continuous Time Fourier Transform

CW: Continuous Wave

DFT: Discrete Fourier Transform

DSP: Digital Signal Processor

DTFT: Discrete Time Fourier Transform

FFT: Fast Fourier Transform

FM: Frequency Modulation

FMCW: Frequency Modulated Continuous Wave

FOD: Foreign Object Debris

GPIB: General Purpose Interface Bus

GPRS: General Packet Radio Service

GUI: Graphical User Interface

HPF: High Pass Filter

IDRA: IRCTR Drizzle Radar

IRCTR: International Research Centre for Telecommunication and Radar

LNA: Low Noise Amplifier

LPF: Low Pass Filter

OPAMP: Operational Amplifier

PRI: Pulse Repetition Interval

RADAR: Radio Detection And Ranging

RCS: Radar Cross Section

SFT: Strip Flex Taped

SMA: Sub Miniature version A

SNR: Signal to Noise Ratio

TDR: Time Domain Reflectometry

TOBB: Türkiye Odalar ve Borsalar Birliği / The Unioun of Chambers and Commodity Exchanges of Turkey

USB: Universal Serial Bus

WSR: Weather Surveillance Radar

CHAPTER 1

INTRODUCTION

RADAR is an acronym for RAdio Detection And Ranging. A radar system can be used to determine the range, altitude, direction, or speed of any object. In this modern age, the usage areas of radars are various, including astronomy, outer space surveillance systems, air traffic control, air-defense systems, altimetry control systems, ocean surveillance systems, ground-penetrating systems for geological observations, and meteorological precipitation monitoring which is also related with this study.

The main working principle of a radar is transmitting electromagnetic waves and inspecting a reflected signal. The transmitter block of a radar system generates and radiates electromagnetic wave. This electromagnetic wave hits any target placed in the range of the radar and reflects back to many places including the receiver system. After capturing the back scattered signal, the range of the target is calculated by measuring the travel time of the signal between the radar and the target.

Travel time of an electromagnetic wave can be measured in time or frequency domains. Therefore, a radar system can use either pulsed or continuous waveforms. In a pulsed radar system, the transmitter radiates a short burst and then the receiver of the system waits for the echo signal from a target. The transmitter and receiver blocks of a pulsed radar do not usually work at the same time, but they work sequentially. Specifically, while the receiver is listening for a scattered signal, the transmitter of the radar is at rest and while the transmitter is sending a pulse, the receiver is off. Since pulse repetition intervals (PRI) of radars are in general much longer than pulse durations, radar stays in the receiver state for longer times than in the transmitter state. If a scattered signal is sensed by the receiver, it shows there is a

target in the range of radar and the range of the target is related with the time difference between transmitting the signal and receiving the echo[1].

In contrast, for continuous wave (CW) radars, both transmitter and receiver parts are working at the same time and continuously. The transmitted and received signals are not bursts rather continuous signals. The transmitter radiates a signal and the receiver listens for an echo continuously. Therefore, discrimination of the echo signal from the transmitted one is different from pulsed radar.

There are two types of continuous-wave radars: unmodulated CW and modulated CW. Distinguishing different targets and obtaining range information with unmodulated CW radars are not possible[2]. They can detect moving targets and their speed. Since reflected signals from stationary and slow-moving objects are interfered with and overwhelmed by the leakage of transmit signal, it is hard for unmodulated CW to detect stationary and slow-moving objects, and they cannot differentiate between two or more reflecting objects[2]. Additionally, since the transmitted signal is changing in neither time domain (burst) nor frequency domain (modulation), the travel time of the scattered signal cannot be measured. That means calculation of the range information of the targets is not possible. Based on the Doppler Effect, the frequency of the scattered signal is shifted away from the transmitted frequency for targets which are moving. This variation in frequency makes the echo signal distinguishable from the leakage of the transmitted signal. And this effect makes moving targets detectable. Since the variation of Doppler Frequency is related with the speed of the objects, calculation of the speed is possible by measuring the deviation in frequency. The main advantage of this type of radars is their prices. They are cheaper and typically used with competition sports, like golf, tennis, baseball, and racing.

To make CW radars capable of detecting stable targets and measuring the range information, a modulation in the frequency of the transmitted signal is needed. By doing that, the received signal is separated from the transmitted one and time difference between the transmitted and received signals become measurable. This type of CW radars is called Frequency Modulated Continuous Wave (FMCW) radars.

FMCW radars are used in many places including weather surveillance radars. Several studies are performed with FMCW radars to make atmospheric measurements [3], [4].

The basic motivating factor behind this study is establishing an FMCW radar assembly with instrumental tools and measuring distances and velocities of the buildings, cars, and water particles in a cloud or on the air during a rain. The most advantageous property of the established setup is that it uses less powerful devices and this makes it more affordable. Since both of the transmitter and receiver parts of an FMCW radar are active during the whole time, they can reach the same energy level with the pulse waveform radars by using less powerful devices. Pulse radars generally transmit electromagnetic waves for significantly shorter intervals of time than their reception period. This means that they need to have more powerful devices to transmit at a high level of energy. However CW radars transmit and listen during the same interval which makes them use the whole time interval to transmit wave. This ability of the established FMCW radars makes them more affordable and easier to establish.

In Chapter 2, fundamentals of FMCW radar are described. Firstly, the common usage areas of FMCW radars are examined, and then radar principles such as range ambiguity, resolution, velocity, and return power calculations are described for FMCW radars.

In Chapter 3, essential information about the established radar setup is given. The system block diagram, the transmitter and receiver blocks and power measurement of the system are described. The graphical user interface of the radar is also described.

Chapter 4 covers signal processing steps performed during range and velocity calculation in fast and slow time.

Experimental results of the study are presented in Chapter 5. Results of building detection, car speed calculations, cloud range calculations, and speed of wind calculations while it is raining are given.

Finally, the study is concluded in Chapter 6 and future works are stated.

CHAPTER 2

FUNDAMENTALS OF FMCW RADAR

The radiated wave in FMCW radars are frequency modulated where, the frequency of the signal varies with time. This deviation in frequency generates frequency difference between transmitted and received signals since the received signal is a time shifted version of the transmitted one. Frequency difference is proportional with the travel time of the wave which is a measure for the range of the target. By multiplying the received signal with the transmitted one by a mixer, the frequency difference between the transmitted signal and echo is derived. After this process which is called “deramping”, range information of the target can be obtained from the frequency of the beat signal. In digital radars beat signals are passed through an Analog to Digital converter and then digital signal processing is performed.

In weather radars the targets are water or ice droplets on the air. Electromagnetic waves hit the particles on a cloud or on the air and scatter back to the receiver. The return power and time delay gives the information about the precipitation type and amount. Dual polarimetric radars which are able to transmit radio waves on both horizontal and vertical orientations can obtain further information about the size and shape of water particles. Horizontally transmitted waves gives information about the horizontal dimension of water particle while vertical ones give essential information on vertical dimension [5].

2.1 FMCW Radar Applications

FMCW radar systems are low cost techniques generally used in shorter range applications[6]. Most of the theoretical and practical works on FMCW radar were published during a period from late 1940s to early 1960[7]. The capability of detecting and ranging targets, and both the reliability and simplicity of FMCW radar

systems are the main advantages of using them. Mostly, they have been being used in radio altimeters in military and civil aircraft since World War II[7]. In addition to proximity fuse and radio altimetry, FMCW radars have been developed for many military and civil applications such as laboratory test instruments, avalanche detection, and volcano eruption onset and runway debris monitoring [6]. A few important example applications are described below.

Foreign Object Debris (FOD) Detection: FOD is a substance, debris, or article which is not a part of a vehicle or system. Since they are alien, they potentially cause damage to the safety and performance of systems. These systems are located along airport travel surfaces for high-resolution and high-speed detection of FOD. Tarsier® is an example of FMCW radar designed and built by QinetiQ Malvern for the detection of debris on airport runways [6].

Naval Navigational Radar: FMCW radar systems can be used as navigational radar. Although they are used for several kilometers they are the most useful at short ranges, from tens to hundreds of meters. Surveillance systems inform when vessels arrive under bad visibility conditions at sea or large river. FMCW radar does not only detect vehicles but also measure range and relative speed of them [7].

Level Measuring Radar: Level measuring radars are most commonly used for measuring liquid level on a tank. The radar signal is radiated from the cover of the tank and scattered from the surface of the liquid. The echo is captured by the receiver. Then the empty distance from liquid surface to top of the tank is measured. By subtracting the empty distance from the total height of the tank the liquid level is calculated [7].

Radio Altimeter: Radio altimeter is one of the early applications of FMCW radar used to measure the distance of an aircraft to ground. Particularly, in conditions where visibility is limited, it is crucial for landing. Besides, it is used as terrain awareness and warning system which prevent terrain accidents for low altitude flies [7].

Proximity Fuse: Proximity fuse is used to denote automatically when the distance of the target is smaller than a certain, predetermined value. This fuse is used

to increase the damage of bombs by exploding them before they hit the land. They are invented during World War II and secret guarded to a similar level as the atom bomb project [8].

Car Collision Avoidance System: The radars covering four side of a vehicle (front, tail, left and right) provide a warning to the driver when there is an imminent collision or take action autonomously such as braking, steering, or both without any driver input. Danger is determined by measuring the range and relative velocity of the targets. These systems have high potential for future use such as automatic driving system [9].

Measurements of Very Small Motions: Measuring and detecting small motions without any contact is also one of the areas that FMCW radars are used. The information on the phase angle of the beat signal is used to handle this mission [7].

Weather Radar: Weather radar, also called weather surveillance radar (WSR), is a type of radar specialized to make measurements on precipitation and estimate its type (rain, snow, hail etc.). During World War II, military radar operators noticed that the water particles on the air also reflect the radiated electromagnetic wave. This reflection is much related with the amount of water particles on a cloud and makes possible to talk about the amount of rain before it starts[10]. Much more recently, the advantage of polarimetry for a better estimation of the type of precipitation has been recognized. By transmitting and receiving radar signals with different combination of the polarization and then analyzing their correlation gives much more information about the amount of precipitation and its type. Therefore most modern meteorological radars are slowly migrating towards polarimetric capability.

2.2 FMCW Radar Principles

In FMCW radars transmitted signal is a continuous wave and its frequency is modulated by a periodic function such as a sinusoid or a sawtooth[11]. The variation in the frequency of transmitted signal is linear for linear FMCW radars (i.e., sawtooth with up – down chirps or triangular). The main working principle of FMCW radars is reflecting a signal from an object and generating a frequency

difference between the frequencies of the currently being transmitted signal and the echo by modulation. The frequency difference between the received and transmitted signals represents the range of the target. This difference in frequency is formed by the time until the transmitted signal travels in space, reaches the target, hits it, and scatters back to the receiver antenna. This period of time is related with the range of the target. Speed of propagation for electromagnetic waves is exactly equal to the speed of light in a vacuum and nearly equal to that value on air. Travel time of the transmitted signal along the paths from the transmitter antenna to the target and from the target back to the receiver antenna is calculated as

$$\tau = \frac{2\,R}{c}. \tag{1}$$

where τ stands for the travel time, R stands for range of target and c is the speed of light.

When the received signal is compared with the transmitted one at the arrival time, it is seen that received signal is a delayed version of the transmitted signal. Also this delay is exactly equal to the time of travel. For FMCW radar this delay forms a difference between the frequencies of the transmitted and received signals and it keeps the range information of the target. This frequency difference is named as the beat frequency. During deramping process, the received signal is mixed with a duplicate of the transmitted signal. The low pass term of the output which is the response of the target is called beat signal and it is a signal with frequency equal to the beat frequency. Hereby, in FMCW radars the range information of a target lies in the frequency domain, unlike a pulse radar where it is usually obtained in time domain. In Figure 1, the frequency deviation on the carrier signal versus time plots for the transmitted, received, and beat signals (LPF portion of mixed signal) are shown.

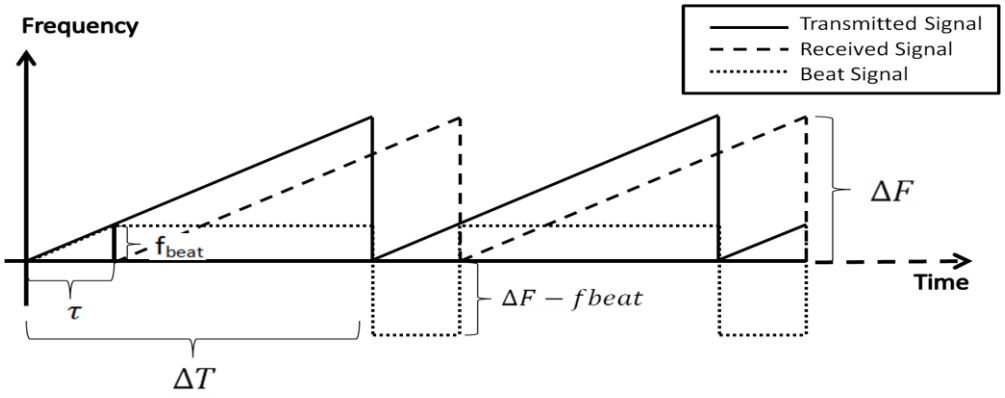

Figure 1: Frequency of Transmitted, Received, and Beat Signals vs. Time

The frequency of transmitted signal is swept as a sawtooth on the carrier frequency. The frequency excursion is shown with ΔF, and the sweep time is represented by ΔT. τ represents time delay between the received and transmitted signals and f_{beat} stands for beat frequency. Simply by taking the slope of the frequency deviation function for just in a single sweep interval, the relation between the beat frequency and range information is obtained.

$$m = \frac{\Delta F}{\Delta T} = \frac{f_{beat}}{\tau} \tag{2}$$

By using (1)

$$\frac{\Delta F}{\Delta T} = \frac{f_{beat}}{\frac{2R}{c}} = \frac{f_{beat}\, c}{2R} \tag{3}$$

$$f_{beat} = \frac{2\,\Delta F\, R}{\Delta T\, c} \tag{4}$$

$$R = \frac{f_{beat}\,\Delta T\, c}{2\,\Delta F} \tag{5}$$

The beat signal generated by a single target in an arbitrary range, composed of two different frequency components. As it is seen on Figure 2, for each sweep interval ΔT, the frequency of the signal is ΔF- f_{beat} during the first τ second and its frequency is f_{beat} for the remaining time (i.e., from τ to ΔT second). Because of the proportion between range and time delay τ, duration of the signal with beat frequency f_{beat}

decreases as the range increases. Having double frequency component for a single target may cause confusion of different targets. To avoid this, it is possible to switch to frequency domain after clipping the first part of the time domain signal which contains the component with frequency ΔF- f_{beat}.

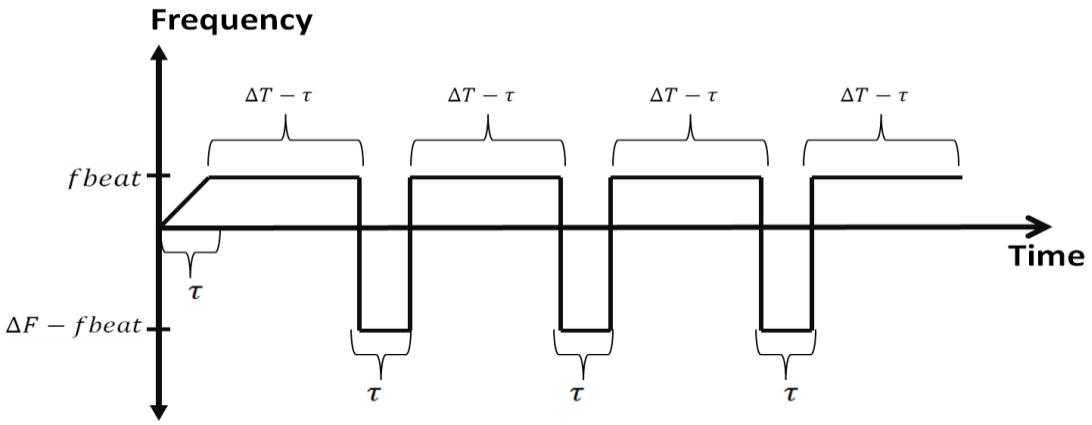

Figure 2: Frequency of Beat Signal vs. Time

As it is also seen on Figure 3, the time domain model of a beat signal which represents a single target contains two different frequency components divided in time. A beat signal is composed of two different signals which are shaped with a rectangular window.

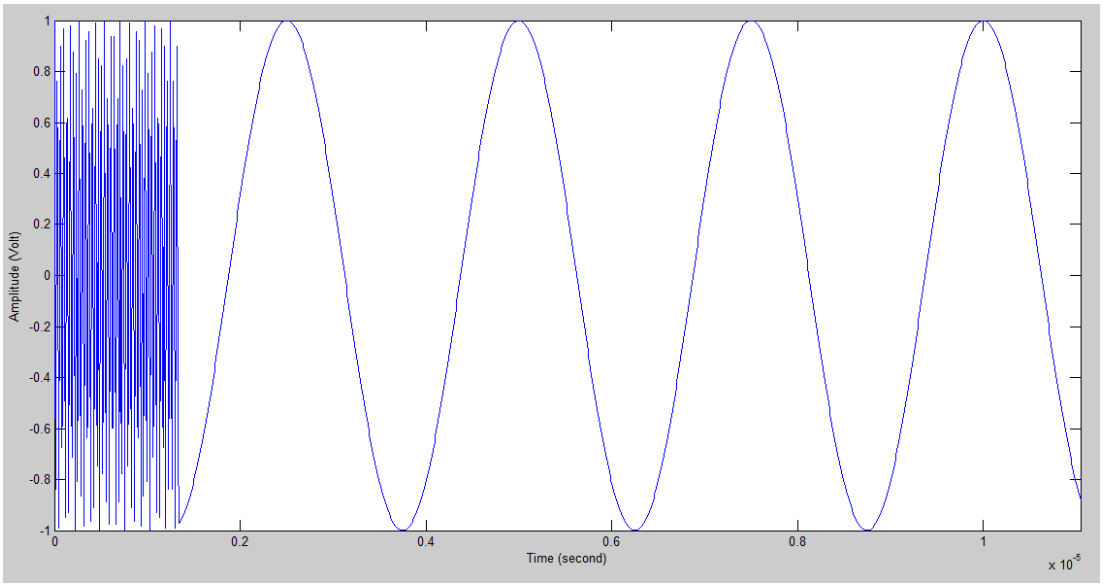

Figure 3: Beat Signal Model vs. Time

The spectrum of a beat signal is depicted on Figure 4. The beat signal is composed of two different frequency. Since this may reason confusion when handling multiple targets and the spectrum includes too many periodic components (spectral leakage), clipping the first region of the beat signal in time domain may be required. Unlike from pulse radars, this process does not prevent radar from seeing close region. Details of clipping algorithm is described in Chapter 4.1.2 (Clipping)

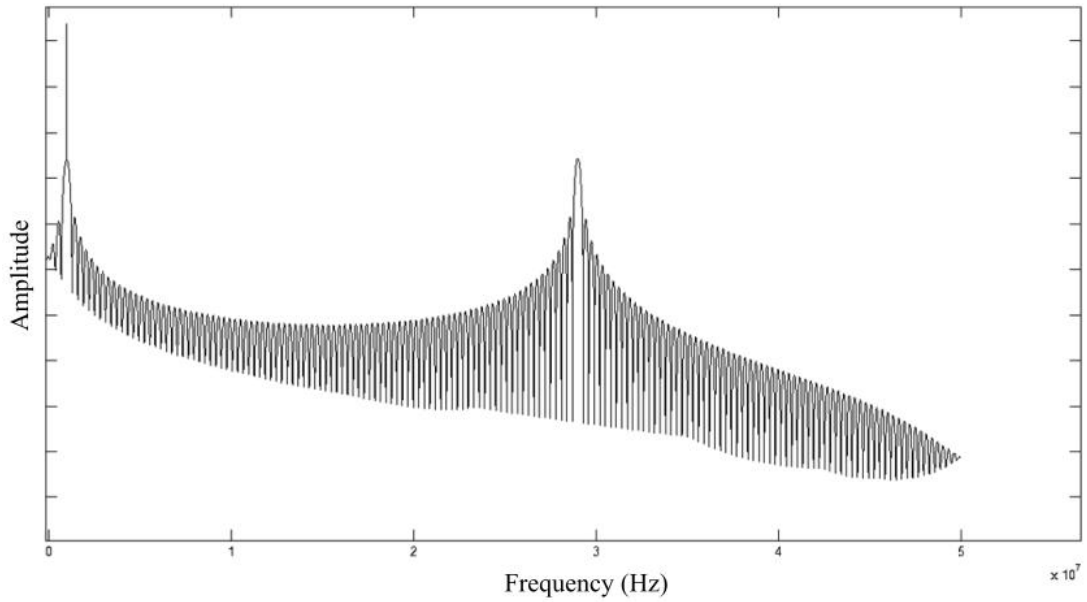

Figure 4: Beat Signal in Frequency Domain

Because of the rectangular windows in time domain, the frequency domain signal includes sync envelopes. To avoid these envelopes in frequency domain special windows such as Hanning or 4 steps Blackman Harris are implemented. These topics are focused on Chapter 4.1.3

2.2.1 Range Ambiguity/Max Range:

The targets whose range is far enough from the radar, for which the travel of the transmitted signal on the path back from the target takes more than a single sweep interval ΔT, form the ambiguous range of a radar[12]. The maximum unambiguous range is the maximum distance from the radar at which a target is located so as the backscatter signal from the target is received before a single period of frequency modulation is completed. Although it is not practical to detect near the edge of the unambiguous range since duration of the signal with beat frequency diminishes as

the range of the radar increases, the theoretical peak frequency that can be measured unambiguously is the frequency deviation ΔF itself. When the receiver is digital, the beat signal is sampled and converted to frequency domain with fast Fourier transform (FFT) algorithms. Since the range information is represented on the frequency domain, the maximum detectable range of a target which is computed unambiguously is also related with the sampling frequency of the receiver. By Nyquist criterion the widest detectable bandwidth is half the sampling frequency f_s. Hence the maximum unambiguous detectable frequency is the maximum of $f_s/2$ and ΔF.

When $f_s/2$ is greater than ΔF, the limiting factor is ΔF and by using the formula given in (5) the maximum unambiguous range becomes

$$R_{max} = \frac{\Delta F \, \Delta T \, c}{2 \, \Delta F} = \frac{\Delta T \, c}{2} \tag{6}$$

In the experimental results of this study ΔF is going to be the limiting factor and maximum unambiguous range will be determined by modulation sweep time, ΔT. As sweep time goes longer the maximum unambiguous range will also be farther.

When ΔF is greater than $f_s/2$, the limiting factor is f_s and by using the formula given in (5) the maximum unambiguous range become

$$R_{max} = \frac{(f_s/2) \, \Delta T \, c}{2 \, \Delta F} = \frac{f_s \, \Delta T \, c}{4 \, \Delta F} \tag{7}$$

2.2.2 Range Resolution:

The frequency spectrum representing range information is divided into finite frequency cells so called range resolution cells. For digital receivers, the frequency resolution of the FFT applied target response depends on the sampling rate f_s and the size of the recorded data (the number of acquisition points)[13]. The number of frequency bins in the spectrum is n_s which is also the number of signal points captured in time domain. The frequency spectrum of an FFT applied real-valued signal is symmetrical. Only one half of the spectrum is sufficient to obtain the range information since the other half is a replication. Hence, for that reason $n_s/2$ frequency bin represents the frequency domain from 0 to $f_s/2$. Frequency lines are spaced at

intervals of f_s/n_s Hz and this determines the resolution in the frequency domain. They are commonly referred as frequency bins or FFT bins and represent range resolution cells. Since the amount of sampled data (n_s) is collected for a single sweep interval ΔT with the sampling frequency f_s, it is equal to ΔT x f_s. By using formula given in (5) and having the frequency resolution of f_s/n_s, range resolution of digital FMCW radar is calculated as:

$$\delta R = \frac{\delta f_{beat}\, \Delta T\, c}{2\, \Delta F} = \frac{f_s\, \Delta T\, c}{2\, n_s\, \Delta F} = \frac{f_s\, \Delta T\, c}{2\, f_s\, \Delta T\, \Delta F} = \frac{c}{2\, \Delta F} \quad . \tag{8}$$

As a result of formula (8) the range resolution of FMCW radar depends on the frequency deviation parameter,ΔF. As the amount of frequency deviation increases the range resolution also increases.

2.2.3 Moving Targets

By using FMCW radars it is possible to detect speed of moving targets. The frequency of the transmitted signal changes if it is scattering back from a moving object. The amount of change in the frequency is given as $\frac{2\,v}{\lambda}$ where v stands for the velocity of the target and λ stands for the wavelength of the radiated signal. The change on the frequency is positive for the approaching targets and it is negative for diverging ones.

As it is discussed earlier, it is known that FMCW radars detect ranges from the frequency of the beat signal. And now it is mentioned that moving targets changes the frequency of the beat signal. By combining these two properties, FMCW radars may be expected to fail while detecting the range information of moving targets correctly. However, it is not the case for the established setup and scenario of this study. The maximum speed level for a potential target of this radar is about 120 kmph (≈ 34 m/s). This corresponds to a Doppler frequency about 227 Hz for the carrier frequency at X-Band. This difference in the received signal frequency is directly transferred to the beat signal. Hence we have 227 Hz error in frequency calculation. However, even this maximum error on the frequency caused by the motion of the target is very small compared to the range resolution. The frequency

resolution of a system is given by f_s/n_s and this amount is about 10 kHz in design of this thesis.

Doppler frequency of moving targets is calculated through slow time data processing. The signal in frequency domain which keeps the range information is a complex signal. The phase of this signal changes if the target is moving. Hence, Fourier transform is applied to slow time data for a particular range bin. The sampling period of slow time data is equal to ΔT. By Nyquist criterion, the maximum frequency that can be measured in slow time is$\frac{1}{2\Delta T}$. This is the maximum unambiguous Doppler frequency that can be measured.

$$f_{Doppler,max} = \frac{1}{2\Delta T} = \frac{2\,V_{max}}{\lambda} \tag{9}$$

$$V_{max} = \frac{\lambda}{4\,\Delta T} \quad . \tag{10}$$

The maximum speed that can be measured unambiguously is proportional with wavelength and inversely proportional with sweep duration.

The resolution of the measured velocity is related with the frequency resolution of the Fourier transformed slow time data. The amount of stored fast time data in a slow time data block is denoted by N. Speeds of moving targets are calculated by taking Fourier transform of N complex valued range samples. The number of frequency bins in the slow time spectrum is equal to the number of signal points captured in slow time (N). Only one half of the spectrum is sufficient to obtain velocity information since the other half is an indicator of the direction. For that reason N/2 frequency bin represents the slow time frequency domain from 0 to $\frac{1}{2\Delta T}$. Frequency lines are spaced at intervals of $(\frac{1}{\Delta T})$/N Hz and this determines the resolution in the slow time frequency domain. Speed resolution of digital FMCW radar is calculated as:

$$\delta f_{\text{Doppler}} = \frac{2\,\delta V}{\lambda} = \frac{1}{\Delta T\,N} \quad . \tag{11}$$

$$\delta V = \frac{\lambda}{2\,\Delta T\,N} \tag{12}$$

As a result of formula (12) the speed resolution of FMCW radar depends on duration of sweep interval, the number of data in slow time and the wavelength. As the sweep duration and number of slow time data increases the velocity resolution also increases.

2.2.4 Return Power Calculation for Weather Targets

The radar range equation represents the dependencies of the received power P_r to the parameters such as power of transmitted wave, the gain of the antennas, the wavelength, the range of the target etc. The performance of the radar system is defined by the radar range equation.

Weather radar equation is a specialized form of primary radar equations and has many equivalent principles. Therefore, the basic form of radar range equation is commemorated as [1]

$$P_r = \frac{P_t\,G_t\,G_r\,\lambda^2\,\sigma_b}{(4\pi)^3\,R^4\,L_{atm}^2(R)}. \tag{13}$$

P_r = Received Power — λ = Wavelength of Radiated Signal

P_t = Transmitted Power — σ_b = Radar Cross Section

G_t = Transmit Antenna Gain — R = Range of Target

G_r = Received Antenna Gain — L_{atm} = Atmospheric Attenuation

The main difference on radar range equation for weather radar is the target. The reflection area of an aircraft or any other flying object is rigid and small while hydrometeors are normally sparse, much larger, and more fluid [14]. The mass of water particles in the air is composed of small size water or ice droplets. When the radius of water droplets is much smaller compared to wavelength (which is even the case at X band), specifically when $\frac{2\pi a}{\lambda} \ll 1$, the reflection area of a 'single' water drop is given by the Rayleigh backscatter equation [4]

$$\sigma_i = \frac{\pi^5 \, |K|^2 \, D_i^6}{\lambda^4} . \tag{14}$$

where

σ_i =Radar Cross Section of a single particle

$|K|^2$ = 0.93 for water particles and 0.197 for ice from L to X band radar[1]

D_i = rain drop diameter

Now, it is easy to compute radar reflectivity from a single particle to a unit volume which contains M such scatterers.

$$\eta = \frac{1}{\Delta V} \sum_{i=1}^{M} \sigma_i \ . \tag{15}$$

η stands for scattering cross section per unit volume

$$\eta = \frac{1}{\Delta V} \sum_{i=1}^{M} \frac{\pi^5 \, |K|^2 \, D_i^6}{\lambda^4} = \frac{\pi^5 \, |K|^2}{\lambda^4} \, x \, \frac{1}{\Delta V} \sum_{i=1}^{M} D_i^6 \ . \tag{16}$$

The term $\frac{1}{\Delta V} \sum_{i=1}^{M} D_i^6$ in this equation is called as meteorological reflectivity and denoted with Z.

$$Z = \frac{1}{\Delta V} \sum_{i=1}^{M} D_i^6 \ . \tag{17}$$

$$\eta = \frac{\pi^5 \, |K|^2}{\lambda^4} \, Z \ . \tag{18}$$

The contribution of every single point scatterer in the resolution volume is not the same. Hydrometeors located in the direction of maximum antenna gain are going to contribute more. The radar cross-section, σ_b for meteorological scatterers is approximated by Probert-Jones as following [4]

$$\sigma_b = \eta \, \Delta R \, R^2 \, \frac{\pi \, \theta^2}{8 \, \ln 2} . \tag{19}$$

θ stands for minimum beamwidth of transmitter and receiver antenna.

This approximation requires the following assumptions

i) Both the transmitter and the receiver antennas are illuminating the same resolution volume,

ii) Within the resolution volume the scatterers are randomly spaced and have the same radar cross-section

iii) The range resolution is much smaller compared to the actual range

By combining (13) and (19) the radar range equation for weather radars becomes

$$P_r = \frac{P_t\, G_t\, G_r\, \lambda^2\, \theta^2\, \Delta R\, \eta}{\pi^2\, R^2\, L_{atm}^2(R)\, 512\, \ln 2} \quad . \tag{20}$$

In this radar equation η and R are the parameters that affect return power but do not depend on the radar system. Here R is target range and the scattering cross section per unit volume η is a parameter depends on the amount of water particles in the air or in a cloud and the precipitation rate. A number of models are used to relate the amount of precipitation and scattering cross section. Meteorologists prefer to express the strength of echo from hydrometeors in terms of Meteorological reflectivity Z in unit dBz. Reflectivity value in dBz unit is 10 times base-10 logarithm of reflectivity in the unit of mm^6/m^3. The most common model that relates the reflectivity with the precipitation rate is seen on Table 1. This model is used in the U.S. National Weather Radar System NEXTRAD [1]. It relates Rain Fall Rate with the reflectivity in dBz at 6 levels.

Table 1: Reflectivity vs. Precipitation Type Table used in NEXTRAD

Level	**Rain Fall Rate (mm/hr)**	**Category**	**Z - Reflectivity**	
			(dBz)	**(mm^6/m^3)**
1	0.49 to 2.7	Light Mist	18<Z<30	63<Z<1000
2	2.7 to 13.3	Moderate	30<Z<41	1000<Z<12600
3	13.3 to 27.3	Heavy	41<Z<46	12600<Z<39800
4	27.3 to 48.6	Very Heavy	46<Z<50	39800<Z<10^5
5	48.6 to 133.2	Intense	50<Z<57	10^5<Z<5x10^5
6	133.2 and higher	Extreme	Z > 57	Z>5x10^5

As a result of this table, it is possible to compute the return power that the receiver antenna handles for a specific fall rate and range. This will be also used from the reverse, by measuring the received power it is possible to estimate the rain rate.

Atmospheric attenuation which is also a function of the range affects the return power of the electromagnetic wave. Besides target range, it also depends on the frequency being used. Atmospheric attenuation of electromagnetic waves for the specified frequency and altitude is seen on Figure 5 [1]. According to this figure, attenuation usually increases as the frequency of transmitted signal increases. The loss factor α is given in decibel per kilometer and for just one-way propagation. In (20), $L_{atm}^2(R)$ represents the attenuation in linear unit per meters and for two way propagation. To calculate this value from given loss factor the following calculation is needed.

$$L_{atm}(R)\ (dB) = 2\alpha\left(\frac{R}{1000}\right) = \frac{\alpha R}{500} \tag{21}$$

In linear unit

$$L_{atm}(R) = 10^{\frac{\alpha R}{500}} \tag{22}$$

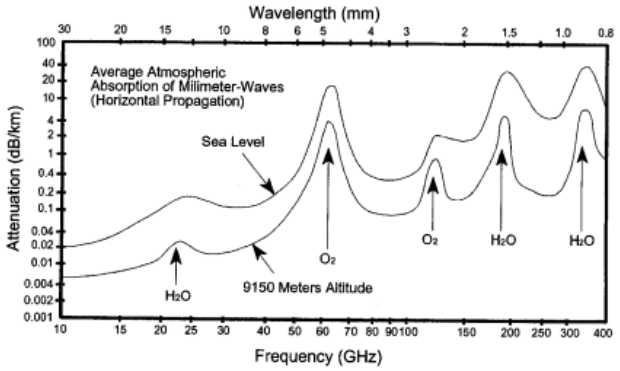

Figure 5: One-way Atmospheric Attenuation of Electromagnetic Waves[1]

CHAPTER 3

SYSTEM DESCRIPTION

The FMCW weather radar system is set up on top of the tower at Ayaslı Research Center in Ankara at latitude 39°53'27.2"N and longitude 32°46'53.6"E. Figure 6 shows a picture of the system at its location.

Figure 6: Tower in Ayaslı Research Centre

3.1 System Block Diagram

The experimental FMCW weather radar system used in this study is constructed by using commercial on the shelf (COTS) test equipments. The system unit is composed of the following equipments:

- Agilent E8267D PSG Vector Signal Generator
- Agilent DSO 6102A Oscilloscope
- Agilent GPIB to USB converter cable
- A computer with MATLAB as the signal processing and user interface unit
- Microsemi AML218L1502 Low Noise Amplifier
- Marki M1-0310 Double Balanced Mixer
- Power Divider
- TriQuint TGA2501 Power Amplifier
- High Pass Filter designed with Analog Device AD9631 OPAMPs
- Horn Antennas
- Dish Antennas
- USB flash memory stick
- Several SMA cable

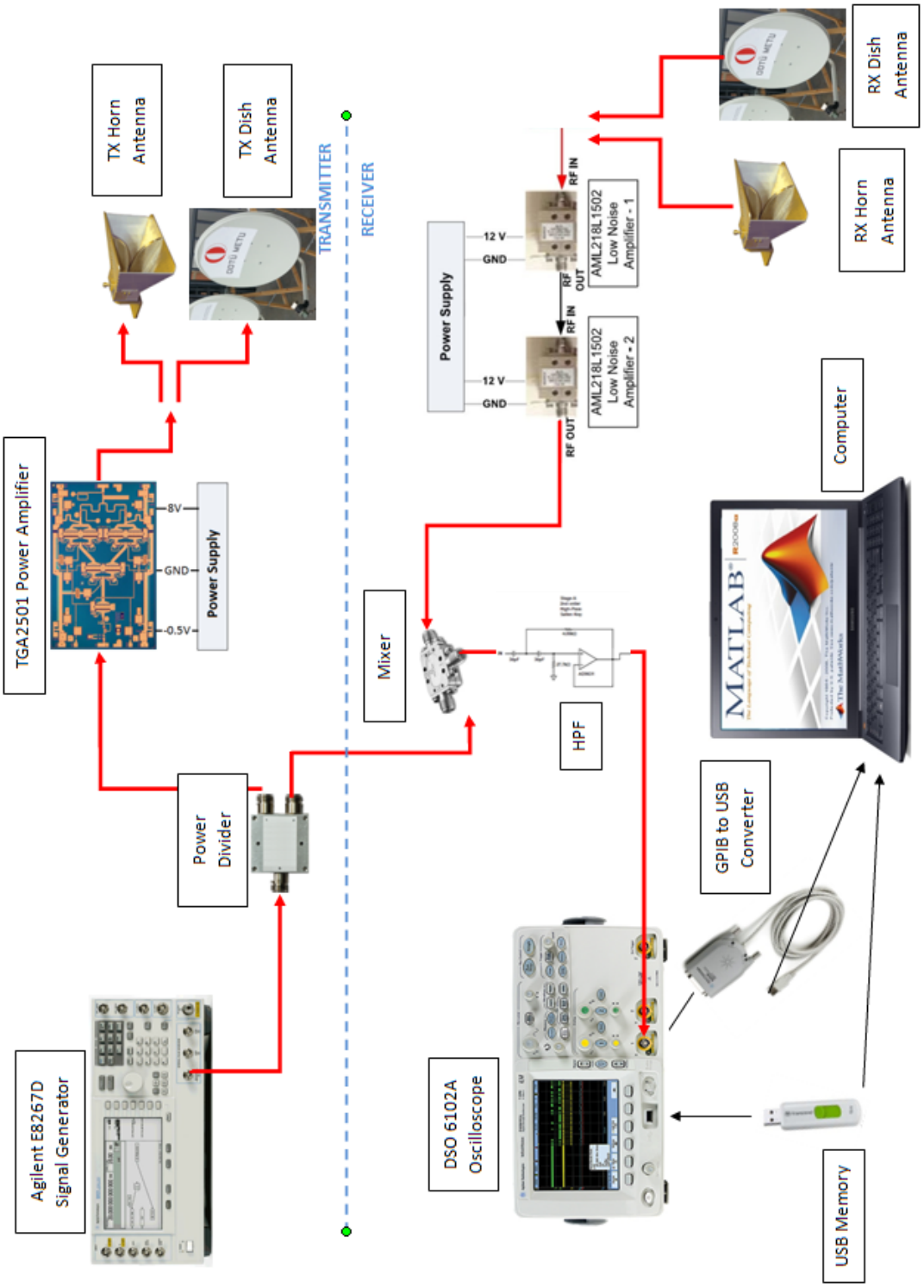

Figure 7: System Block Diagram

The general block diagram of FMCW weather radar system is depicted in. A brief explanation of the system operation is as follows:

A continuous wave whose frequency is modulated as a positive ramp sawtooth is generated by using Agilent E8267D signal generator. This signal is divided into two portions by a signal divider. While one of these portions is going to the transmitter part, the other one merges with the received signal. Transmitted signal is strengthened with a TGA2501 power amplifier and then radiated from one of the horn or dish antennas with the chosen polarimetry.

The receiver part of the system proceeds from two edges. One of the edges starts from the power divider with a duplicate of the transmitted signal. The other edge starts with the receiver antenna. Dish or horn antenna is used as the same with the transmit antenna. Then two cascaded low noise amplifier are used to strengthen the echo of the transmitted signal.

Following the LNA step, the edges of the receiver system meet at the mixer. The difference of the frequencies between the received and transmitted signal is obtained by mixing them. After this deramping process, beat signal is obtained and passed to Agilent DSO 6102A oscilloscope. Oscilloscope is used as an analog to digital converter and also as the data storage of the system.

There is a high pass filter (HPF) between the mixer and the oscilloscope which eliminates the effects of close region returns. The transmitter and receiver antennas are very close to each other and some portion of the transmitted signal leaks to the receiver antenna without reflecting from any surface. Besides direct leakage between the antennas, short range targets reflect more powerful echoes in relation to the far range targets. Because of these two effects, beat signals with low frequency components are more powerful. This situation, especially leakage between antennas requires high dynamic range to detect far range targets. To decrease dynamic range requirement HPF attenuates the low frequency high power components which are produced by the close region targets. The cut-off frequency of the filter is adjusted as 750 kHz and this frequency corresponds to 375 meters of range.

Highpass filtered signal captured by the oscilloscope and taken in binary format by either a USB flash memory or directly by the radar interface program from GPIB interface with the help of an Agilent GPIB to USB converter. If data is captured and stored into USB flash memory, it is processed offline. On the other hand, GPIB interface is used to take real time data with the intervals of 1 second and process it as online.

The last step of the system is handling the captured data. The program which is generated using Matlab takes the parameters from the graphical user interface, takes the offline or online data, processes it, and shows the results on graphical user interface again.

3.2 System Design Parameters and Working Principles

In this study the parameters such as carrier frequency, the amount of FM deviation, the duration of sweep interval etc. are determined to optimize the radar properties with the limiting values of the devices in our hand. The first limiting factor was the number of data points that Agilent DSO6102A Oscilloscope can provide to us. The maximum number of digitized data is captured when the oscilloscope is not in the acquisition mode. This value is equal to 1 million points with time and voltage values[15]. The number of captured data points affects the amount of captured fast time data, duration of a single sweep and also the sampling frequency.

Design Parameter Decision 0: Total number of captured data = 1 Mpts. This decision is the limiting factor of the used oscilloscope. The maximum number of points that can be stored into the oscilloscope memory is 1 million when the waveform is captured in single mode of the oscilloscope.

Design Parameter Decision 1: Carrier frequency of the transmitted signal is 10 GHz. The main reason of choosing carrier frequency at X band is the limitations of components in hand. The most restrictive limitation is related to the dishes that we used. Since dishes that can be easily accessed in the market are designed for satellite TV broadcasting, they are appropriate for X band as it is shown in Figure 8 which is a picture of an LNB that works with the same dishes. Hence, 10

GHz is chosen as the carrier frequency to be compatible with the tested band of the dishes.

Figure 8: Picture of LNB for the Used Dishes

Other polarimetric weather radars such as IDRA also encouraged us to use X Band as the carrier frequency [4]. In weather surveillance radars, using X band has some advantages over L and C bands. One of the advantages is that X-band components are, generally, less bulky, cheaper, and less power consuming.

The advantage of X band radars increases with the effect of polarimetry. In polarimetric weather radars, the backscatter differential phase is used as a good indicator when the size of the drop is larger than about a tenth of the wavelength. When it exceeds that value, differential phase exhibit an abrupt increase [11]. The corresponding size of the drops for 3, 5, and 10 GHz are 10 mm, 6 mm and 3 mm. Since water drops are smaller than 10 mm, the advantage of X band is significant for the backscatter differential phase [16].

Other components also do have limitations as enlisted below.

- Agilent E8267D PSG Vector Signal Generator can generate signals from 250 kHz up to 44 GHz.
- Power divider divides 10 GHz signal with 3.3 dB attenuation.
- Microsemi AML218L1502 Low Noise Amplifier can work from 2 to 18 GHz.
- Marki M1-0310 Double Balanced Mixer can work from 3 to 10 GHz.
- TriQuint TGA2501 Power Amplifier can work from 6 to 18 GHz
- Horn Antennas can work from 1 to 12 GHz
- Dish Reflectors are tested from 10 to 12 GHz and feed horns can work from 8 to 12 GHz.

- SMA cables works with 1 dB loss per meter at 10 GHz.

Design Parameter Decision 2: Modulation Type is Positive Ramp Sawtooth.

Agilent E8267D PSG Vector Signal Generator can generate frequency modulated signals with the waveforms of sine, square, positive ramp sawtooth, negative ramp sawtooth, and triangle. The most appropriate ones for us to measure range and Doppler with signal processing are linear ones, triangular and sawtooth modulations. The frequency of beat signals for both of these two modulation types affected by the range of the target and the Doppler shift (velocity). Although sawtooth waveform cannot extract the range component from Doppler effect without doing slow time signal processing, triangular waveform can do it in a single sweep measurement[17].

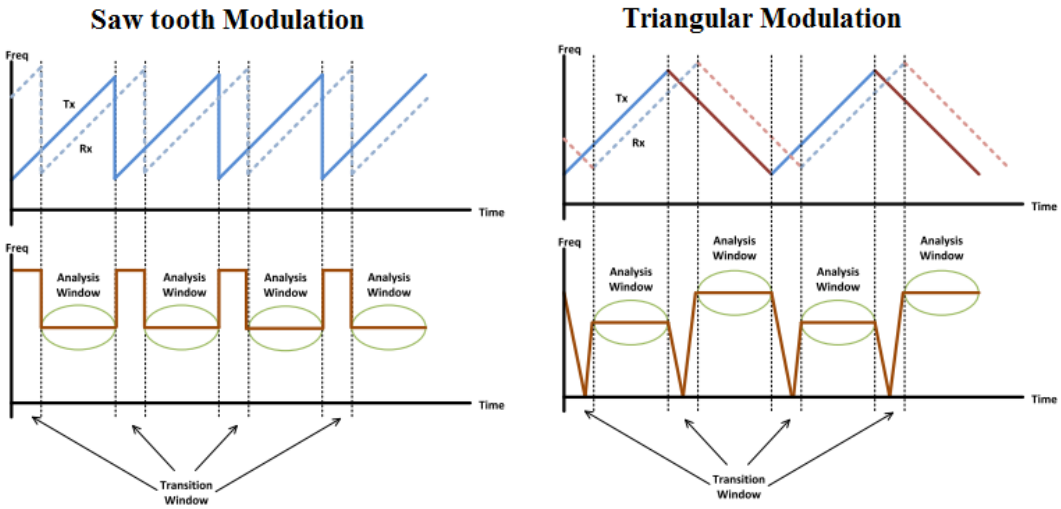

Figure 9: Sawtooth Modulation vs. Triangular Modulation[17]

Beat signal for one of the analysis interval in a triangular waveform case has a frequency equal to the sum of the range and Doppler frequencies and the other has the difference of them. Hence, it is possible to find both of range and Doppler frequency with basic addition and subtraction operations. By this operation, triangular waveform modulated radars can eliminate the error on measurement of range caused by the Doppler frequency. However sawtooth modulated radars calculate the range of moving targets with an error caused by the Doppler Effect.

Although triangular waveform is seen to be advantageous over sawtooth in the range and Doppler involvement aspect, it is not useful for the scenario of this study. First of all, range calculation error of a moving object does not make even a single resolution

cell for the speediest potential target. As it is exemplified earlier, a vehicle or a cloud which is moving with 120 kmph radial velocity (which is pretty high) causes 227 Hz error in calculation of its range at X band. However the range resolution of the radar in this system corresponds to 10 kHz. Therefore the ability of triangular waveform is not an advantage for this study and it also needs slow time signal processing operations to have Doppler capability.

The main disadvantage of triangular waveform over sawtooth is it takes twice as long time to perform a single measurement. In other words, for the limited capacity of oscilloscope memory, triangular waveform modulation generates less data for slow time signal processing operations. This causes decreases in the resolution of velocity measuring.

The practical reason to choose sawtooth modulation is the difference between the frequencies of analysis and transition windows. It is easy to find the starting point of the first sweep when using ramp modulation. The frequencies of the first and second regions differs more for the short range targets and this makes easy to separate them. This difference helps the signal processing unit to find the starting point of the sweep without any triggering signal. However that is not the case for the triangular ones. Frequency difference is very small for the case of triangular and changes smoothly and this makes hard to detect the starting point.

For these reasons, sawtooth modulation with positive slope is chosen as the modulation waveform and the parameters such as frequency deviation and FM rate are adjusted as described in previous Chapter.

Design Parameter Decision 3: N=100. Number of fast time data that will be captured during an observation is defined by rule of thumb. 100 fast time data is seemed sufficient and decided to check its compatibility after deciding on other parameters.

Design Parameter Decision 4: ΔF=30 MHz Equation (8) implies that, to increase the range resolution of the radar, frequency deviation should also be increased. Therefore, the greater frequency deviation means the better range resolution. Since there is no other parameter that depends on deviation, the maximum

possible value for that parameter is chosen. The transmitted signal is generated by Agilent E8267D PSG Vector Signal Generator. This device has a limitation for the deviation of the frequency. The maximum amount of frequency deviation at 10 GHz is given as 32 MHz. Since this amount is at the edge of maximum limit, 30 MHz is selected as the frequency deviation.

Result of Design Parameter Decisions 0, 1, 2, 3 and 4: By choosing ΔF as 30 MHz, range resolution of the radar is determined by (8) as:

$$\delta R = \frac{c}{\Delta F \; x \; 2} = \frac{3 \; x \; 10^8 \; (m/s)}{30 \; x \; 10^6 \; x \; 2 \; (1/s)} = 5 \; m \qquad (23)$$

Design Parameter Decision 5: ΔT=100 usec, f_s = 100 MHz. Before deciding on the duration of a single sweep interval, the parameters that it affects are considered. In the first place, it affects the sampling frequency of the oscilloscope. It is determined that 100 fast time data is going to be captured. This makes the duration of complete interval 100xΔT. During this time interval 1 million points will be sampled. This makes the sampling period $\frac{100x\Delta T}{10^6}$. By taking the inverse of the period, the sampling frequency becomes $\frac{10^4}{\Delta T}$ Hz. This value should be large enough to catch the maximum beat frequency which is the deviation itself. Hence, by Nyquist Criterion sampling frequency should be larger than 60 MHz.

Secondly, as (7), (10) and (12) implies, by choosing ΔT, the maximum unambiguous range, the maximum calculated speed and the resolution of measured speed are determined respectively. Although the maximum speed measure is inversely proportional, to increase the maximum range, and have better speed resolution, duration of single sweep should be increased.

Before deciding, some candidate of ΔT is examined and the affected parameters are listed on the table.

Table 2: Candidates for Single Sweep Duration

ΔT	$\boldsymbol{Fs}$: $\frac{\mathbf{10^4}}{\mathbf{\Delta T}}$	**Rmax**: $\frac{\mathbf{\Delta T\ c}}{\mathbf{2}}$	**Vmax**: $\frac{\lambda}{\mathbf{4\Delta T}}$	**δV**: $\frac{\boldsymbol{\lambda}}{\mathbf{2\ \Delta T\ N}}$	**Comments**
1 usec	10 Gsps	150 m	7500 m/s	150 m/s	Sampling frequency is above the limit, maximum range is too low, speed resolution is too low
10 usec	1 Gsps	1500 m	750 m/s	15 m/s	Maximum range is low, speed resolution is too low
50 usec	200 Msps	7500 m	150 m/s	3 m/s	Speed resolution can be increased more
100 usec	100 Msps	15000 m	75 m/s	1.5 m/s	Sampling frequency is enough. Speed resolution increased
1 ms	10 Msps	150000 m	7.5 m/s	0.15 m/s	Sampling frequency is too low, detectable maximum speed is too low

According to the comments on the table, duration of single sweep is determined as 100 usec. This is done by setting "FM Rate" of FM modulation parameters of Agilent E8267D PSG Vector Signal Generator to 10 kHz. Also horizontal zoom parameters of oscilloscope need to be set to 1 msec per division to capture at 100 sweeps during 10 msec interval.

Result of Design Parameter Decision 5: By choosing ΔT as 100 usec, maximum unambiguous range of the radar, maximum speed that can be measured, the resolution of calculated speed values, and the sampling frequency of analog to digital conversion are determined as:

$$\mathrm{f_{beat}} = \frac{\Delta F\ 2\ R}{\Delta T\ c} = \frac{30\ 10^6\ 2\ R}{100\ 10^{-6}\ 3\ 10^8} = 2\ R\ (KHz) \tag{24}$$

$$R\ = \frac{\mathrm{f_{beat}}\ \Delta T\ c}{2\ \Delta F} = \frac{\mathrm{f_{beat}}\ 100\ 10^{-6}\ 3\ 10^8}{60\ 10^6} = \frac{\mathrm{f_{beat}(kHz)}}{2} \tag{25}$$

$$R_{max}\ = \frac{\Delta T\ c}{2} = \frac{100\ x\ 10^{-6}(s)\ x\ 3\ x\ 10^8\left(\frac{m}{s}\right)}{2} = 15.000\ m \tag{26}$$

$$V_{max}\ = \frac{\lambda}{4\ \Delta T} = \frac{0.03\ (m)}{4x\ 100\ 10^{-6}(s)} = 75\ m/s\ = 270\ km/h \tag{27}$$

$$\delta V = \frac{\lambda}{2\ \Delta T\ N}\ = \frac{0.03\ (m)}{2\ x100\ x100\ x10^{-6}(s)} = 1.5\ m/s\ =\ 5.4\ km/h \tag{28}$$

$$f_s = \frac{10^4}{\Delta T} = \frac{10^4}{100\ 10^{-6}(s)} = 100\ MHz \quad (29)$$

At this point, all the parameters are decided and all the properties seem good for a weather radar. This shows the starting point, i.e. the rule of thumb was appropriate.

The transmitter part of the system mainly consists of four instruments: a signal generator, a power divider, an amplifier, and a transmitter antenna. By activating and adjusting the modulation option of signal generator it generates a frequency modulated signal. As described in system design parameters chapter sawtooth modulation with 30 MHz bandwidth is generated.

The maximum output power that signal generator can produce is 18 dBm and this maximum value is adjusted. The cables between the signal generator located inside the operator room and the power amplifier have a total loss of 13 dB together with the divider. Hence 5 dBm powers reach to the input of the power amplifier. The TGA 2501 amplifies the signal by 24 dB nominal gain and a 29 dBm (close to 0.8 Watts) signal is radiated through the transmitter antenna. By decreasing the distance between the signal generator and power amplifier it is possible to increase the radiated power. However the instruments need to stay in the operator room because of a potential rain.

The receiver part of the system consists of mixer, LNA, HPF, oscilloscope and signal processing unit. This system applies deramping process to the received and strengthened echo as described earlier. The cascaded LNA's generates 30 dB gains for the received echo. The specification of the used device is seen on Figure 10.

The parameters of the oscilloscope are adjusted to take 100 slow time sweeps. To be able to do that, horizontal scale of the oscilloscope is adjusted to 1 ms/div. This makes 10 ms of total observation interval and it contains 100 sweeps with the length of 100 us. The digitized and stored signal in the oscilloscope is taken by the Matlab generated program and signal processing operations are performed there.

Select Property Type	Symbol	Min	Typ	Max	Unit
DC Current (mA)	mA		160.00		mA
Flatness	Flatness (dB)		1.00		±dB
Frequency	F	2.00		18.00	GHz
Gain	Gain		15.00		dB
Noise Figure @ 25C	NF		3.00		dB
Output IP3	$IP3_{Out}$		24.00		dBm
P1dB	P1dB		14.00		dBm
VSWR	VSWR		2.00		x:1

Figure 10: Low Noise Amplifier Specifications

3.3 Antennas

There are two types of antennas used in this study. The first antenna is a horn antenna with a larger beamwidth and a lower gain. Although its gain is not too much, the width of its beam is used as advantage to superpose the enlightened regions easily. Horn antennas used in this study is seen on Figure 11.

Figure 11: Horn Antennas

The gain and bandwidth specification of the horn antenna is calculated in a prior M.S. thesis [18]. The details of the gain measurements are provided in Table 3.

Table 3: Gain of Horn Antennas[18]

	Antenna 1 (GAH-1042)
@ 9GHz	15.5257 dBi
@ 10GHz	15.3757 dBi

Additionally, the radiation pattern of the horn antennas on the E-plane is obtained from [18] and is presented in Figure 12. The 3dB beamwidths of the antenna in the azimuth plane is around 30 degree.

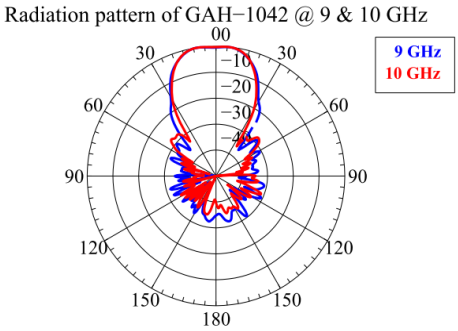

Figure 12: Radiation Pattern of Horn Antennas[18]

During power calculations, these values are used among the antenna parameters. The gain parameter G and the beamwidth parameters for both azimuth and elevation in radar range equation are calculated in power calculation part according to these values.

As a second choice, to increase the gain and decrease the beamwidth, a dish reflector and a small horn antenna are used. Satellite TV dishes which can work at X-band are used as reflectors and a small horn is used as the feed of the antenna. A picture of the dish antennas and the feed horn is shown in Figure 13 and Figure 14.

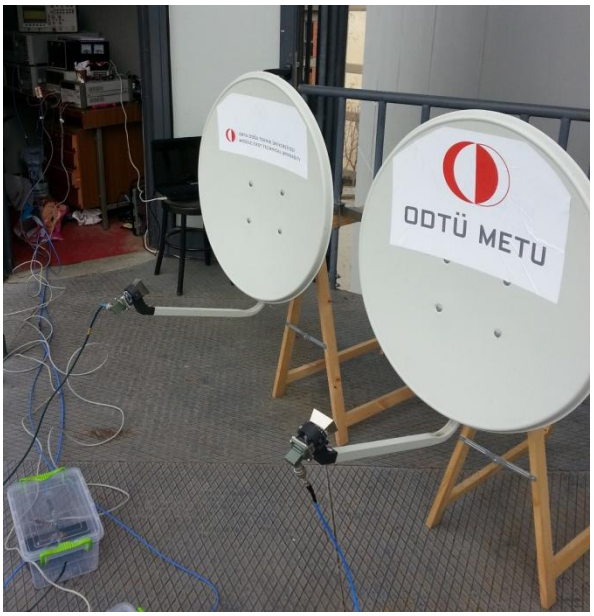

Figure 13: Dish Antennas

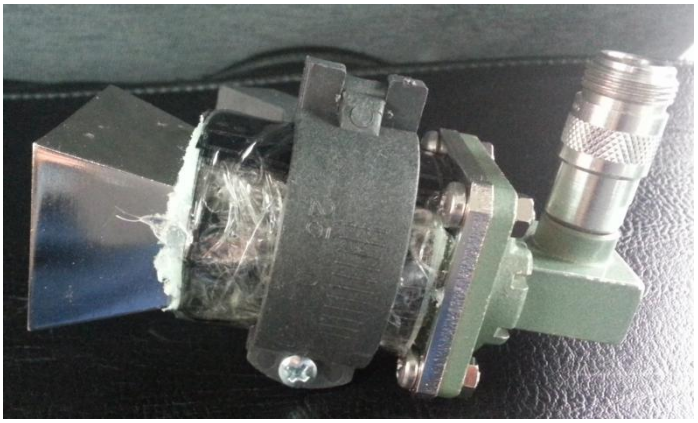

Figure 14: Feed of the Dish Antennas

Dish antennas are modeled by using CST Studio Suit and their simulations are performed with the help of Mert Çelik to be able to have information about the gain and beam with of them.

According to the simulation result in Figure 15, the gain of the feed is calculated as 12 dBi. Then, total gain of the dish reflector and feed horn is also calculated with the same simulation program.

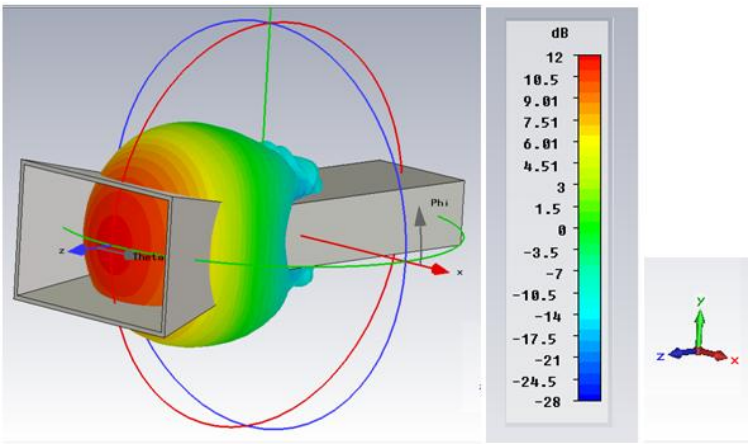

Figure 15: Model of Feed of Dish Antennas

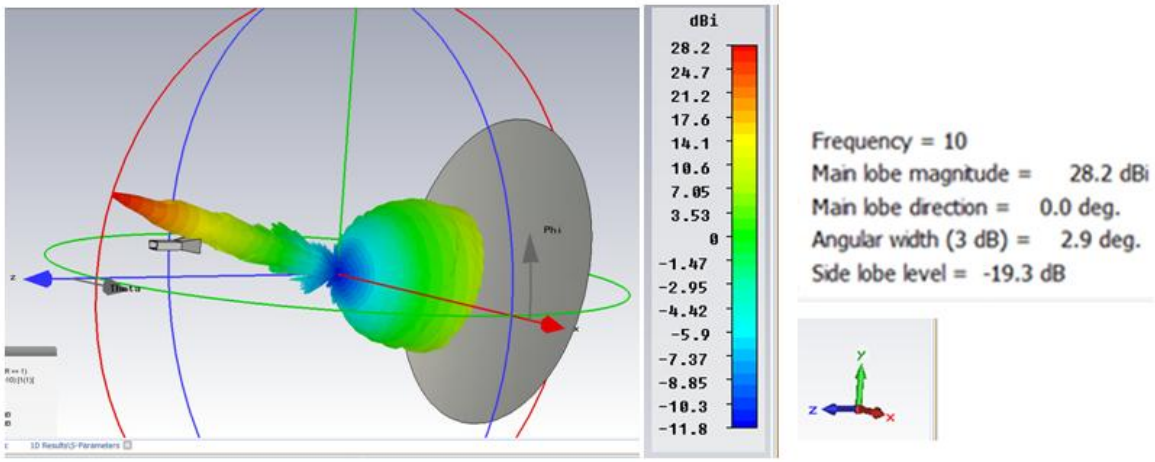

Figure 16: Model of Dish Antenna Set

According to simulation results depicted in Figure 16, gain of dish antenna is calculated as 28 dBi and 3 dB beamwidth is calculated as 3 degree. Power calculations are performed according to these values in the next section.

3.4 Power Calculation of the System

Research motivation of this study was reducing the power need of the FMCW system while receiving the same amount of energy with pulsed radars. Hence, the transmission power of the system is desired to be low. The amplifier that we have in our hand was TGA2501 power amplifier with maximum output of 34.5 dBm. However the limiting factor was the maximum output level of signal generator and the losses caused by the cables and divider. Hence the maximum power level that

reaches to the transmitter antenna is calculated as 29 dBm (≈0.8 Watts) in Section 3.2.

The return power in case of a rain is obtained according to the strength of rain. The corresponding reflectivity, Z is given in Table 1. These values are multiplied with 10^{-18} to have the unit of m^3.

According to Figure 5, atmospheric loss factor for X band can be taken as 0.01 dB/Km.

$$\alpha = 0.01\ dB/Km$$

$$L_{atm}^2(R)\ (dB) = 2\alpha\ \left(\frac{R}{1000}\right) = \frac{2R}{10^5}(dB) \tag{30}$$

$$L_{atm}^2(R) = 10^{2R/10^6} \tag{31}$$

By placing the system parameters for the horn antennas to the radar range equation (20) for weather radars the equation become:

3 dB beam with is 30 degree = 0.523 radian

$$G_t = G_r = 10^{1.53} = 33.8$$

$$P_r = \frac{P_t\ G_t\ G_r\ \lambda^2\ \theta^2\ \Delta R\ \eta}{\pi^2\ 512\ \ln 2\ R^2\ L_{atm}^2(R)} = \frac{0.8\ x\ 33.8^2\ x(0.03)^2\ x\ (0.523)^2\ x\ 5\ x\ \eta}{\pi^2\ 512\ \ln(2)\ R^2\ L_{atm}^2(R)}$$

$$= 0.000321\ x\ \frac{\eta}{R^2\ L_{atm}^2(R)} \tag{32}$$

For a moderate rain at 5 km

$$Z\ (avarage) = 6800\ x\ 10^{-18}\ \ m^3$$

$$\eta = \frac{\pi^5\ |K|^2}{\lambda^4}\ Z = \frac{\pi^5\ x\ 0.93}{(0.03)^4}\ x\ 6800x10^{-18} = 2.389\ x\ 10^{-6}\ (1/m)$$

$$L_{atm}^2(R) = 10^{2x5x10^3/10^6} = 1.023 \tag{33}$$

By using (32) the received power is calculated as:

$$P_r = 0.000321\ x\ \frac{2.389\ x\ 10^{-6}}{(5000)^2\ x\ 1.023} = 3x\ 10^{-17} W = -135\ dBm \tag{34}$$

By the same way from 100 m during moderate rain the received power is calculated as:

$$P_r = 0.000321\ x\ \frac{2.389\ x\ 10^{-6}}{(100)^2\ x\ 1}$$

$$= 7.67\ x\ 10^{-14}\ W = -101.1\ dBm \tag{35}$$

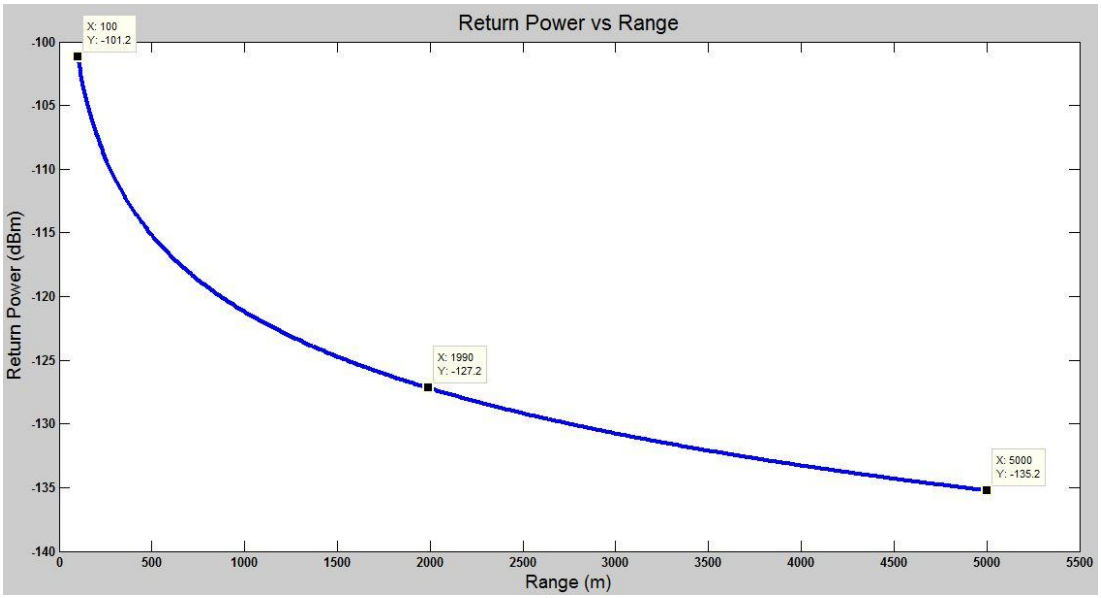

Figure 17: Return Power vs. Range with Horn Antennas

Return power from 100m to 5 km is plotted on Figure 17. The average value is -127 dBm. By using the low noise amplifiers this value is increased by 30 dB to average of -97 dBm.

For the dish antennas

$$G_t = G_r = 10^{2.82} = 660.7$$

3 dB beam with is 2.9 degree = 0.0506 radian

Than radar range equation becomes:

$$P_r = \frac{0.8\ x\ 660.7^2\ x(0.03)^2\ x\ (0.0506\ )^2\ x\ 5\ x\ \eta}{\pi^2\ \ 512\ \ln(2)\ R^2\ \ L_{atm}^2(R)} \tag{36}$$

$$= 0.00115\ x\ \frac{\eta}{R^2\ x\ L_{atm}^2(R)}$$

For the moderate rain at 5 km

$$P_r = 0.00115\ \ x\ \frac{2.389\ x\ 10^{-6}}{5000^2\ x\ 1.023} = 1.074\ x\ 10^{-16}\ W = \ -129.6\ dBm \qquad (37)$$

By the same way from 100 m

$$P_r = 0.00115\ x\ \frac{2.389\ x\ 10^{-6}}{100^2\ x\ 1} = 2.74\ x\ 10^{-13}\ W = \ -95.6\ dBm \qquad (38)$$

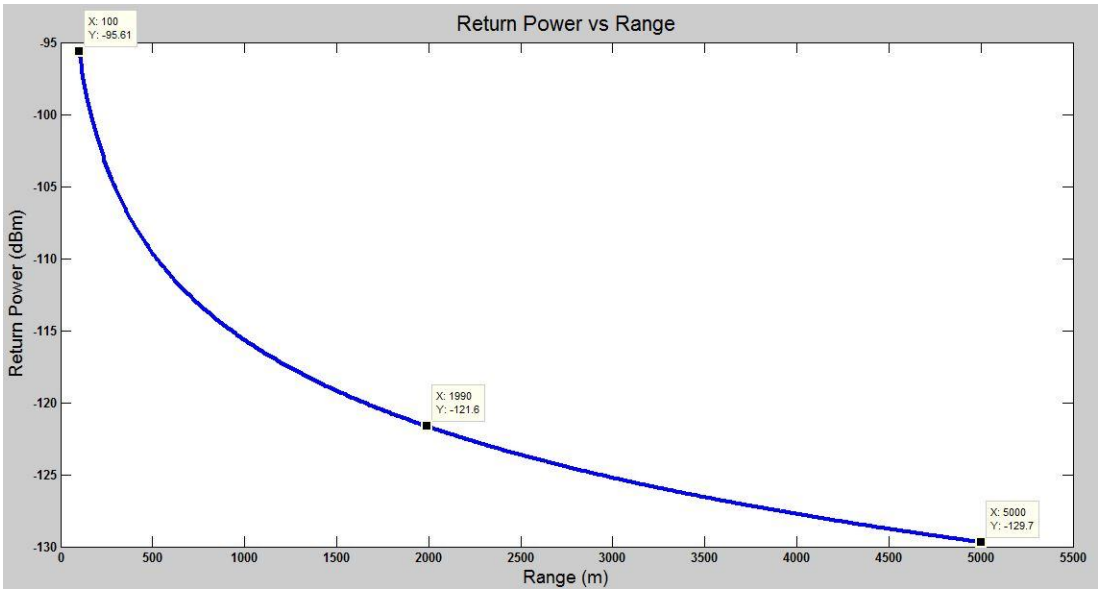

Figure 18: Return Power vs. Range for Dish Antennas

Return power from 100m to 5 km with dish antennas is plotted on Figure 18.

Dynamic range of the system is calculated from 5 km to 100 meters as -95 + 129 = 34 dB.

3.5 Graphical User Interface (GUI)

The Matlab generated program takes online or offline digital data, processes it according to the given system parameters by the GUI. The results of the signal processing unit are also showed on the GUI screen. The range of the targets and speed of them are examined with the help of this GUI. A screenshot of the GUI is

shown on Figure 19 with the additional numbering. Explanation of the GUI is made with the help of this numbers.

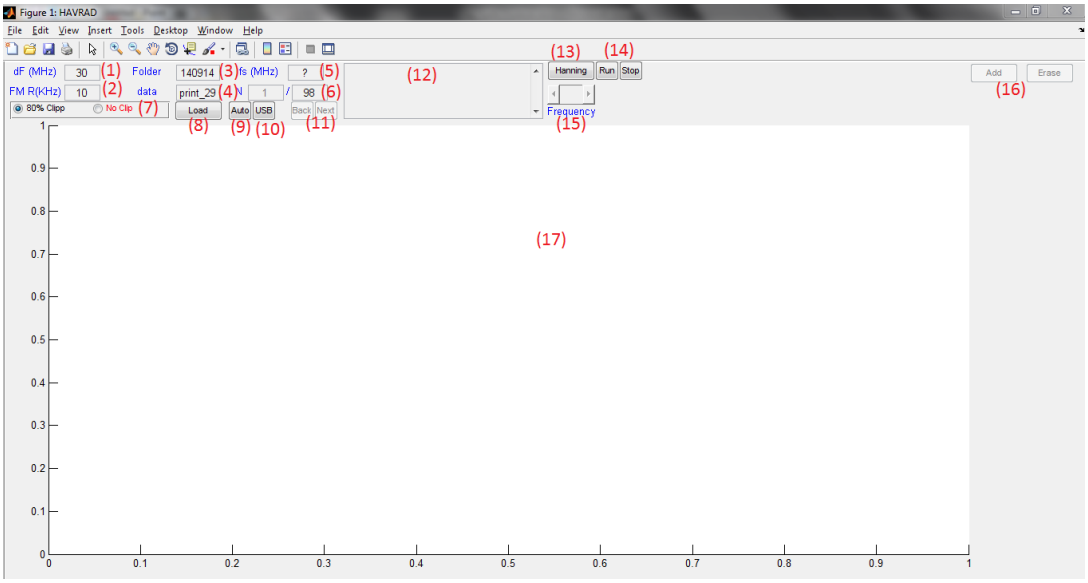

Figure 19: Radar Graphical User Interface

1. <u>ΔF / Frequency Deviation:</u> The frequency deviation of the transmitter signal is needed to be written at this portion. Range calculation of the targets directly depends on this value. Default value is 30 MHz and it must be updated if it changes.
2. <u>FMR / FM Rate:</u> FM rate is the inverse of the duration of a single sweep interval. Since this value is also a parameter used in the calculations, this value is needed to be updated in case of any change. Default value is 10 kHz and corresponds to 100 usec of sweep duration.
3. <u>Folder:</u> When an offline data is going to be handled, the name of the folder where the corresponding binary file is placed should be written into this textbox. This folder and the programming .m file must be at the same directory.
4. <u>Data:</u> The name of the binary file which stays on the "Folder" need to be written here while doing offline processing.
5. <u>Fs / Sampling frequency:</u> This box is an output box. Sampling Frequency of the oscilloscope chances by depending on the length of the given data. The sampling frequency is calculated from the stored data into memory and used while doing

Fourier Transform. In this textbox, it is showed to the operator as control information.

6. N / Slow time data amount: This portion has two textbox. The one on the right is an input while the other is an output. It asks to operator how many fast time data should be processed on slow time. Given value need to be at least one less than the stored value since the first point of the recorded data is not always the starting point of a sweep. The amount of stored value is showed on the information text bar (12) after data is loaded. The portion on the left is just an output and shows the number of current fast time data on the screen. The back and next buttons (11) refresh this output.
7. Clipping on / off: This input gives the ability to clip the first 20% of a sweep in time domain or continue without clipping. More information about this operation is given in section 4.1.2 Clipping Section.
8. Load/Choose or Go/FFT Button: Loading data into the system and processing it start and continue with this button. There are 3 different forms of data loading and signal processing. These forms are chosen from button (9) and described as the following.
    a. Manual: If processing type is chosen as "Manu" from button 9, the starting point of the first sweep need to be adjusted by hand. This is the primitive version of the signal processing algorithm. Every click on this button converts it in a loop as it is shown in Figure 20

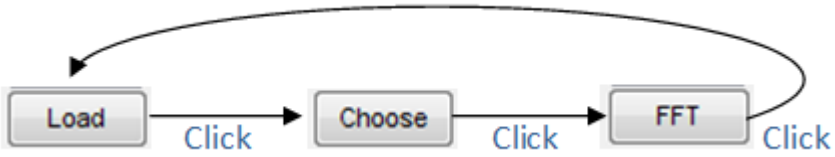

Figure 20: Load Button Flow in Manual Mode

When the *"Load"* button is clicked, data is loaded from the binary file at the specified folder if offline data processing is chosen from button (10). If the choice is online, then data is taken from the GPIB interface. All of the loaded data is shown on the screen and button is converted to *"Choose"* mode to define the starting point of the first sweep.

After zooming near the beginning of the first sweep "*Choose"* button should be clicked. By this action, the mouse cursor changes its type. By clicking on the starting point of the first sweep on the data graph, all fast time data are parsed from each other and taken into memory arrays. By default the first fast time data is seen on the screen. It is possible to see all the fast time data from the next/previous buttons. By this choosing operation, choose button is converted to *'FFT'* mode.

By clicking *'FFT'* button, Fast Fourier Transforms of all individual fast time data are taken. At first, average of Fourier Transforms of all fast time data is shown on the screen. It is possible to see fast time data individually from the next/previous buttons. On this step, all targets are seen on the power vs. frequency plot. To see the corresponding range values of the targets "Add/Erase" buttons which has just became active should be used.

b. Step: If processing type is chosen as "Step" from button 9, the starting point of the first sweep is going to be adjusted automatically. However steps of signal processing are shown to the operator. This form is a moderate version between the primitive and automated ones. This form gives the ability to see and control all the steps of data processing. Every click on this button converts its state in a loop as it is shown in Figure 21.

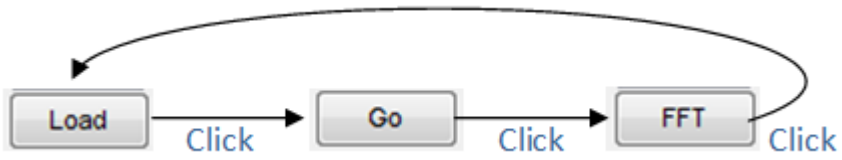

Figure 21: Load Button Flow in Step Mode

When the *"Load"* button is clicked, data is loaded from the binary file at the specified folder if offline data processing is chosen from button (10). If the choice is online, then data is taken from the GPIB interface. The starting point of the first sweep is found automatically and showed with a red line on the screen for the operator's approval. Starting point finding algorithm is implemented with a digital high pass filter. Since the 1st region of every sweep contains higher frequency terms, the first value above the average of

the result of HPF is determined as the starting point of the first sweep. Then button is converted to *"Go"* mode to approve the found starting point.

The button "Go" is just to approve the starting point that algorithm defined automatically. After clicking the button it changes itself to *"FFT"* and by clicking it again it does the same thing for the FFT case above.

c. Automated: If processing type is chosen as "Auto" from button 9, the starting point of the first sweep is adjusted automatically and this time just the result of FFT is showed to the operator. This form is the fully automated version and user clicks only to *"Load"* button and see the FFT results. The state of the button in this case is stable and stays at *"Load"* as shown in Figure 22.

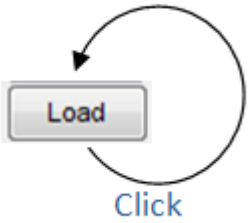

Figure 22: Load Button Flow in Automated Mode

9. Auto/Step/Manu: This button is to choose the mode of signal processing. Its function is described above. Its flow is seen on Figure 23. The value written on the button is the current value that is being applied. Default choice is *"Auto"*.

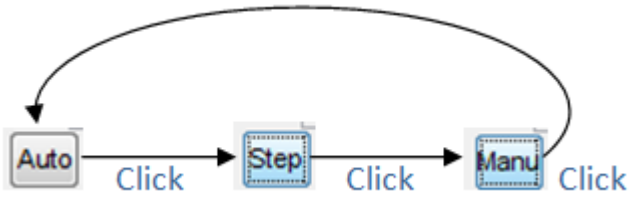

Figure 23: Mode Button Flow

10. USB/GPIB: This button is to make the choice of processing offline or online data. When *"USB"* is the choice on the button, system loads offline data from the folder. On the other hand, *"GPIB"* is the choice of online data which flows from the GPIB interface.

11. Back/Next: This button is to switch between the fast time data. It is possible to traverse between fast time data both at time domain or frequency domain. The current value on the screen can be followed from textbox (6). If "*Back*" button is pressed while the current value is already 1, the average of all the fast time data is printed on the screen. The default value is the average value.
12. Information Text: This textbox is the main screen that the background operations can give some messages to operator such as the range parameters, the value of the picked point etc.
13. Window Button: This button applies special windows to fast time data. The choices are Hanning, 4 steps Blackman – Harris and no window. The window name written on the button is the current value that is applied to the data. When window changes, the value on the screen also changes.
14. Run/Stop: These buttons are also to automate the system. When *"Run"* is pushed the *"Load"* button is clicked for every 1 second. *"Stop"* button stops this action as the name implies.
15. Zoom Slider: This slider is to extend the frequency axis and to be able to see the targets closely. It is active only when FFT of fast time data is on the screen.
16. Add/Erase: These buttons convert the frequency information into range. By clicking the *"Add"* button, program waits user to pick a range bin from the screen. Additionally a new text box and a new button are created as seen on Figure 24. When a point on the graph is picked, range of the clicked point is written on the created textbox. The frequency of the picked point is also shown on the main information text window (12).

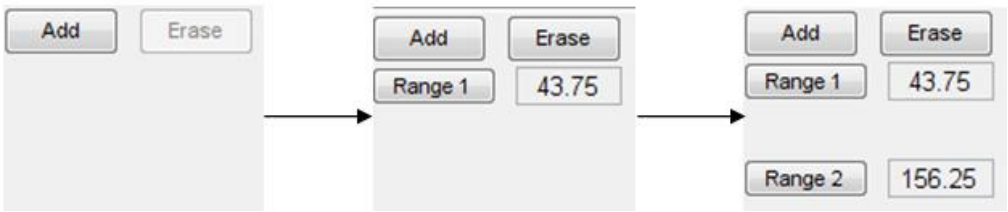

Figure 24: Add Button Flow

The new appeared button performs slow time signal processing. The values for different sweep intervals and Fourier transform of them are showed at two different new windows. At the Fourier transform window, program waits the

operator to pick a frequency bin to measure the speed of the target. The following figures show the real part of the slow time data and its FFT for both stationary and moving targets. Doppler Frequency for the moving object can also be easily seen from the real part of slow time data and it is calculated by FFT algorithm.

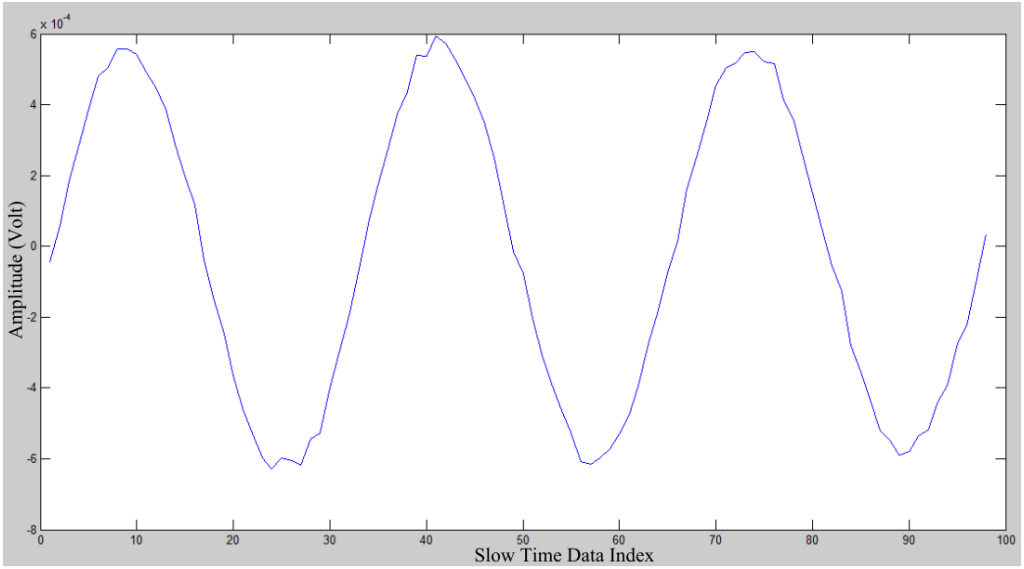

Figure 25: Slow Time Data for a Moving Target

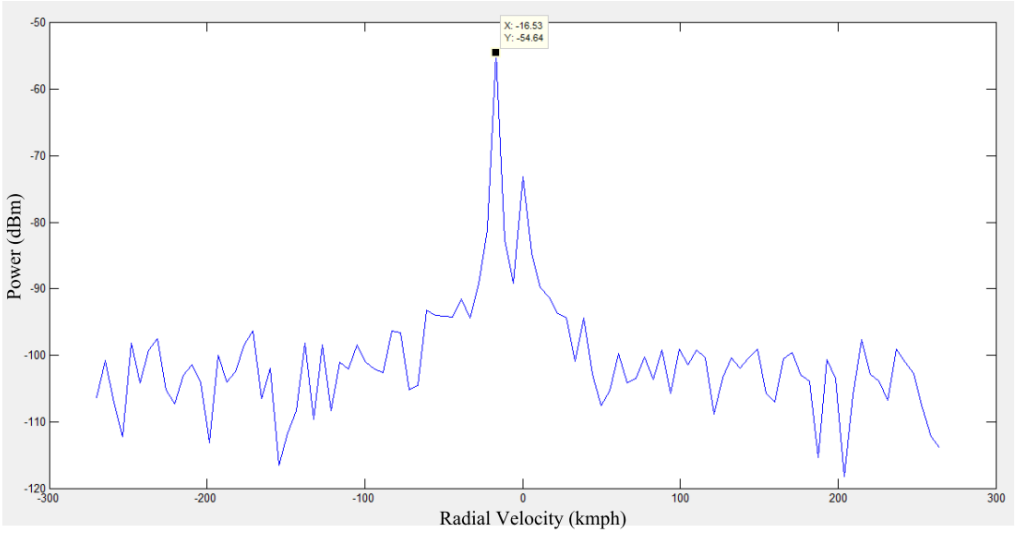

Figure 26: FFT of Real Part of Slow Time Data for a Moving Target

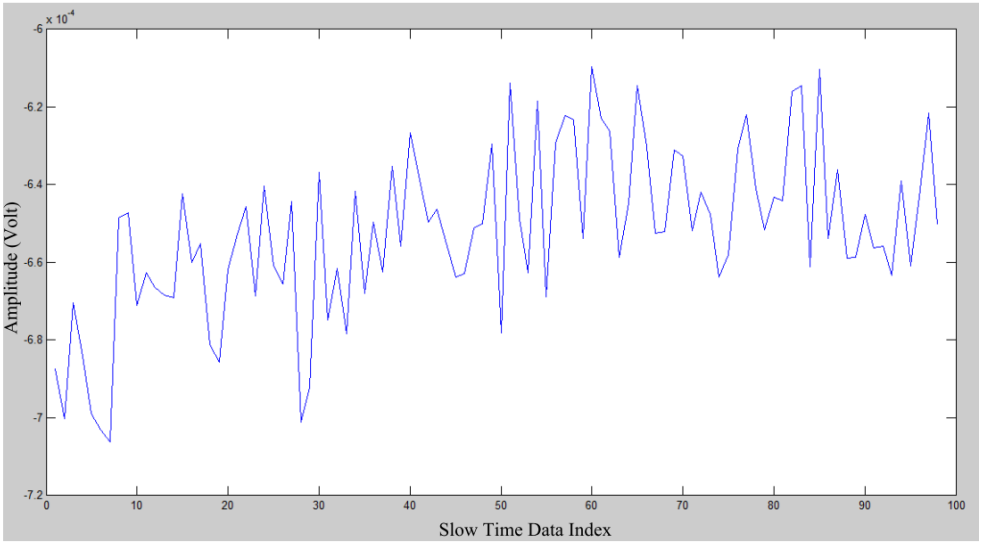

Figure 27: Slow Time Data for a Stationary Target

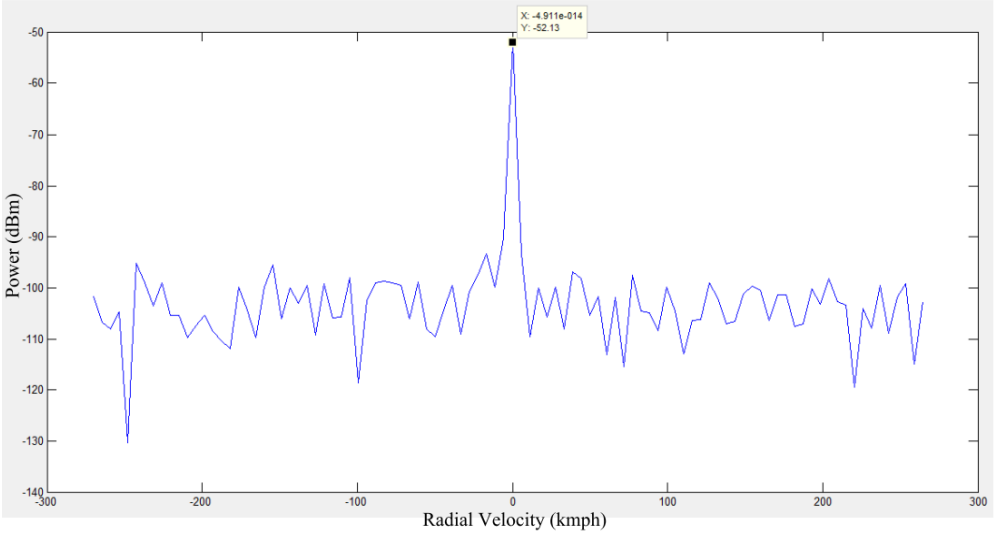

Figure 28: FFT of Slow Time Data for a Stationary Target

CHAPTER 4

DETECTION ALGORITHMS

4.1 Fast Time Signal Processing

Fast time signal processing steps contain the algorithms that detect and obtain range information of targets from the data stored in time domain. The main processes to detect targets and find their range is taking the Fourier Transform of time domain data. By converting the information from time domain to frequency domain the existence of any target at an arbitrary range is converted to the existence of corresponding frequency component in the spectrum. Before converting the information to frequency domain, some necessary algorithms need to be applied to signal in time domain. The first step is finding the starting point of sweep interval. This process is called as "Sweep Interval Trigger Process". In this process the starting point of the first sweep is determined and sequential sweeps are segmented from the continuous fast time data. Then separated sweeps are stored into a matrix.

Following process is clipping the first portion of time domain data to avoid multiple frequency components for the single targets. This process is optional and activated by clicking the clipping radio button (7) in the graphical user interface.

The last step before taking Fast Fourier Transform is applying windowing algorithms to time domain data parcels. This step is also optional and activated by the button 13 in GUI. User can apply Hanning window, 4 steps Blackman-Harris window or rectangular window (closed) to the captured fast time data slices. This process is crucial for avoiding spectral leakage problems.

4.1.1 Sweep Interval Trigger Processing

Since there is not any reference clock from signal generator to the oscilloscope, the starting point of the very first beat interval cannot be determined by the oscilloscope. Hence it takes trig manually by the "Single" button or by "Load" button (8) on the GUI of control program through GPIB interface. Hence, to be able to divide the fast time data into segments and constitute the slow time data the starting point of the first sweep needed to be determined.

To find the starting point, the jump in the frequency difference at the transition points of sawtooth modulation is used. For the 1st region of beat signal the frequency is ΔF - fbeat and it is fbeat for the second region. Fortunately, for the close region targets the frequency of first region signal is much greater than the frequency of the second region. The leakage between the transmitter and receiver antennas behaves like there is a target in the very front of the radar. Since delay generating path caused by the inevitable leakage between the antennas, there are always higher frequency components near ΔF in the first region. This permanent high frequency component on the beat signal is used as an advantageous indicator of the starting point of the first sweep.

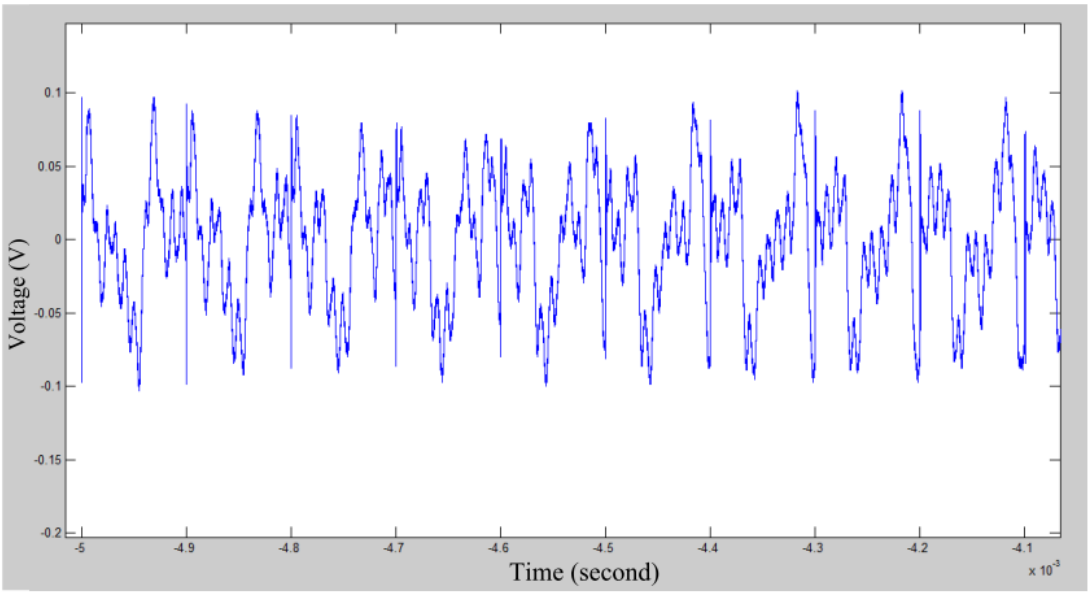

Figure 29: Beat Signal in Time Domain

On Figure 29, a portion of fast time data which contains about 9 sweeps is seen. To determine the starting point, firstly the low frequency components are filtered by a digital HPF.

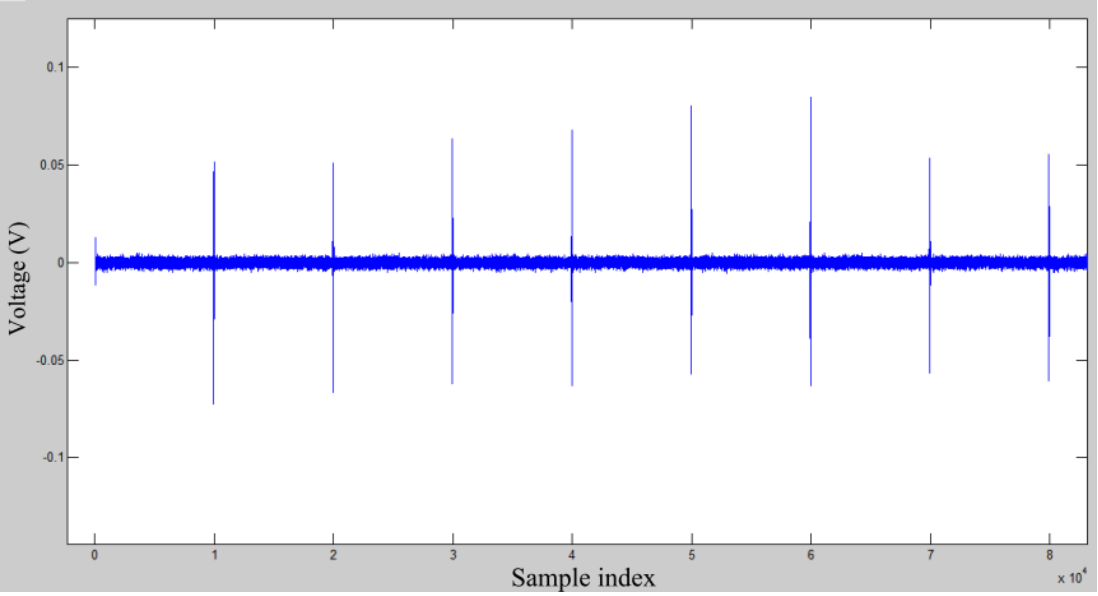

Figure 30: High Pass Filtered Beat Signal

By filtering low frequency components, 2nd region of the fast time data is eliminated. Then the first point exceeding the threshold is picked as the starting point. According to the FM rate entered to GUI the cascaded sweeps from the original data (before filtering) are separated and stored into the memory arrays.

Finding the starting point with the help of a high pass filter is done if the fast time signal processing type is chosen as automatic or step. Starting point finding process can also be made by hand if button 9 is adjusted as manual. User is expected to zoom and find the starting point of the sweep interval totally by hand.

If the button is set to "Step" the control program finds the starting point automatically and shows it to user with a red line and waits for an approve.

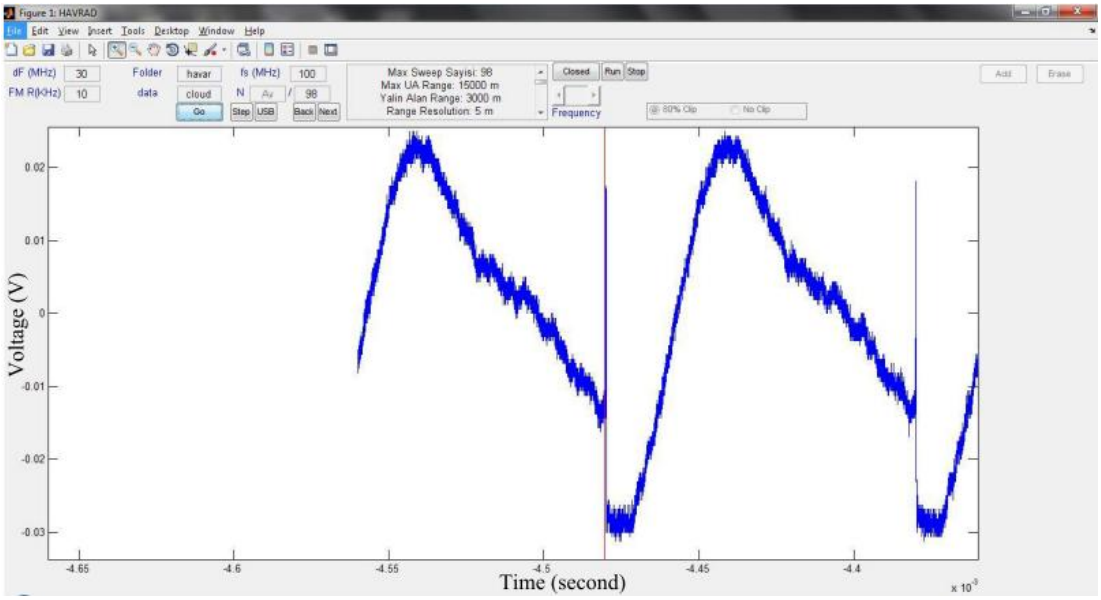

Figure 31: Finding Starting Point of First Sweep

4.1.2 Clipping

As it is mentioned above, while using sawtooth modulation in the frequency, the beat signal generated by a single point target contains two different frequency components. A single sweep interval is seen on Figure 32. This sweep is divided into two regions. The length of the regions depends on the range of the target. The 1st region called the transition region and lasts for τ seconds, the second one called the analysis region lasts for the rest of the sweep interval, ΔT-τ seconds. The duration of the analysis region is longer for close range targets. In the same way, transition region has longer duration for targets located near the unambiguous range border.

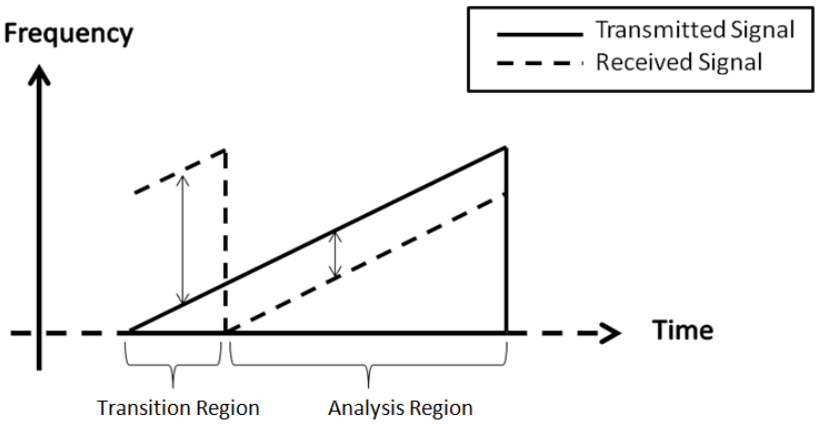

Figure 32: Sweep Frequency vs. Time

Besides duration, the frequency difference between the transmitted and received signals is also different for these two regions. For the analysis region the frequency difference of the transmitted and received signal is equal to the beat frequency, f_{beat}. On the other hand, for the transition region it is $\Delta F - f_{beat}$.

Having multiple frequency components for a single target is not desired since it generates another rectangular window inside a sweep interval and also causes confusion when having multiple targets. To avoid this, transition region of any beat signal is clipped. Since the transition point of regions depends on the range of the target, it is not possible to avoid multiple frequency components for all of the targets. In this thesis the first 20% of the beat signal is clipped in time domain. Since the range information is on the frequency domain it does not blind the radar for any range. This technique leads to a single frequency component for targets whose travel times are less than 20% of ΔT. In Figure 33 the effect of clipping the transition region for a single target is seen.

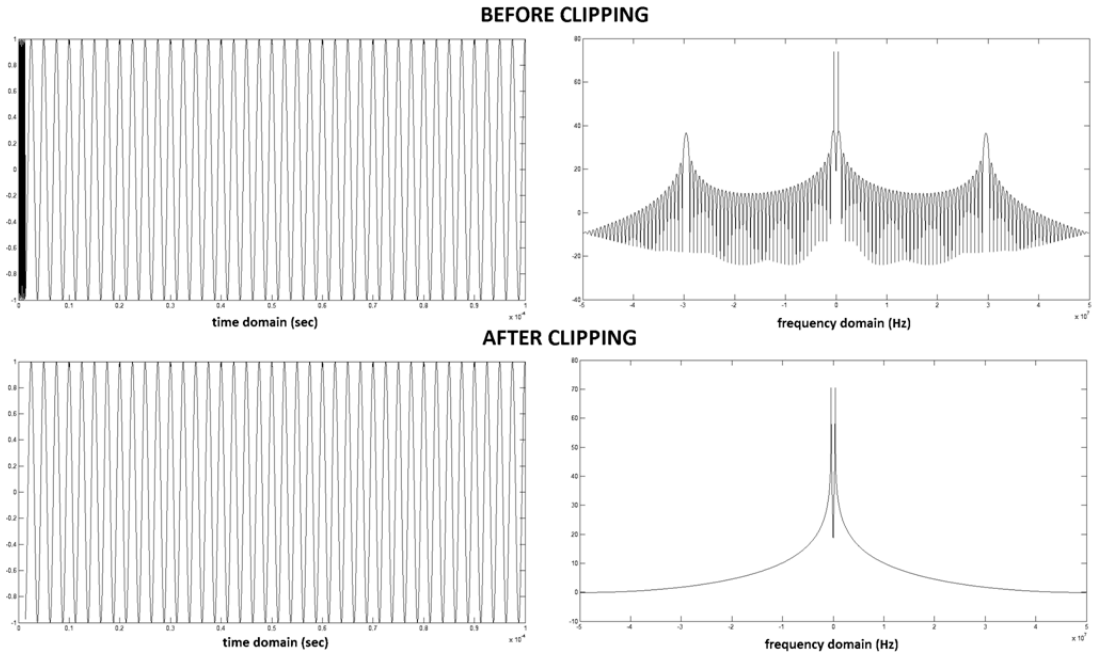

Figure 33: Models for Clipped and Original Beat Signals

Clipping the beat signal decreases the amount of energy per sweep interval. Duration of the beat signal is decreased by this operation and energy of the input signal to the FFT algorithm is decreased. Besides, the range resolution of the system is also

changed. From (8), the range resolution of the radar depends on the number of frequency bins in the spectrum, n_s. The number of frequency bins is equal to the number of signal points in time domain. By clipping 20% of the beat signal, this amount decreases to 80% of the previous value which is denoted as $n_s^c = 0.8 \text{ x } n_s$. Then the distance between frequency bins are increased to $\frac{fs}{n_s^c}$ Hz and this value decreases the resolution in the frequency domain. The amount of data available for FFT after clipping is collected during 80% of sweep interval. Then, n_s^c is equal to 0.8 x ΔT x fs. By using formula given in (5) and having the frequency resolution of $\frac{fs}{n_s^c}$, the range resolution of 20% clipping algorithm is calculated as

$$\delta R = \frac{\delta f_{beat}\ \Delta T\ c}{2\ \Delta F} = \frac{f_s\ \Delta T\ c}{2\ n_s^c\ \Delta F} = \frac{f_s\ \Delta T\ c}{1.6\ f_s\ \Delta T\ \Delta F} = \frac{5\ c}{8\ \Delta F}$$

$$= \frac{3 \text{ x} 10^8 \text{ x } 5}{30\ x\ 10^6\ x\ 8} = 6.25\ m\ . \qquad (39)$$

As a result, the range resolution of the radar with clipping capability decreased by 20%. This clipping operation does not eliminate the second frequency component for all of the targets. Since where the target is located is not known before clipping, first 20% of the beat signal is clipped automatically. This operation only eliminates the second frequency components for the targets inside 20% of the maximum unambiguous range. Hence the maximum range with single tone after clipping becomes:

$$\text{Single Tone } R_{max} = 0.1\ x\ 100u\ x\ 3x10^8 = 3000\ m$$

4.1.3 Windowing / Spectral Leakage

Range information of any target lies in the frequency domain in FMCW radars. Therefore, FFT is applied to the captured and segmented fast time data. The FFT computation assumes that input signal is periodic and identically repeats itself over and over again with infinite duration in time domain. If there is integer number of cycles of a sine wave in the recorded data, it would not cause any spectral leakage. This is because single input data and repeated blocks result the same signal, when the observation time is an integer multiple of the period of the signal.

On the other hand, when the recorded data is not periodic, there would be either discontinuities or overlaps in the signal. To exemplify, a portion of a sine wave where the number of the cycles is not an integer is cascaded twice in Figure 34. Since the signal is not periodic, discontinuities occurred in the vanishing point. This discontinuity generates spectral leakage while applying FFT to this signal.

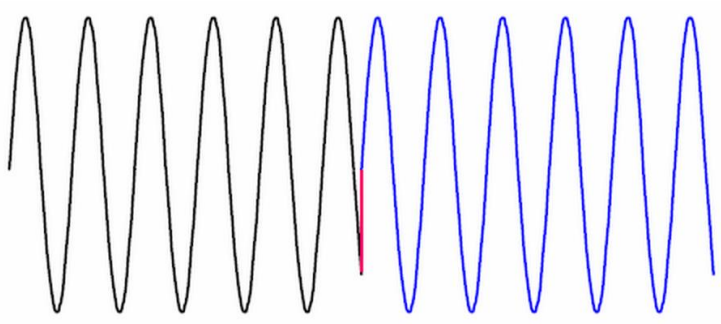

Figure 34: Signal with Spectral Leakage[19]

When FFT of a non-periodic signal is computed, frequency components of the signal change and the resulting frequency spectrum suffers from spectral leakage. This leakage spreads signal energy in a wide frequency range in the frequency.

For both the periodic and non-periodic cases, time domain signals and their FFT results are plotted in Figure 34.

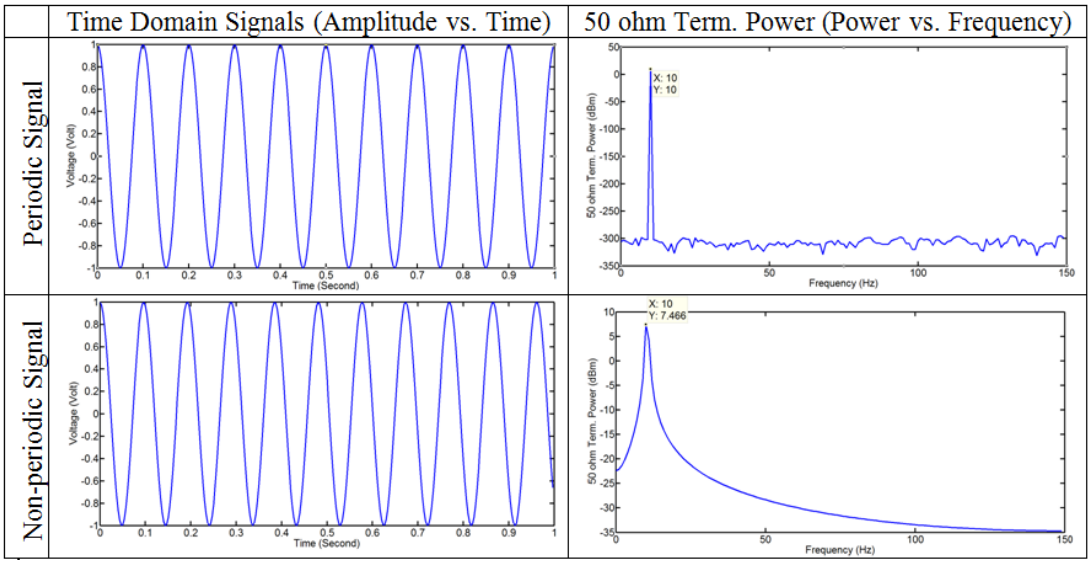

Figure 35: Spectral Leakage

The first row in the graph shows a 10 Hz sine wave which is periodic in the recorded time frame. Voltage information of this signal is converted into power domain for 50 ohm termination resistance by doing necessary calculation on the result of its FFT. In the same row and second column a narrow peak at 10 Hz with a height of 10 dBm is shown as expected[20]. In the second row a sine wave whose frequency is very close to previous one but is not periodic in the recorded time interval is seen. Spectral leakage can be observed on the power domain of this signal. Although the amplitudes of time domain signals are the same for both cases, amplitude of the FFT result for non-periodic case is less than the expected value, 10 dBm. Also the signal energy is more dispersed by the unwanted frequency bins next to the main bin in the frequency domain. This phenomenon which can be regarded as "leakage" from the main frequency bin to the other bins makes it more difficult to identify the frequency content of the measured signal. Especially if there are multiple frequency components in the recorded data, some frequency components with smaller power can disappear because of the leakage from other bins.

In this study, the waveform under analysis, which is the beat signal, consists of multiple frequency components. Since the frequency of the contributor which depends on the range of the corresponding target is not known, the periodicity of the recorded data is also not known. This means, spectral leakage will generally occur on the result of the applied FFT algorithm. The effect of spectral leakage in the application of this study is related with the range resolution of radar. Since the beat signal under analysis comprises multiple sinusoids of different frequencies, leakage can interfere with the ability to distinguish multiple targets spectrally. If the targets are located far away from each other, their frequencies are dissimilar. In such a case, if return power from one target is weaker, then leakage from the target with the larger return power can obscure the weaker one’s presence[20]. However, if the targets are located close to each other, their frequencies become similar. This time, leakage can render them irresolvable even if the return powers of them are equal[19].

Spectral leakage causes mainly two problems and it is possible to decrease their effects: One of them is about signal to noise ratio. Because of the spectral components, the desired signal cannot contain all of the energy; rather it also

contains the energy coming from the spectral leakage of adjacent components and noise. These effects reduce the SNR. On the other hand, spectral leakage of larger signal component may significantly overshadow smaller signals and makes them difficult to detect.

The way of reducing these problems is applying varies windows to the recorded signal [20]. Instead of rectangular window, applying a window function to the acquisition that connects the waveform endpoints in a smoother fashion before computing the FFT will result in a better spectral resolution. This technique which decreases the effect of spectral leakage is also referred to as windowing.

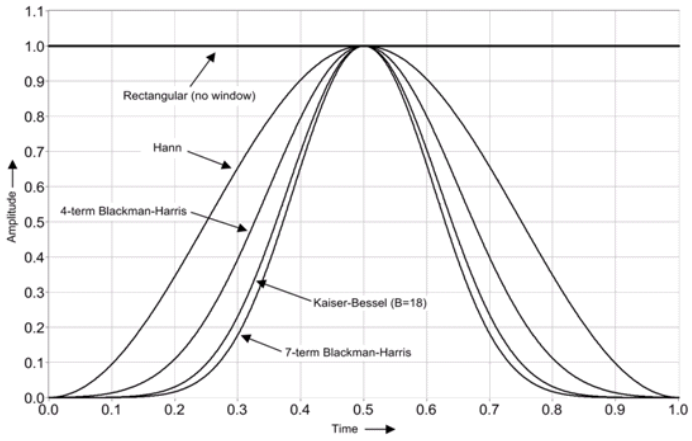

Figure 36: Time Domain Plots of Some Windows[21]

There are different types of window functions preferred for particular applications and each of them has its own advantages for the used application. In Figure 36 time-domain plots of some popular windows are plotted

To be able to provide smooth connections between waveforms, windows begin and end at zero and rise to unity in the middle. Having narrow window in time domain means wide main lobe in the frequency domain, and vice-versa. On the other hand, wider windows in the time domain have higher side lobes in the frequency domain. Since rectangular window function is the widest in the time domain, it has the highest side lobe in the frequency domain and normally is not recommended to use before an FFT. While choosing an appropriate window for a specified application, there is a trade-off between width of the main lobe and height of the side lobes. If more frequency resolution is desired in the application, it is needed to sacrifice more

in the spectral leakage. More specifically, applying a 4-term Blackman-Harris window before FFT reduces the side lobes significantly. On the other hand, the width of main lobe increased from about 1 bin to about 2 bins. Frequency domain responses of the windows in Figure 36 are depicted on Figure 37.

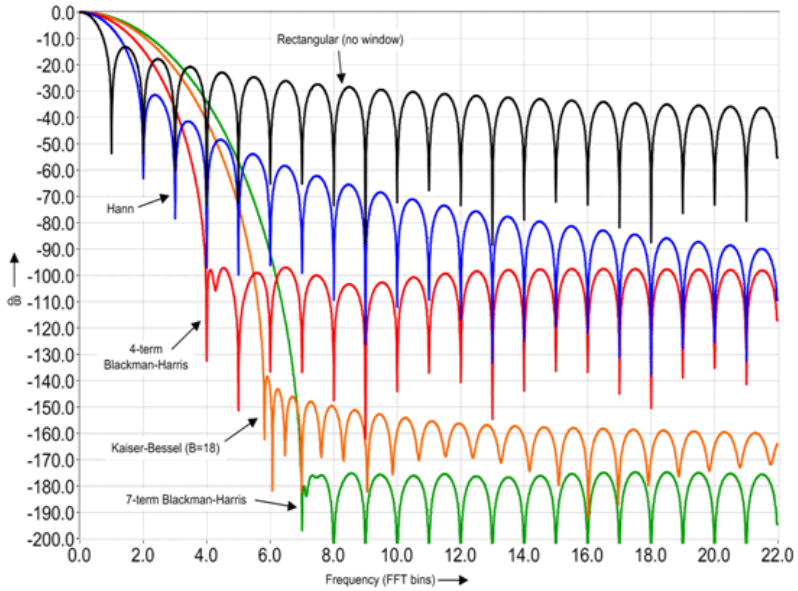

Figure 37: Frequency Domain Plots of some Windows[21]

Since the resolution in the frequency domain represents the range resolution of the FMCW radar, it is not desired to compromise. Therefore, restricted improvement in the spectral leakage is preferred and only the widest most common two types of non-rectangular windows, Hanning and 4-term Blackman-Harris are implemented in this thesis. It is possible to switch between windows by using button 13 in the GUI. By clicking it, three choices are presented interchangeably: No window, which represents rectangular window, Hanning and 4-term Blackman Harris windows. It is possible to see the effects of windows in the GUI both in time and frequency domains.

The leakage from one range bin to the adjacent is measured by testing system with known length cables. Since a known length cable behaves lake a single point target, power level on the neighbor range bin is caused by the side lobe effect. Data cursors on Figure 38 depict the power level on the adjacent range bins. There are 12 dBm differences between the main lobe and side lobe when Hanning window is used.

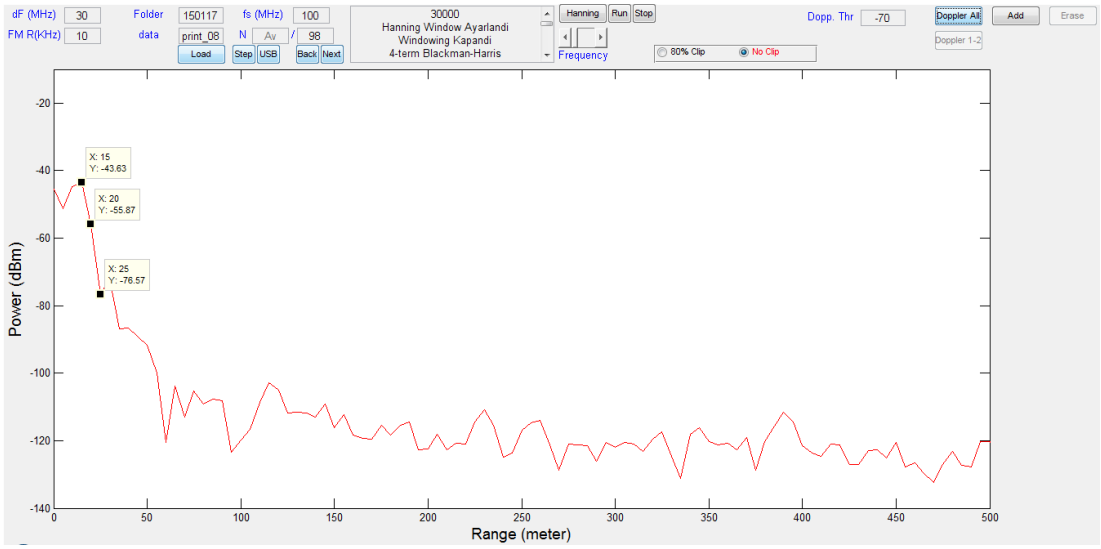

Figure 38: Side Lobe Leakage with Hanning Window

When the used window is changed to Blackman-Harris difference between adjacent bins decreases to 6 dBm

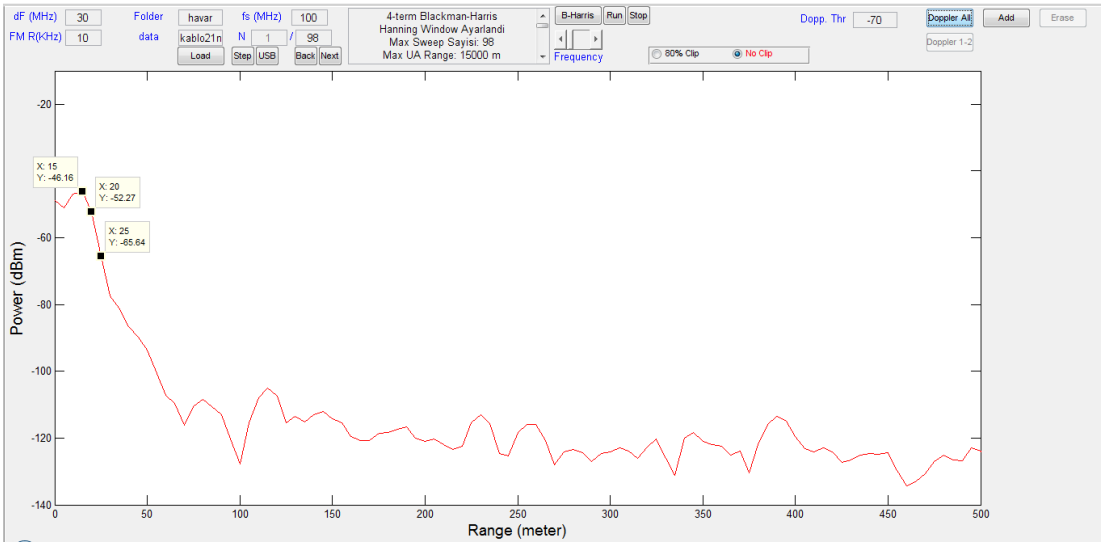

Figure 39: Side Lobe Leakage with Blackman Harris Window

4.1.4 Frequency Transform

In this study, fast time signal processing starts with capturing and recording the beat signal into oscilloscope memory and continues with finding the starting point of the first sweep. After triggering the starting point, all the cascaded beat signal cycles are segmented from each other and stored into a matrix. The Fast Fourier Transform (FFT) is used to convert time domain data into frequency domain.

Let us introduce the sampled and segmented beat signal generated by a single target during a single sweep interval as the following

$$x[m] = A\cos\left(2\pi f_b \frac{m}{f_s} + \phi\right) + w[m], \quad (40)$$

where m ranges from 1 to 10000 samples per sweep interval since sampling frequency of oscilloscope is set as 100 MHz and duration of a sweep (ΔT) is set to 100 usec.

The segmented time domain data is stored in a 100 by 10000 matrix where data corresponds to 100 frequency sweeps is recorded. Then the segmented data in the matrix become

$$x[n,m] = A\cos(2\pi f_b \frac{m}{f_s} + \phi) + w[n,m] \quad n \epsilon [1,N],\ m \epsilon [1,M], \quad (41)$$

where N=100 and M=10000 as described in Chapter 3.2 (System Design Parameters). This means N*M=1 million samples which is the maximum for the device is captured by oscilloscope.

The frequency components in each sweep represent the range of the targets. Therefore Fourier Transforms of the entire segmented beat signals are computed for each by calling FFT in the Matlab and stored into another N by M matrix. One hundred sweeps are recorded for slow time signal processing and both to improve SNR by eliminating the uncorrelated noise components by coherent data integration and to enable Doppler processing.

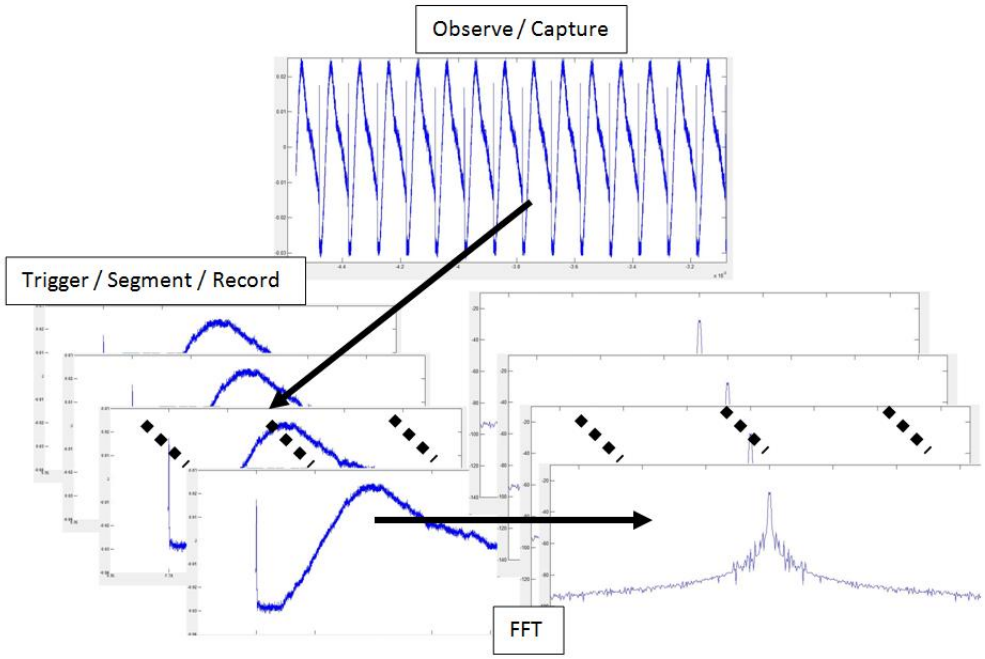

Figure 40: Fast Time Signal Processing Steps

When Button 8 in the implemented GUI is clicked to compute FFT of the segmented waveforms, the frequency domain signals are exhibited on the screen and operator can interchange between the sweeps results by clicking the button group 11 (next/previous). In the frequency domain the components with higher power can easily be distinguished. Every single frequency component represents different targets with different ranges. The operator clicks to "Add button" (13) to compute the corresponding range for a target. By clicking this button, a cursor on the graph appears and waits for the operator to click on a frequency bin which is suspected to be a target. Then the frequency of the clicked point is grabbed and used to find the range of the corresponding target.

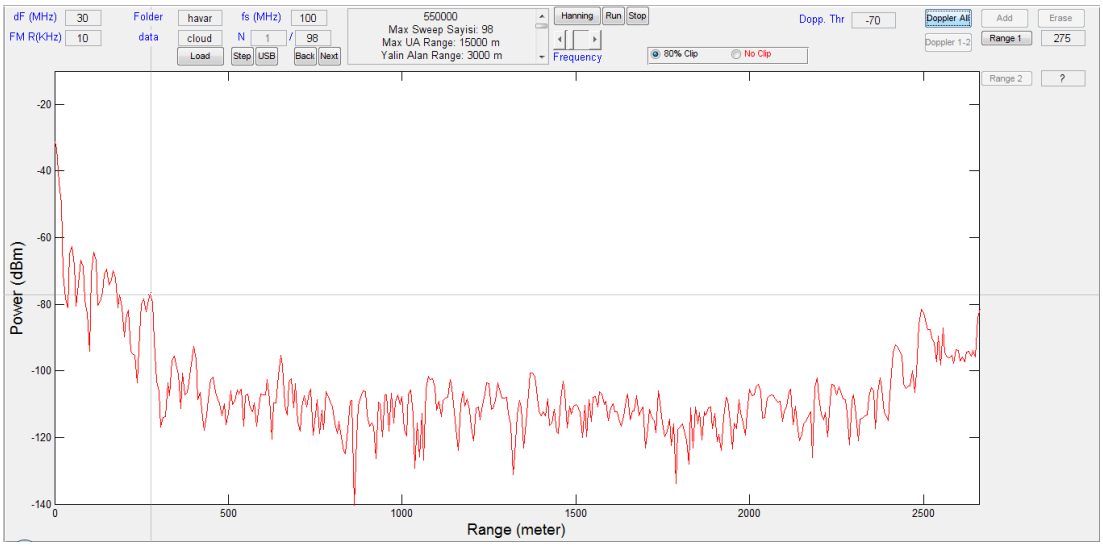

Figure 41: Target Detection by Operator

4.1.5 Coherent Data Integration

Integration of beat signals obtained from different sweeps is a fundamental operation in radar signal processing to improve signal to noise ratio. As described in [1], there are two types of data integration; *coherent integration*, *non-coherent integration*. With coherent integration, integrating process is inserted before amplitude detection where it is performed by human operator in the case of this study. The signal processor program samples, segments and stores the beat signals generated by each of the transmitted sweeps and adds N of them. After it accumulates N beat signals, radar operator performs the amplitude detection and threshold check [22]. The fundamental property of coherent integration is adding complex signals with magnitude and phase. On the contrary, non-coherent data integration refers to integration based only on the magnitude of data. Since the squared or log magnitude of the complex signal is obtained for detection before data integration, the phase information of the signal is lost. The non-coherent integrator also adds N beat signal from different sweeps but with only in magnitude.

The model of a beat signal which is generated by a single point target during a single sweep and corrupted by additive white Gaussian noise w is defined as

$$s = A\cos(2\pi f_b t + \phi) + w\,. \tag{42}$$

The noise component is modeled as a white Gaussian random process with power σ^2. The power of beat signal is equal to $A^2/2$ and the single sweep SNR is defined as

$$SNR = \frac{signal\,power}{noise\,power} = \frac{A^2/2}{\sigma^2} = \frac{A^2}{2\,\sigma^2} \tag{43}$$

When N sequential beat signals generated by the same single point target are added up by a coherent integrator, the result becomes

$$z = \sum_{n=1}^{N} A\,cos(2\pi f_b t + \phi) + w[n] \tag{44}$$

The RCS of targets for Swerling Case 0, Case 1, and Case 3 does not change from sweep to sweep. Hence the level of beat signal at the input of the coherent integrator does not change for different sweeps in a scan and the same deterministic signal is sampled for each sweep. Besides, noise components at the output of the coherent integrator have the same statistical properties with the noise at the single sweep case. Additionally, the noise samples are independent for each time and they have zero mean.

$$z = N\,A\,cos(2\pi f_b t + \phi) + \sum_{n=1}^{N} w[n] \tag{45}$$

Then the power at the output of data integrator becomes $N^2A^2/2$ and power of uncorrelated noise components is calculated as the sum of individual noise samples. Then the corresponding SNR is defined as

$$SNR = \frac{N^2A^2/2}{N\,\sigma^2} = N\frac{A^2}{2\,\sigma^2} \tag{46}$$

The integrated SNR value is improved by a factor of N by integrating N sweeps perfectly by a coherent integration process[23]. This increase is called the integration gain and costs extra time and energy for the system to collect data and make computation.

In the non-coherent integration case, the integration gain is smaller and it is less efficient. Integration gain for non-coherent integration is equal to N^{α} where α is between 0.7 and 0.8 for small N and reduces down to 0.5 for large N [1]. This is expected since non-coherent data integration is done after losing the phase information of the signal.

Therefore, in the experimental part of this study, coherent data integration is implemented to the segmented beat signals. To normalize the integrated signal to the received one, the result of the summation is divided into the number of components in the integration. After Fourier transform, coherent integration is applied to the complex signal in the frequency domain. Since the order of sequential integration and Fourier transform is not going to change the result, integrating time domain signal and then applying FFT to the result of integration is the same with integrating the FFT applied signals. However in the computing program, the latter choice, integrating the segmented and FFT applied signals are preferred to be able to see both the integrated beat signal and a single beat signal generated by an arbitrary sweep preferably by clicking on the *"next"* and *"back"* buttons (buttons 11 in the GUI). The coherency of the beat signal for different sweeps is provided by protecting phase information during the starting point triggering and segmentation process. Phase of the beat signals are aligned by segmenting them from the correct position.

Additionally, special care must be taken to integrate signals by superposing the same range bins. Range information in FMCW is in frequency domain and the same range bin means the same corresponding frequency bin. Since the lengths of the beat signals for different sweeps are equal and they are sampled with the same sampling frequency by oscilloscope, the same amount of samples per each sweep interval is captured. This means the length of the data for the DFT, and the bandwidth of the stored signal was equal for different sweeps. By having these equalities the frequency bins become identical for different beat signals. To accommodate this, the signal generator and the data capturing oscilloscope must be synchronized.

The result of the FFT applied signal is a complex signal where the real part represents the cosine terms and imaginary part represents sine terms in the input signal. On the GUI only the magnitude of the result is shown. The Button Group 11

is used to interchange between the captured beat signals and their transformations in the frequency domain. To see the result of the integrated data, back button should be hit when the current data is seen as “1” in Text Box 6. Then it turns out to “Av” and the integrated and proportioned data is seen on the graph. The following figure shows the result of the integrated and a single sweep signal.

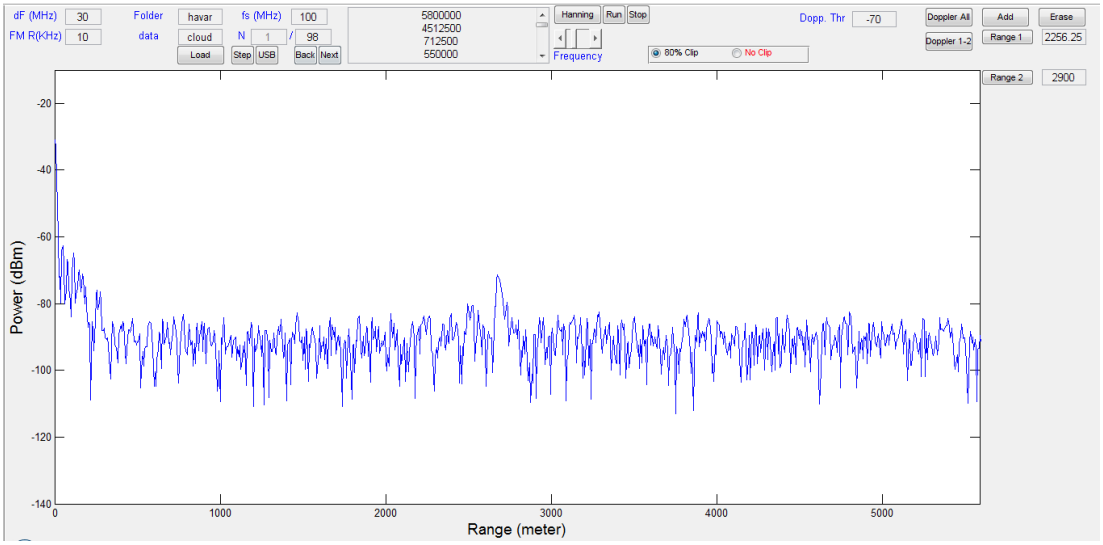

Figure 42: Beat Signal from Single Sweep

Figure 42 shows a beat signal belongs to cloud. A single sweep interval is used to obtain this data and this result belongs to first sweep as it is seen on textbox 6. The average noise level apart from the target range is about -90 to -95 dBm. The targets can be easily detected by the operator since they are about 20 dB higher than the noise level. However, it is not clear for him to understand it represents a cloud.

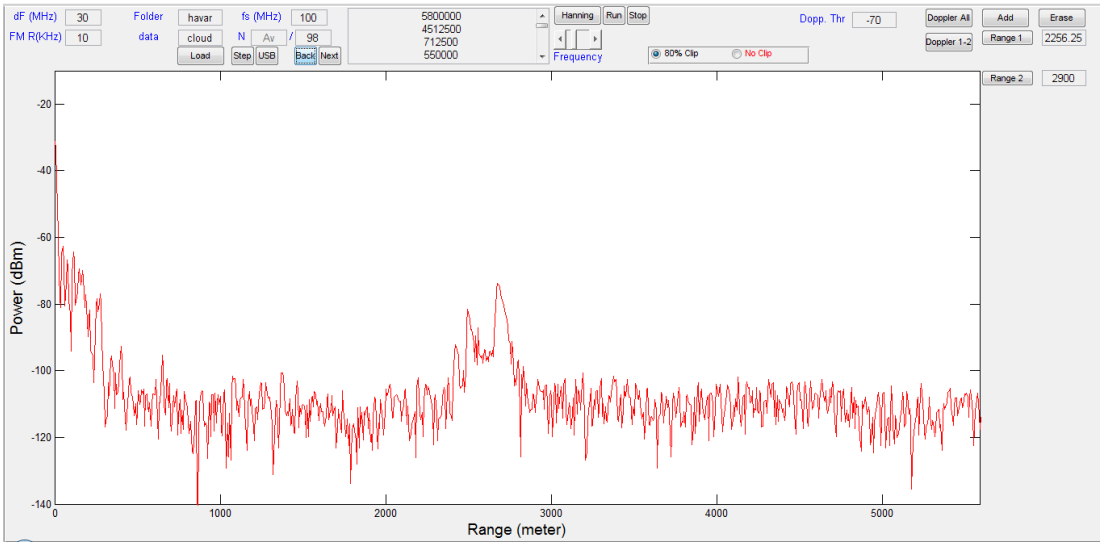

Figure 43: Integrated Beat Signals

On the other hand, integrated data gives more information about the target. In the first place the noise level decreases about the level of -105 to -110 dBm and the peak power of the target stays the same about -70 dBm. This means an increase of 20 dB on the SNR. Integration gain on the SNR is mentioned as N in (46). Where in this experiment 98 cascaded beat signals are integrated and the expected gain on the SNR at dB scale is 10*log (98) = 19.9. The expected integration gain on SNR perfectly matches the experimental results.

Let’s do the same experiment for less partition to the integration and show the consistency of the system. In the following figure 10 beat signals are integrated and the noise level decreased by 10 dB to about -100 dB which is exactly the expected value by 10*log (10) =10 dB.

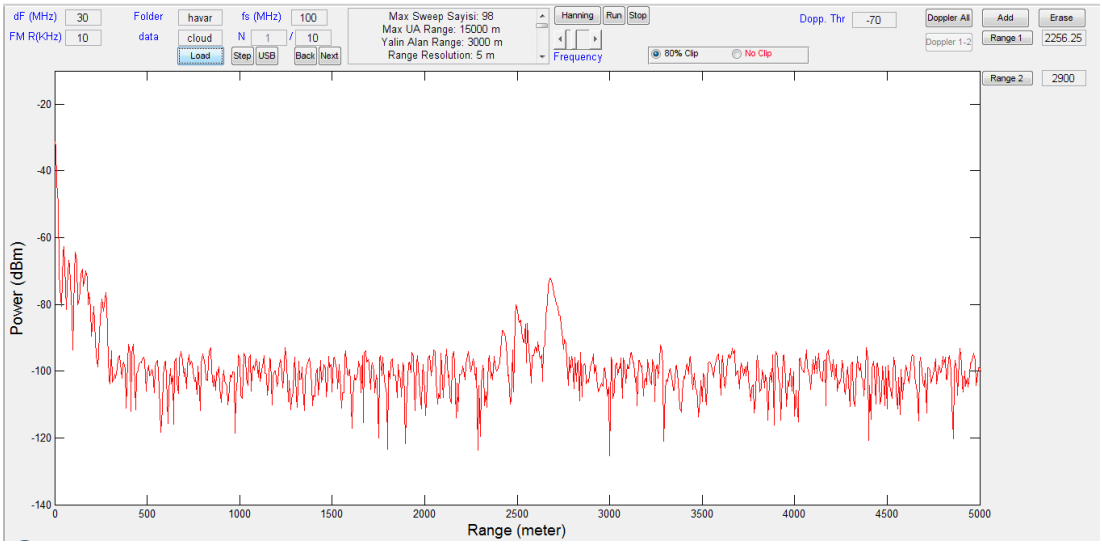

Figure 44: Integrated Beat Signal (less partition)

For moving targets, the phase of the beat signal is changing from sweep to sweep because of the corresponding Doppler frequency. Therefore, summing up samples of a cosine signal with different phase may weaken it. Except the very fortunate cases, the integrated signal power for moving targets will be less than A^2N^2. In Figure 45 the red graph shows the magnitude for 98 integrated beat signals for the case of zero Doppler and the blue one shows the magnitude of 2^{nd} beat signal. Integrated data result overlaps with the single sweep result except the places where noise is dominant and there is a moving object. For example, the targets in the red circles in Figure 45 differ in magnitude for the integrated and single data cases. Since these frequency components are stronger than the noise level, differences in magnitudes represents moving object. They are also examined by Doppler analysis with mesh graphs plotted in both range and velocity axes.

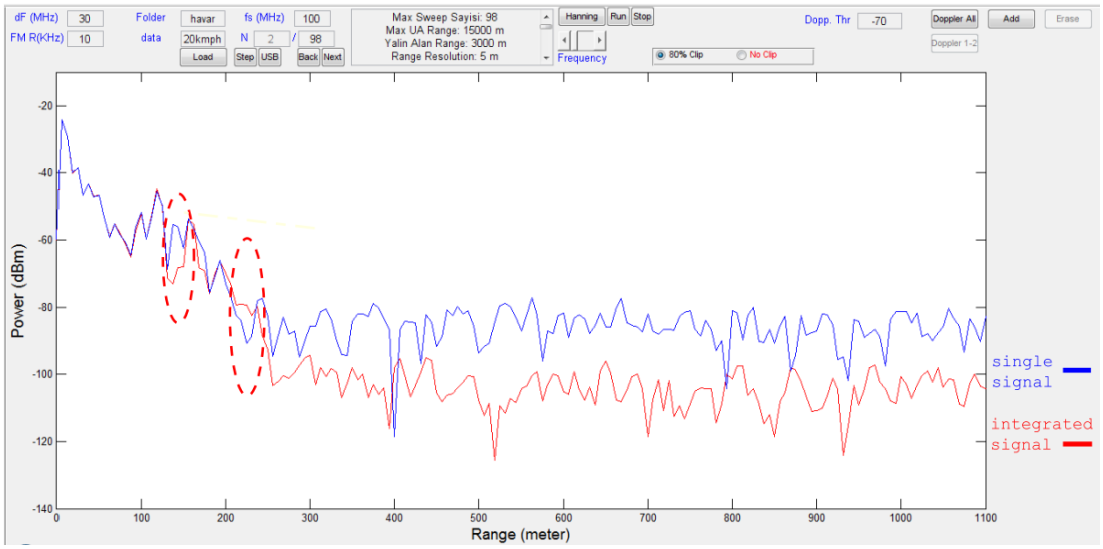

Figure 45: Integrated Beat Signal for Moving Targets

The real part of the frequency domain data for that specific range bin during 98 different sweep intervals is presented on Figure 46. As it is seen, inphase part of the signal is oscillating with slow time data index. That means the phase of the signal is changing from sweep to sweep. Similar situation is valid for the quadrature component. Summing up the magnitude of these samples and dividing the result to N, decreases the magnitude of the integrated data.

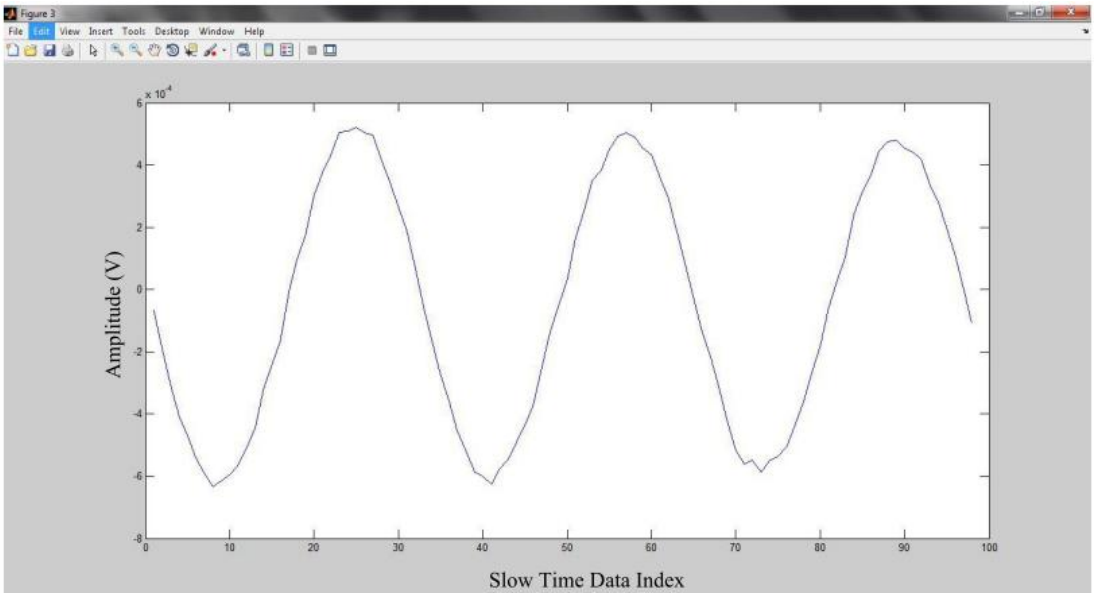

Figure 46: Real Part of Slow Time Data for a Moivng Target

Another description of this situation is mentioned on Figure 47. The sum of complex quantities with changing and constant phases for 5 samples is plotted on the

coordinate system. As it is obvious the magnitude with changing phase is smaller. Addition of 5 vectors with a constant phase and magnitude makes 75 units. On the other hand, the magnitude of the result for changing phase case is less (72.6 units). The same happens with the moving targets.

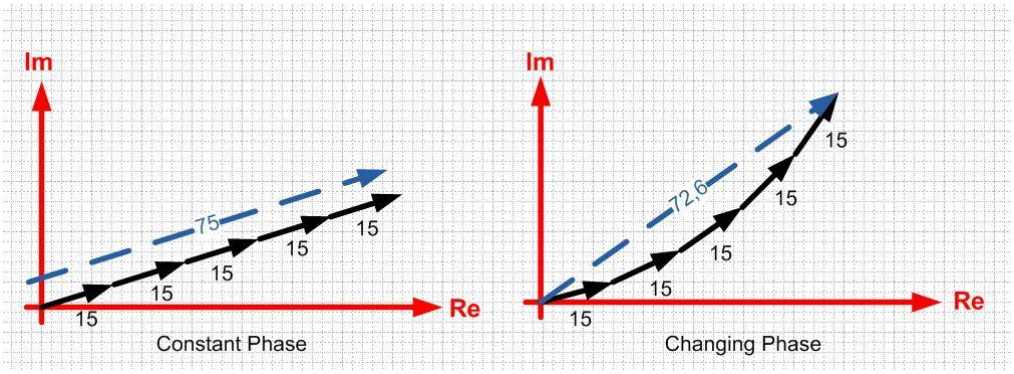

Figure 47: Summing Signals with Constant and Changing Phase

Although this situation may be seen as a drawback for moving targets and need to be compensated, it is an advantage for the operator to distinguish moving targets from plot of both integrated and single beat signal data without doing any slow time signal processing operations. Any frequency component where the averaged data does not overlap with an arbitrary single sweep data indicates moving targets.

On the other hand, it is possible to increase integration gain to N for also moving targets. To be able to do this, Doppler frequencies of moving targets need to be known. After calculating Doppler frequency by slow time signal processing operations, phase progression of the signal component can be compensated before data integration process[1]. Adding or subtracting the corresponding phase from the real signal makes it a stable target. By this way, the magnitude of the cascaded data is rectified and the integration gain increased.

4.2 Doppler Processing

Slow time signal processing for FMCW radar consists of analyzing and getting speed data from the same range bin of the cascaded beat signals. This step is performed to have Doppler capabilities. The phase of the beat signal for moving targets is changing from sweep to sweep. To be able to detect and measure this difference, cascaded beat signals are analyzed.

The fast time data was converted into frequency domain by Discrete Fourier Transform since the range information is in there. The result of the conversion was a complex signal with inphase and quadrature components. Slow time operation is finding the frequency changes in the frequency domain data. Hence another Fourier Transform is needed. For a specific target in a determined range bin, all of the cascaded fast time signals are combined and slow time signal set for that range is generated. (This set can be seen on Figure 46) This operation is performed by clicking on Button 16 and picking up a range bin from the graph in the GUI. The computing program takes all of the cascaded data for the specified range bin into memory, shows them on another plot, and applies FFT to this signal set. After DFT operation is applied to this slow time signal set, the result is displayed on the screen as in Figure 48. Frequency components in the spectrum represent Doppler frequencies of moving targets. By clicking on top of the frequency bin the corresponding speed of the moving target is printed on the text box.

A very important point here is the complexity of the fast time signal. Since the result of the first FFT algorithm is a complex number with representing the inphase and quadrature components, input of the second Fourier transform is a complex number. This situation has two main advantages. The first advantage is having information about the sign of the frequency. Fourier transform of real signal generates only positive frequencies and the negative portion of the result is always the same with the negative part. In other words frequency domain index goes from 0 to N/2 and the rest is just a replication. On the other hand, the complex Fourier Transform includes both positive and negative frequencies by running the index from 0 to N-1. Positive frequencies are represented by the frequency indexes from 0 to N/2 and negative ones represented by N/2 to N-1[24]. This property is crucial for assigning direction of movement. Since Doppler frequencies of approaching and diverging targets have opposite signs, distinguishing them is possible with complex Fourier transform.

The second advantage is related with the SNR of the data. Since both inphase and quadrature components are used to evaluate Fourier transform, complex Fourier transform has 3 dB gain.

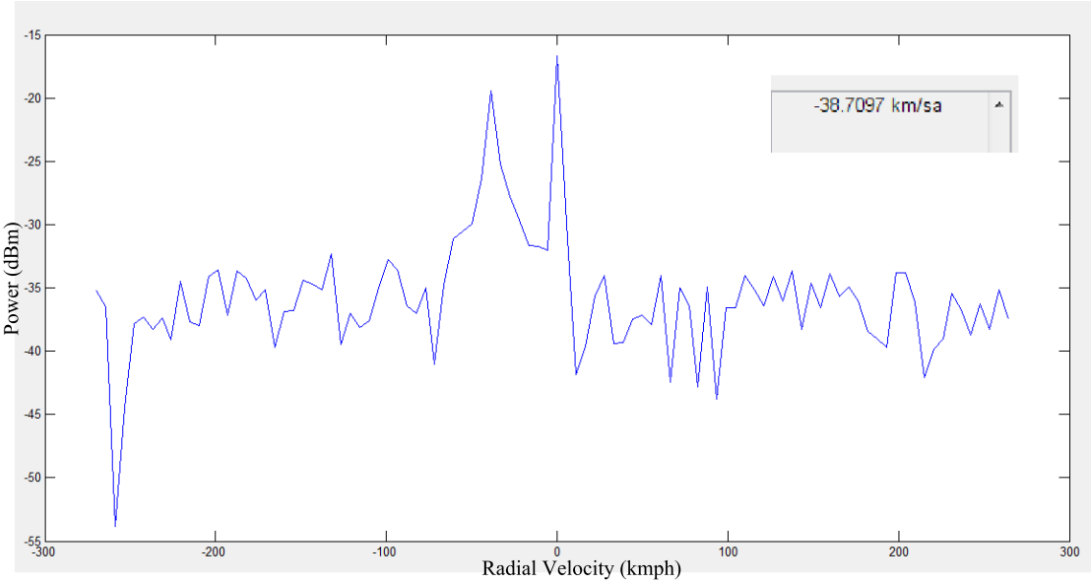

Figure 48: Result of FFT Operation in Slow time

CHAPTER 5

EXPERIMENTAL RESULTS

Experimental studies of this study started in the laboratory and then continued in the tower at Ayaslı Research Center. Before establishing the whole radar system, all the components and cables are tested in the lab. After establishing it, the accuracy of the system is tested first with cables of known length. This step required knowing the speed of electromagnetic propagation in the cables and it is measured with specific components which will be mentioned in the next sections. After succeeding in the cable length measurement tests, next step was verifying the system, especially the antenna parts by measuring the distance of huge buildings from the tower. Since the reflectivity of the buildings was great enough to detect, they were good opportunities for aligning and testing the antennas.

To confirm the Doppler ability of the radar, speed of a car which was driven by a constant and known speed is measured. After verifying the range and velocity measurement capabilities of the radar system, the main study is performed on the range and velocity detection of water particles on the air.

5.1 Component Tests

The first step of the study was gathering information about the materials that will be used. Since it was not possible to reach datasheet of some components, real measurements are performed in the laboratory to be on the safe side.

5.1.1 Loss Calculation of the Power Divider

The loss of the divider which was used to divide the transmitted signal is measured by applying a known power signal from the signal generator without any connecting cable, and the power at the output is measured with a spectrum analyzer. A cable

with a loss of 2.5 dB is used between the output and the analyzer. The results are seen on Table 4.

Table 4: Loss Calculation of Divider

Input Power (dBm)	**Single Channel Output Power (dBm)**	**Total Loss (dB)**	**Divider Loss (dB) (Total Loss – 2.5 dB)**
10	4.35	5.65	3.15
20	13.81	6.19	3.69
-10	-15.7	5.70	3.20
-20	-25.64	5.64	3.14
-50	-55.8	5.80	3.30
-70	-75.67	5.67	3.17
Average divider Loss			3.27

5.1.2 Testing Mixer for the Operating Frequency

The used mixer has a conversion loss of 8 dB for X band. Typical performance characteristics of it taken from its data sheet can be seen on Figure 49.

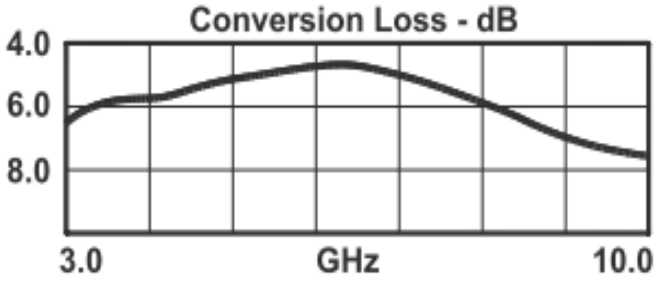

Figure 49: Mixer Conversion Loss

5.1.3 Cable Loss Calculation Tests

Since majority of the used cables in the setup does not have any part number or datasheet, loss of them are calculated by doing measurements. One edge of the SMA cables is connected to signal generator and a continuous and constant power single tone signal at X band is generated. The power of the cable at the other edge is measured by spectrum analyzer and the losses on the cables are calculated.

Table 5: Cable Loss Calculation

No	Amount	Type	Color	Length (m)	Measured Loss (dB)	Loss/Meter (dB/m)
1	1	SFT 205	Turquoise	10	10.0	1.00
2	1	Unknown	Turquoise	2	2.5	1.25
3	1	Unknown	Blue	5	10.0	2.00
4	1	Unknown	Metallic	0.5	1.5	3.00
5	2	Unknown	Blue	2	3.0	1.50
6	3	Unknown	Blue	1	1.6	1.60

5.1.4 Antenna Tests

Before observing reflection from targets, antenna to antenna transmission is performed at 10 GHz. To make sure about the antennas, the radiation from one antenna is tried to be caught by the other. Since dish reflector and feed horns are used together for the first time in this study, such an experiment is needed. The reflected and received powers are noted and these values are seen on Table 6.

Figure 50: Antenna to Antenna Transmission

Table 6: Antenna Power Test Results

Antenna to Antenna Distance	Radiated power From Signal Generator	Maximum Measured Power at Spectrum Analyzer	Transmission Loss
5 Meter	0 dBm	-25.0 dBm	25.0 dBm
5 Meter	10 dBm	-8.5 dBm	18.5 dBm

5 Meter	15 dBm	-7.5 dBm	22.5 dBm
5 Meter	20 dBm	-3.5 dBm	23.0 dBm
5 Meter	25 dBm	1.5 dBm	23.5 dBm

While doing this experiment, antennas were not stable and aligned by hand. We explain the variability of the transmission loss by this instability.

5.2 Velocity Factor Calculation

The first trial of the system was performed by using cables instead of reflecting signals from targets. Since the propagation speed of electromagnetic wave in a cable is different from the speed on the air, the velocity factor of the cables should be known to be sure about the reliability of the system.

The velocity of a signal in a cable is known to be V_{cable} and equals to $c\ (\mu_r\ \varepsilon_r)^{-1/2}$ where c is the speed of light in m/s, μ_r is the relative permeability and ε_r is the relative permittivity [25]. The materials of coaxial cables used in the experiments are non-magnetic with $\mu_r = 1$ and then velocity of propagation becomes almost completely dependent on the properties of the dielectric. If the dielectric constant of the cable (ε_r) is known, the approximate velocity factor is calculated as:

$$velocity\ factor = \frac{1}{\sqrt{\varepsilon_r}}\ . \tag{47}$$

The types of cables used in the experiments were not the same. One of the cables was SFT-205 type and relative permittivity (dielectric constant) of this type is given as 1.73. This makes the velocity factor 0.76 and the speed of propagation 2.28 x 10^8 m/s. On the other hand we do not have any information about the types of the other cables. Hence we had to measure them.

To measure the velocity factor of the cables, Time Domain Reflectometry (TDR) circuit is used. In this technique a square wave with short rising time is generated and divided into two channels. One of the channels enters directly to oscilloscope while the other channel is for the cable under test. A cable with a certain length is connected to the second channel as being open ended. The square wave goes into both channels and while it reaches quickly to oscilloscope through the first channel, it travels through the edge of the open ended cable and reflects back to the first

channel. This structure causes a ladder shape on the oscilloscope. The duration of the first step in this ladder gives the travel time of the wave through the cable. And by using the travel time and length information of the cable, calculating the propagation velocity and velocity factor is possible. The length of the folded cable is seen as 2.46 meters in Figure 51 and it makes the length of the cable 4.92 meters.

Figure 51: Length of the Folded Cable

TDR circuit generates a square wave with 15 ns and the ladder structure is seen on Figure 52.

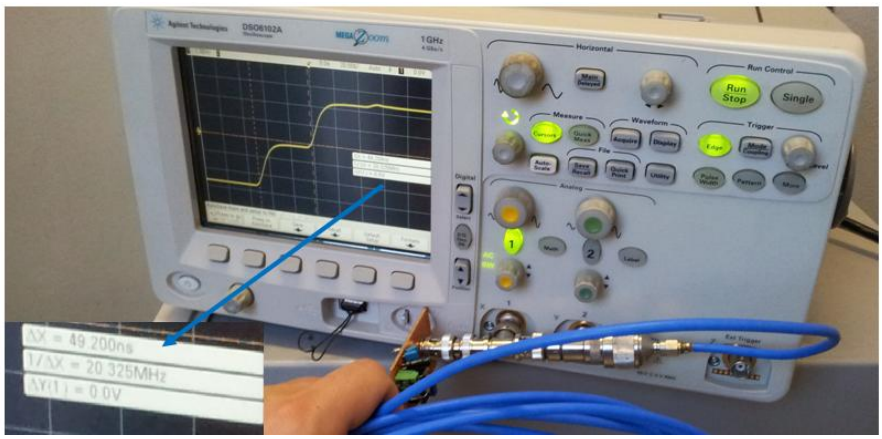

Figure 52: Speed of Propagation Calculations

The length of the first ladder for a 4.92 meters cable is 49.20 ns. This means the wave travels two times 4.92 meters in 49.2 ns. Then the speed of electromagnetic propagation in this cable is:

$$\mathrm{V_{cable}} = \frac{2x4.92}{49.2\ x\ 10^{-9}} = 2\ x\ 10^{8}$$

$$velocity\ factor = \frac{\mathrm{V_{cable}}}{c} = 0.67 \qquad (48)$$

To measure the accuracy of the TDR test, the velocity factor of the SFT-205 cable is also calculated. The experimental and theoretical results found to be compatible. Travel time for 10 meters long SFT-205 cable is measured as 92.4 ns. The

calculation gives the velocity factor for SFT-205 cable as 0.72 which is close to theoretical value, 0.76. The average of datasheet value and measured value, 0.74 can be used as velocity factor for this type of cable. The velocity factors for both of the cables are seen on the following table.

Table 7: Velocity Factors for the Used Cables

Cable Type	Picture	Velocity Factor
SFT-205		0.74
Not Known		0.66

5.3 Delay Generation with Cable

After measuring the characteristics of the used materials, the next step was testing the system without radiating through an antenna. Figure 53 shows the block diagram of the established setup. A cable between the transmitter and receiver ends generates a delay for the transmitted signal. This is a cheap and easy way of modeling the wave hitting a target in the range and scattering back to the receiver.

By this experiment, the complete system except the antenna block is tested. Since there is no radiation through the antennas, the power of the transmitted signal needed to be decreased to avoid any damages to the receiver. A power of – 30 dBm is generated by the signal generator and all the procedure described in 3.1 System Block Diagram is performed.

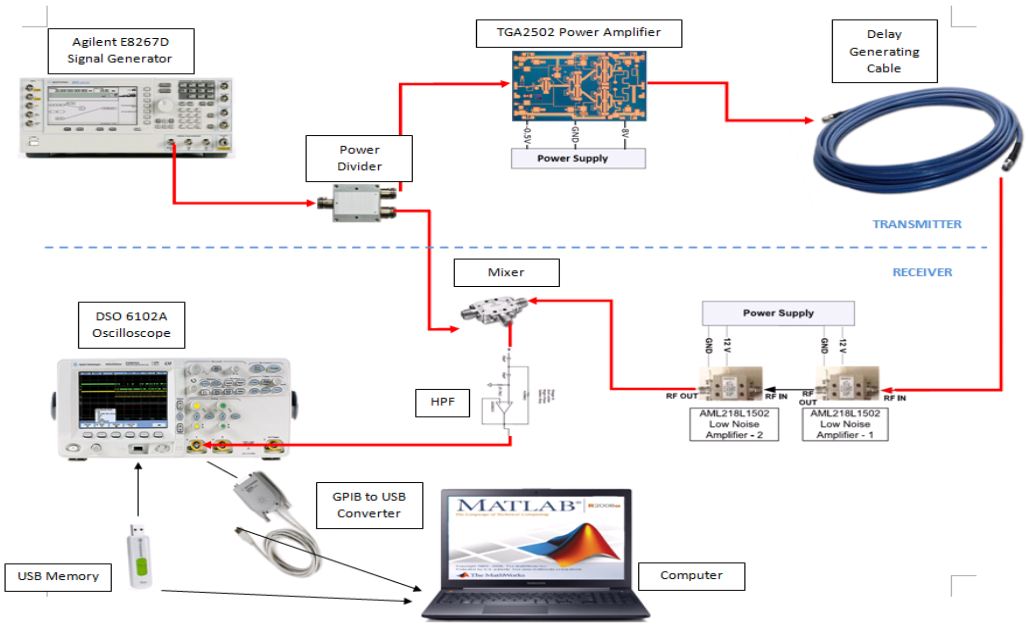

Figure 53: Block Diagram of System Test

There are two important points to mention here. One of them is, since the prorogation speed of electromagnetic wave in a cable is different than in the case of atmosphere, an arbitrary length of a cable models different length of ranges for actual targets. Secondly, the length of the cable represents both the arriving and returning path of the electromagnetic wave. Therefore the computing program is going to measure half of the atmospheric length model of the cable.

The speed of wave in the cable for the mixed type is measured as

$$V_{cable} = 0.7\ c \tag{49}$$

which makes the corresponding length in the atmosphere 1.429 times longer.

$$L_{atm} = \frac{10}{7} L_{cable} = 1.429\, L_{cable}\ . \tag{50}$$

This experiment is performed with 2 cables of different lengths. In the first step a cable set of 21–meter in total is used and, for the sake of consistency, the same experiment is repeated with 13–meter cable in total. The corresponding atmospheric length and range of targets for two cable sets are seen on Table 8.

Table 8: Delay Generating Cable Models

Length of Cable(L_{cable})	Corresponding Length (L_{atm})	Corresponding Range
21 meters	30 meters	15 meters
13 meters	19 meters	9.5 meters

5.3.1 Long Cable Set

In this experiment a 21–meter cable is used between transmitting and receiving units. This set of cables represents an existence of the target located at 15 meters away from the radar. The beat signal in time domain is seen on Figure 54.

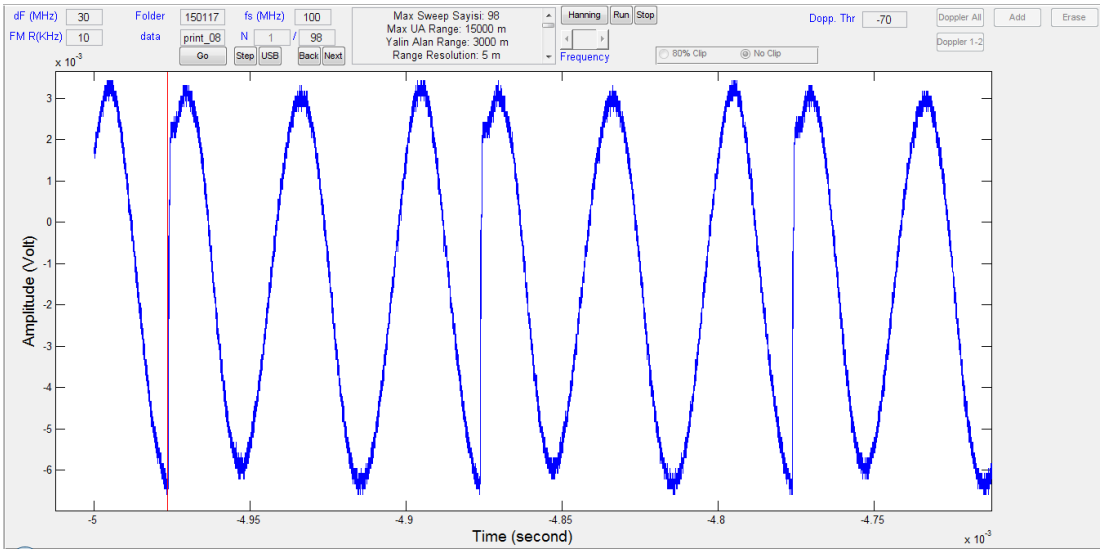

Figure 54: Beat Signal in Time Domain for 21 Meter Cable

Since we are performing short range calculations, the range resolution of the radar should be higher. Therefore clipping option is disabled during this operation. The result of the frequency domain data windowed with Hanning window is shown on Figure 55.

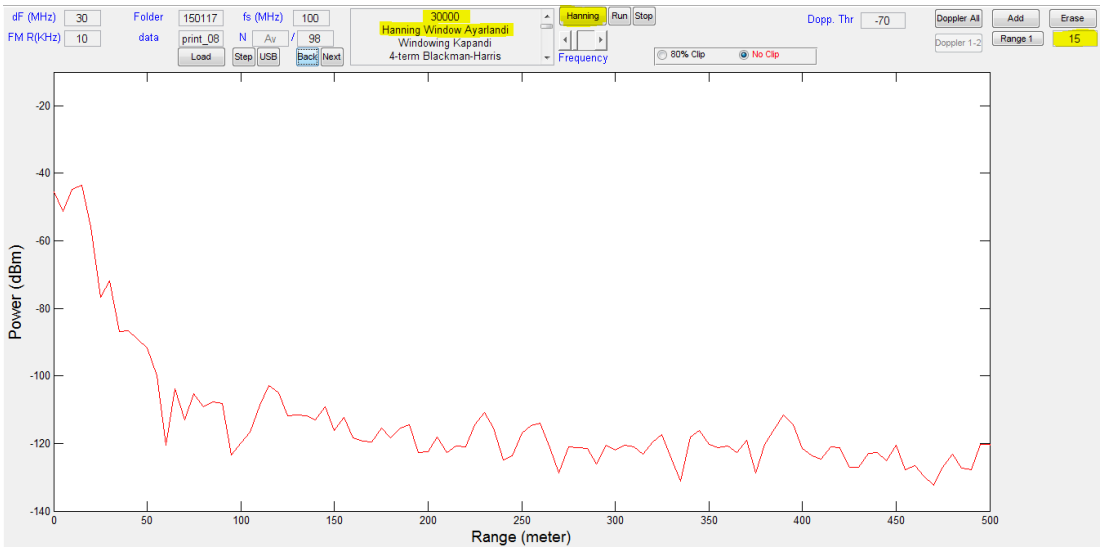

Figure 55: 21 Meter Cable Length Detection

The frequency of the beat signal is calculated as 30 kHz and this frequency corresponds to 15 meters. The range of the target is calculated as 15 meters which was exactly the expected value.

5.3.2 Short Cable Set

This set of cables makes a total of 13 meters and represents an existence of the target located at 9.5 meters away from the radar. The beat signal in time domain is seen on Figure 56.

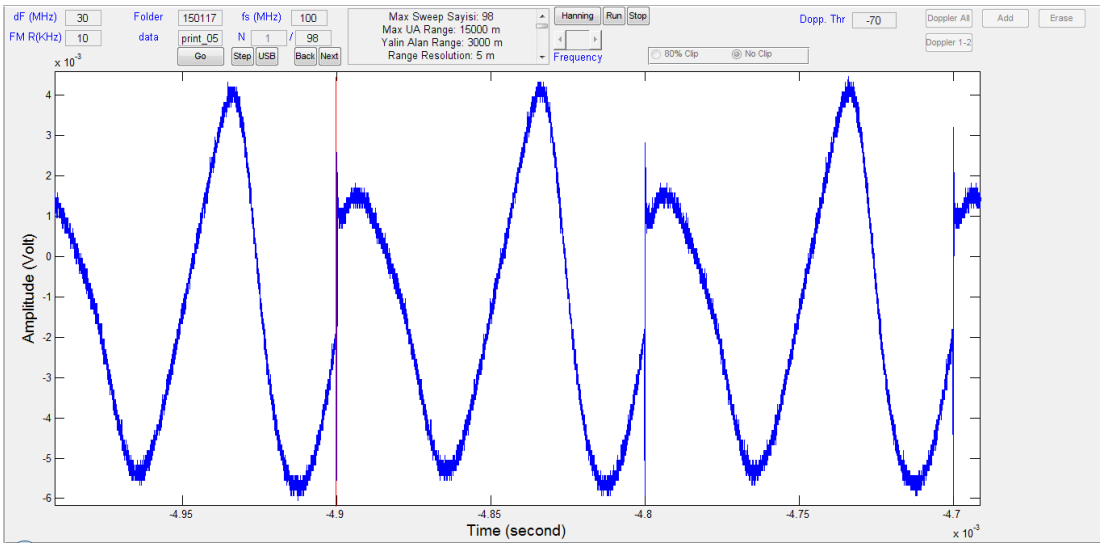

Figure 56: Beat Signal in Time Domain for 13 Meter Cable

Since the range resolution of the radar without clipping is 5 meters, it is not possible for the radar to detect the range exactly. The expected value with 5 meters of resolution is 10 meters for the 9.5 meters of range. The result of frequency domain data windowed with Hanning window is seen on Figure 57. The corresponding beat frequency is calculated as 20 kHz which corresponds to a range of 10 meters.

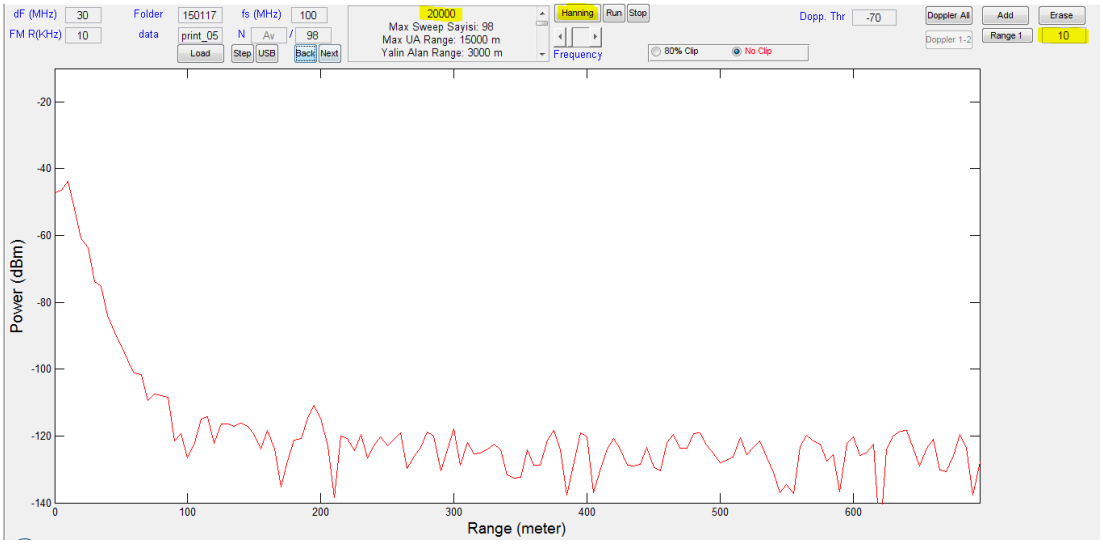

Figure 57: 13 Meter Cable Length Detection

By these two experiments, the reliability of the system in calculations and measurements including signal processing steps and use of the materials is verified. After this point, any encountered problems are should be caused by power and antenna issues.

Another important point need to be mentioned here is related with the second component of the beat signal. Although the clipping option is off, a single frequency component for a single target is observed in the frequency domain. The reason for this situation is related to windowing. Windowing also compressed the first part of the signal which is very short in duration and contains the second frequency component of the beat signal.

5.4 Detection of Buildings

The FMCW radar setup whose block diagram is shown in Figure 7 were moved from lab to the tower on Ayaslı Research Centre and the direction of horn antennas was set to see the brown twin tower blocks of TOBB in Ankara. Since these buildings are huge enough to reflect the transmitted signal with high power, the system was tested in the direction of these buildings in the first trials. The buildings in the field of view can be seen from the photo taken together with both horn and dish antennas in Figure 58.

Figure 58: Picture of Building Detection Setup

For both of the cases the detection of buildings and calculation of the range are performed. It was confirmed that system operates correctly by comparing the measured ranges with the value that Google Maps offers. The detected buildings are divided into two different categories as close and far region buildings for ease of analysis.

5.4.1 Close Region Buildings

The result of the signal processing operation is depicted on Figure 59. The operator clicks on the peaks of the frequency components and measures the corresponding distances.

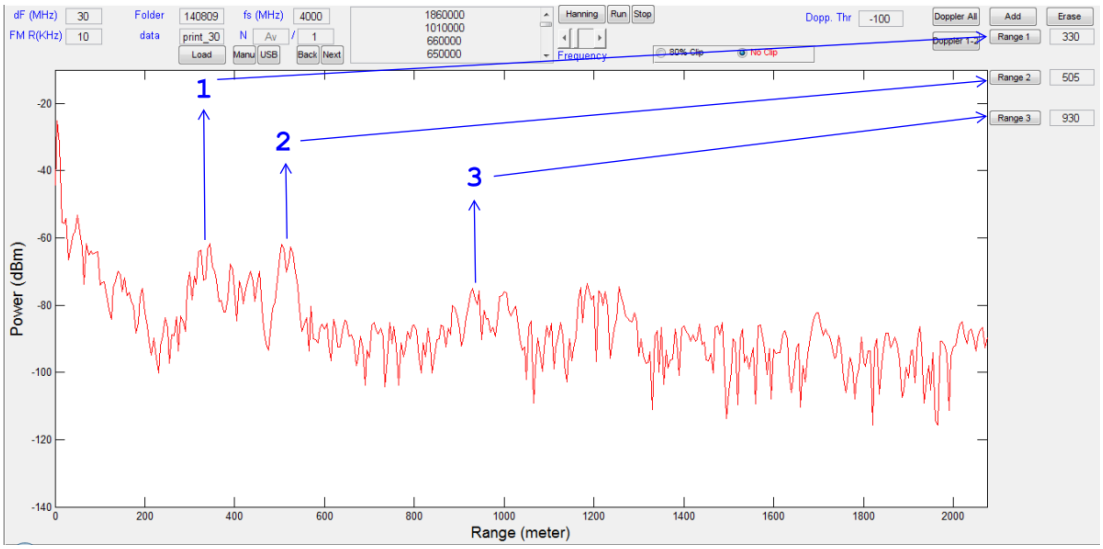

Figure 59: Close Region Detection

For the first step, 3 targets are detected and their ranges are estimated as 331.25, 506.25 and 931.25 meters. Since clipping option is on, the range resolution of the radar is 6.25 meters.

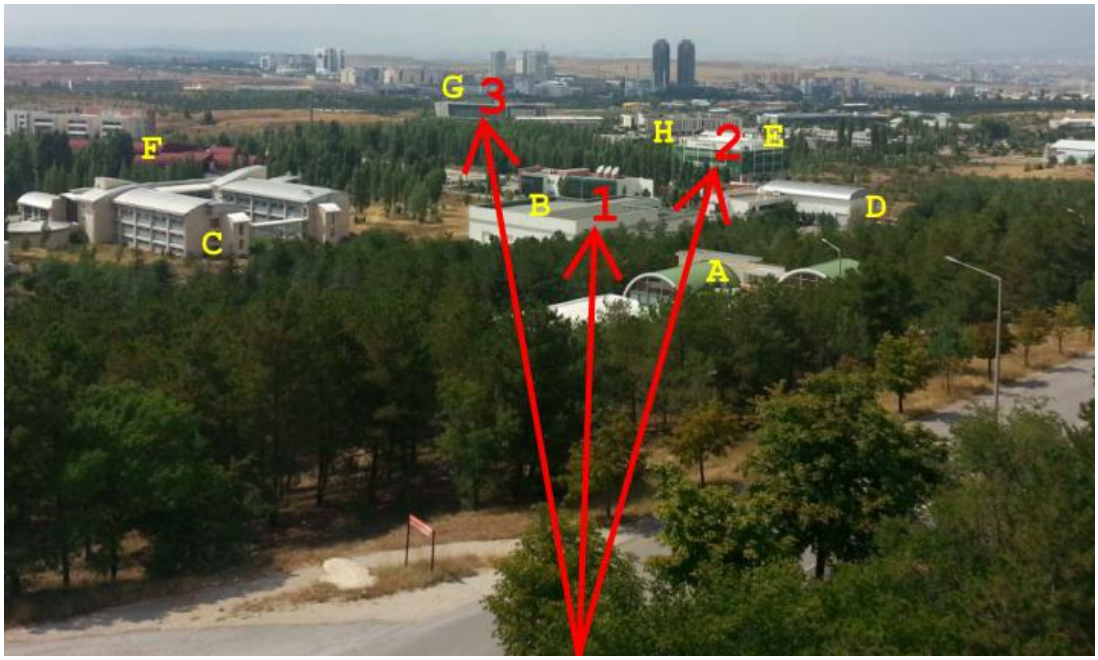

Figure 60: Picture of Close Region Buildings

The close region buildings which are candidates for being detected by the radar are seen on Figure 60 and they are named as A, B, C, D, E, F, G and H. Since only three of them stay inside the field of view of antennas, only they are detected by the radar. They are marked with red arrows and numbered as 1, 2 and 3.

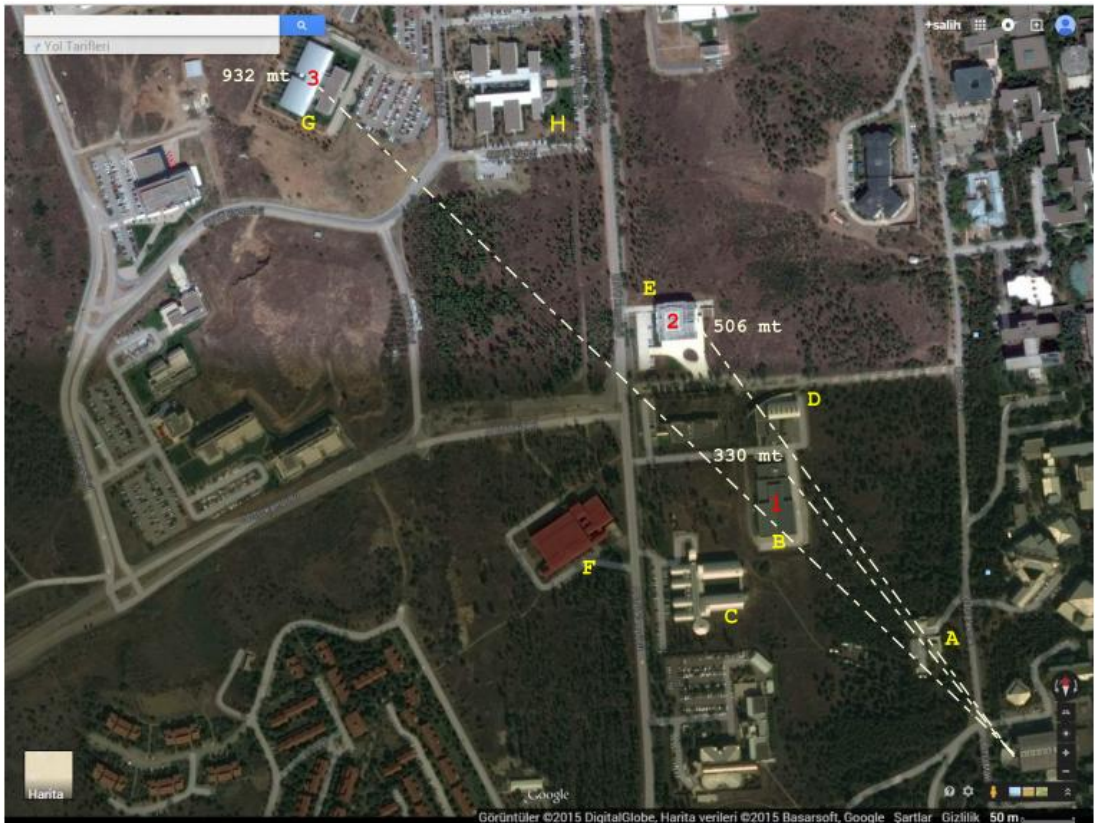

Figure 61: Google Map View of Close Region Buildings

After detecting the ranges of 330,506 and 932 meters, possible buildings are searched from Google Maps in the direction of antennas. First, the buildings named from A to H is found and marked on the map. Then their ranges are measured by the ruler in Google Maps. The results of this inspection are marked on Figure 61. The range of the buildings B, E and G are determined as 330, 506 and 932 meters correspondingly. These are the detected buildings in the close region of the radar.

Since building group H stays in the shadow of building E, it cannot be detected. Additionally, buildings C and F do not stay in the boresight of antennas. Therefore they are also could not be detected.

5.4.2 Far Region Buildings

The second region which can be analyzed in a single picture is the far region whose results of detection are provided in Figure 62. There exist four targets which are chosen by the operator. The ranges of these targets are estimated as 1212.5, 2300, 2650 and 2981.25 meters.

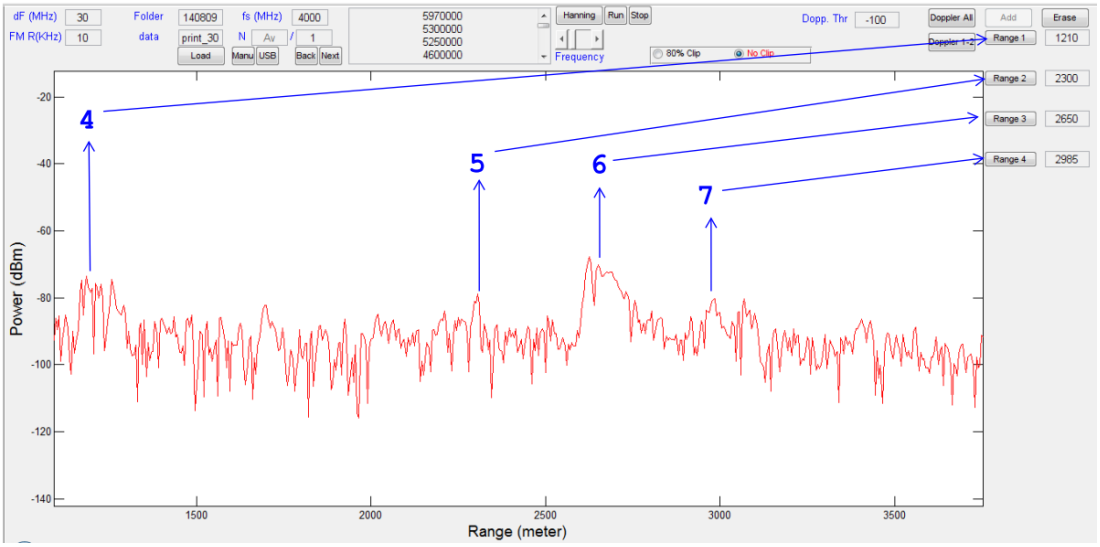

Figure 62: Far Region Detection

The candidate buildings for those ranges are denoted by I, J, K, L, and M and can be observed in Figure 63.

Figure 63: Picture of Far Region Buildings

Buildings I to M are found and marked on the map in Figure 64. The ranges are computed based on Google Maps and the ranges for I, J, K, L and M are determined

as 1200, 1200, 2320, 2640 and 2980 meters correspondingly. These lengths match the estimated values.

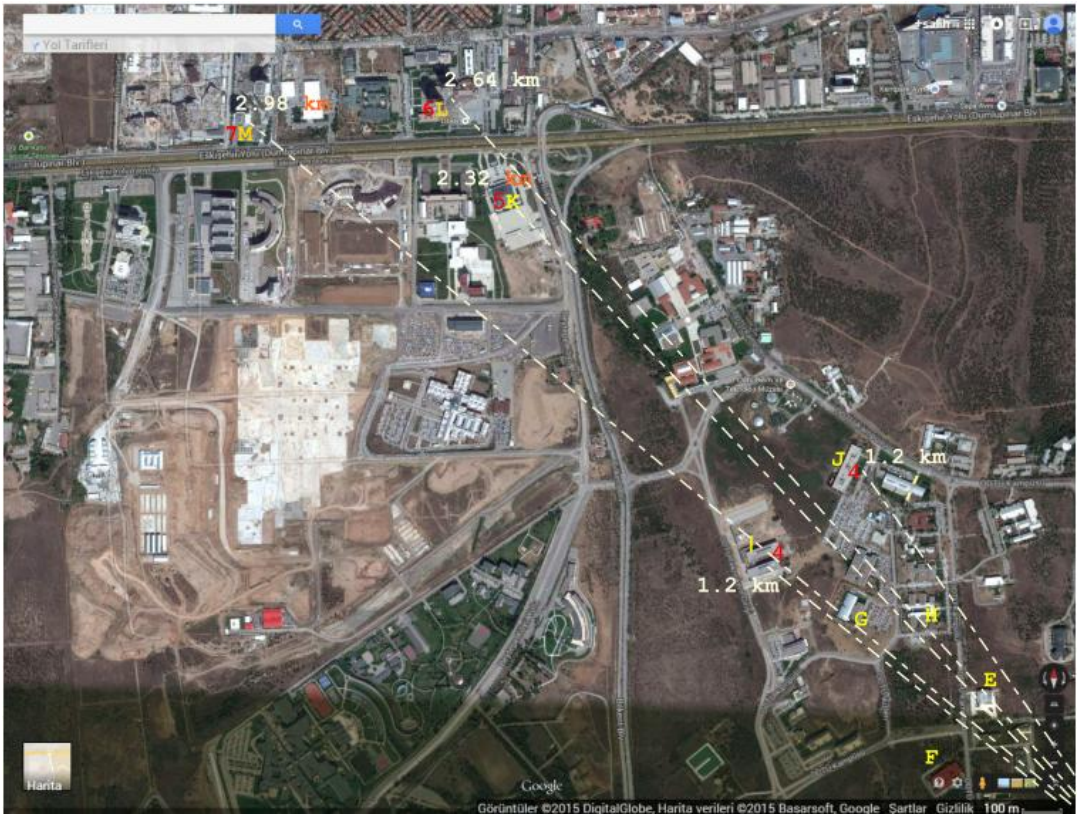

Figure 64: Google Map View of Far Region Buildings

The 4th target may be building I or J or both, and the 5th target is K, 6th is L and 7th is M. The height and width of the buildings L (TOBB) is much higher than the others and the power of the beat signal is higher than the neighbors noticeably.

5.5 Speed Detection

The Doppler property of FMCW radar is tested by measuring the speed of the car cruising in the campus. To compare the measured values with the actual speed of the car, the test car is driven with several constant speeds. Since the test car does not have cruise control, the car was set in a constant speed manually while passing through the testing region.

The speed calculation of the radar system has small differences with the values of the speedometer of the car shows. There are two reasons for this little difference. First of them is the disadvantage of the manual speed regulation. The driver of the car tried

to drive at a constant speed level by just controlling with his eyes. This type of fixing is not very reliable. Besides, the speedometer of the car was not exact. It differs significantly from the speed calculation of several smart devices such as smart phones and car navigation systems which measure the speed from the change of the distance taken by more reliable GPRS devices.

During the experiment, the test car was driven at 4 different velocities, and the speed calculation results are compared with these values. Figure 65 shows the setup established on the road in the campus.

Figure 65: Established Setup to Measure Speed of Cars

While the test car was driven away from the radar system with 20 kmph, its speed was calculated as -22.11 kmph and depicted on Figure 66. The negative sign indicates that car is moving away from radar.

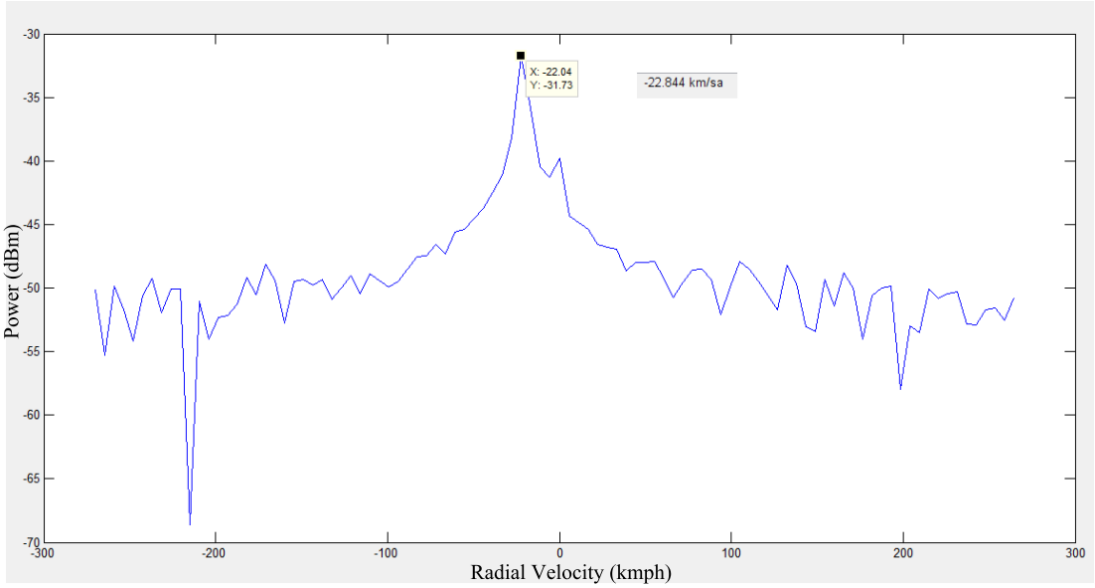

Figure 66: Speed Calculation for 20 kmph

While doing the first speed calculation experiment, the test car moved away from the radar system. According to the test procedure the test car was driven with a speed of 30 kmph in direction towards the radar. The result of 30 kmph speed test is depicted on Figure 67. This time, the direction sign is positive and this indicates the travel of test car towards the radar.

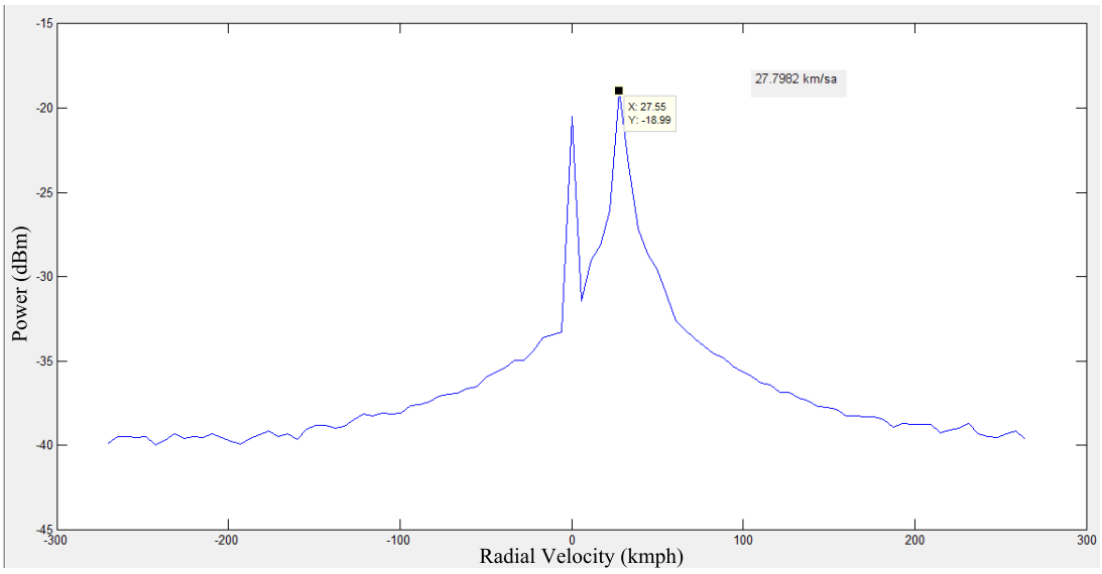

Figure 67: Speed Calculation for 30 kmph

Last time test car came to the radar system and now it is time to move away from radar by increasing the speed of the car. Figure 68 shows speed of the car which is moving away from radar with -38 kmph

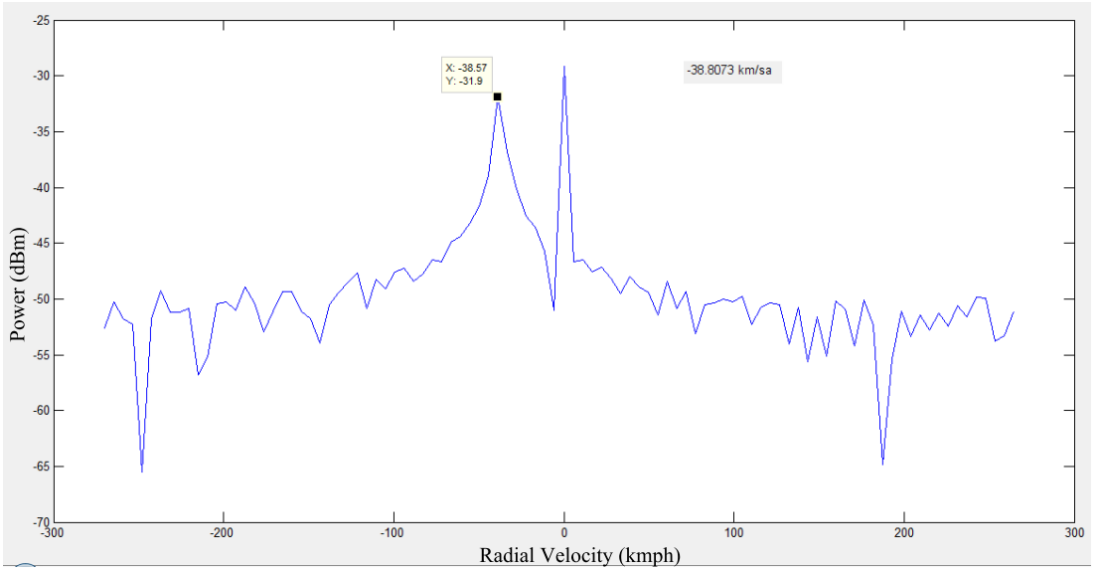

Figure 68: Speed Calculation for 40 kmph

Last step of car speed calculation experiment is performed with 50 kmph and the order of direction is to the radar. Measurement result is seen on Figure 69 with the value of 49.21 kmph.

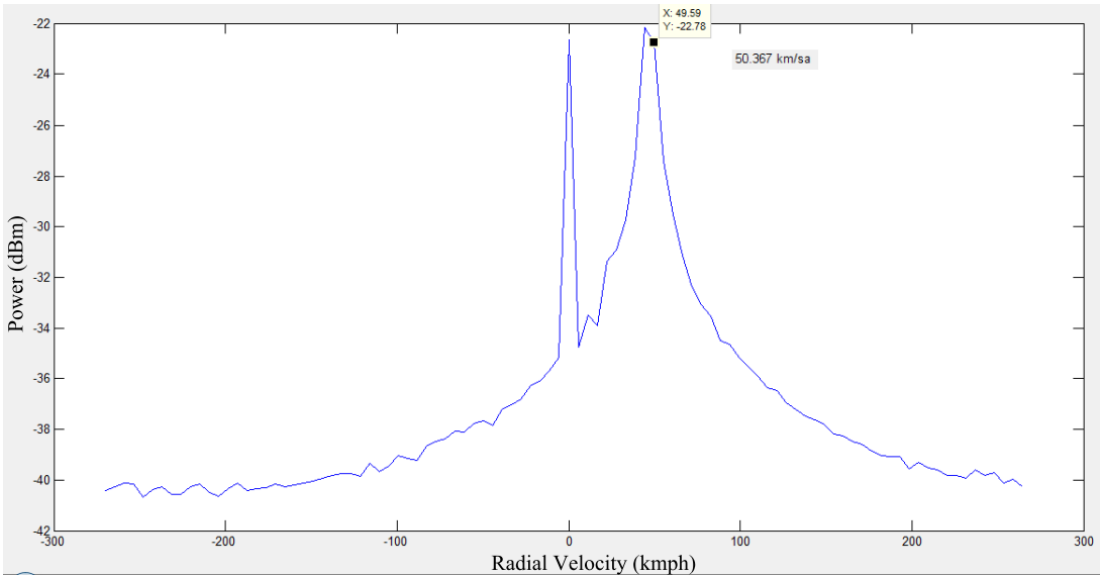

Figure 69: Speed Calculation for 50 kmph

While performing these experiments on the campus pedestrians were also detected by the radar system. Figure 70 shows a picture of people walking with radial velocity on the campus.

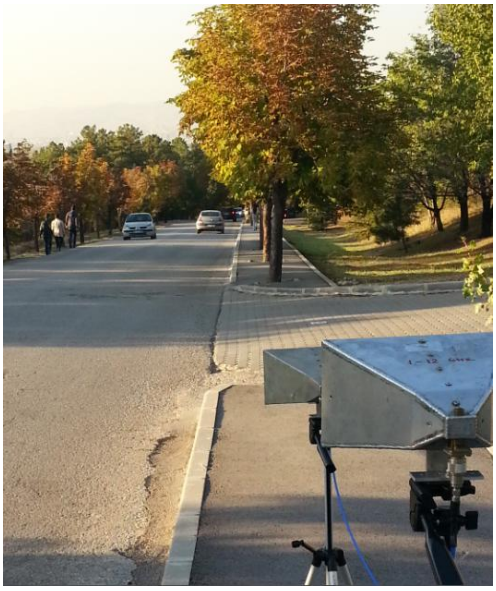

Figure 70: Pedestrians on the Campus

Doppler calculations showing the speed of pedestrians on the campus with a velocity of 5.5 kmph is presented on Figure 71.

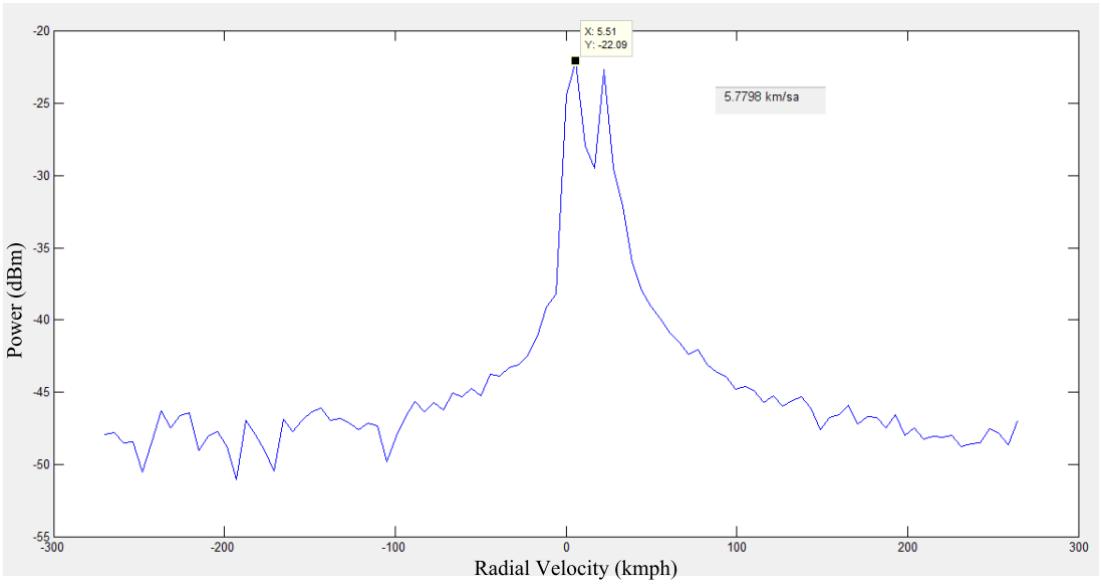

Figure 71: Pedestrian Detection

5.6 Cloud Detection

Last step of this study is cloud and rain detection. Several measurements are done and pictures of them are taken. The first measurement on a cloud was taken on 14 September 2014. Figure 72 shows the picture of the cloud and antennas.

Figure 72: Cloud and Antennas-1

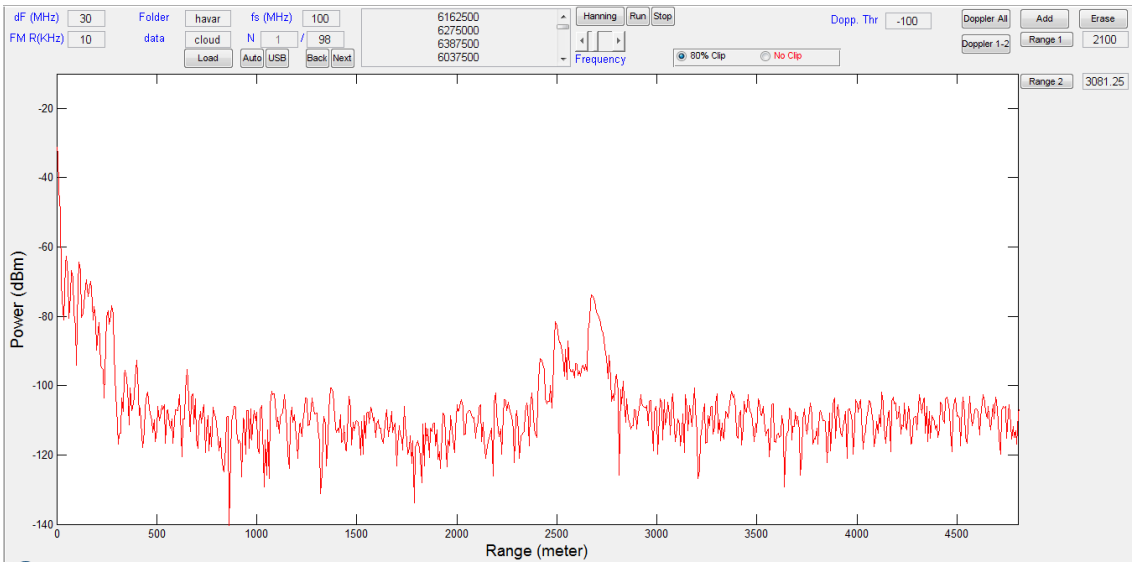

Figure 73: Cloud Detection-1

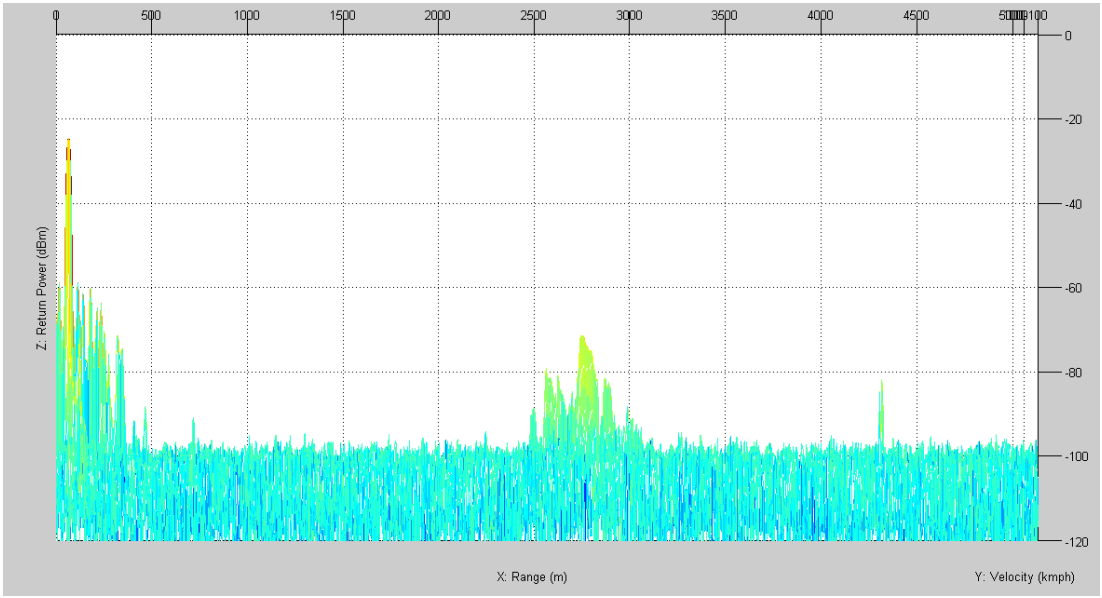

Figure 74: Mesh Plot of Cloud-1

Processing the echo of the transmitted wave from the cloud gave the result on Figure 73. Apart from single point targets, there is a region where the return power is high for a specified range of distance. This was an expected echo from a cloud since cloud has a depth and electromagnetic wave also scatters from the particles inside the cloud. Since the particles on the cloud are moving, Doppler analysis is needed. In Figure 74 mesh plot of the cloud is depicted which shows range of the particles with radial speed. Speed of the particles can be seen by rotating the axis of the 3D plot

When analyzing the range of the target, it is seen that it has a range between 2 km to 3 km. This cloud is a type of stratocumulus and they have altitudes less than 2 km. Since the cloud has also horizontal distance to the radar this amount of range is reasonable.

Another examining point of a cloud is its radial velocity. Movement of the cloud causes Doppler frequency in slow time processing. Since a cloud composes of many single particles, it is not appropriate to examine a single point in slow time. Instead, examining the Doppler Effect for a region is appropriate. To be able to do this operation, Doppler 1-2 button is added to processing program. By clicking this button after choosing two different range bins, Doppler spectrum of the range cell inside these two points is plotted. For this case, range bins between 2118 and 3025 meter is examined and result of the FFT is plotted on Figure 75. The speed measurements of clouds were not exact since the small particles can move independently from each other. However when comparing with a stationary object return, it is seen that their bandwidth is wider. This means there are particles with radial velocities from -5 kmph to 22 kmph as seen in the following figure.

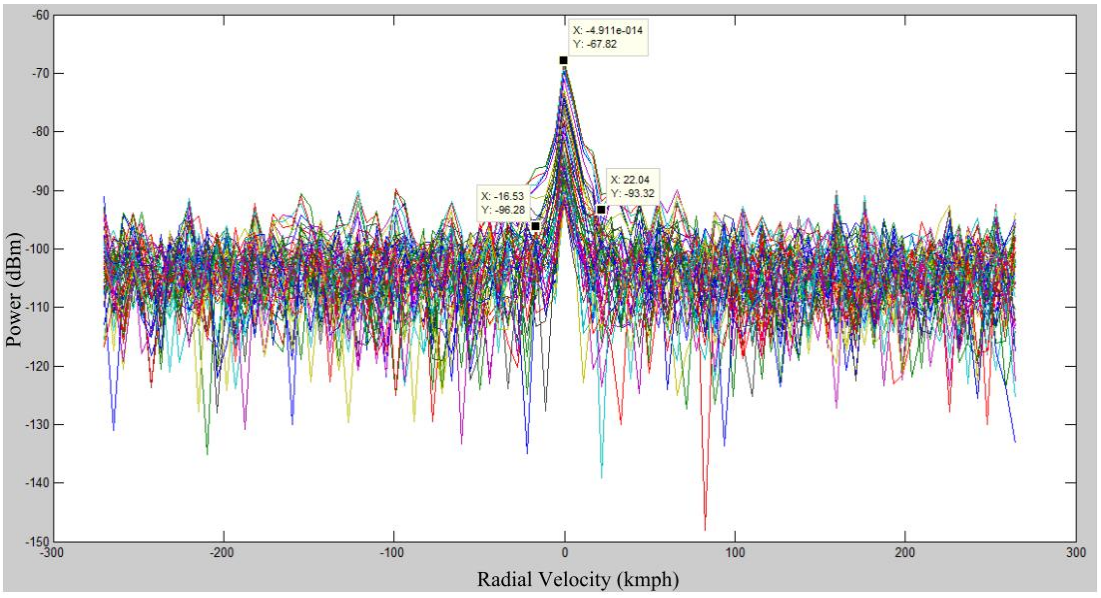

Figure 75: Slow Time Analysis of Cloud-1

The same experiment is repeated on a different day. The picture of the measured cloud is shown on Figure 76.

Figure 76: Cloud and Antennas-2

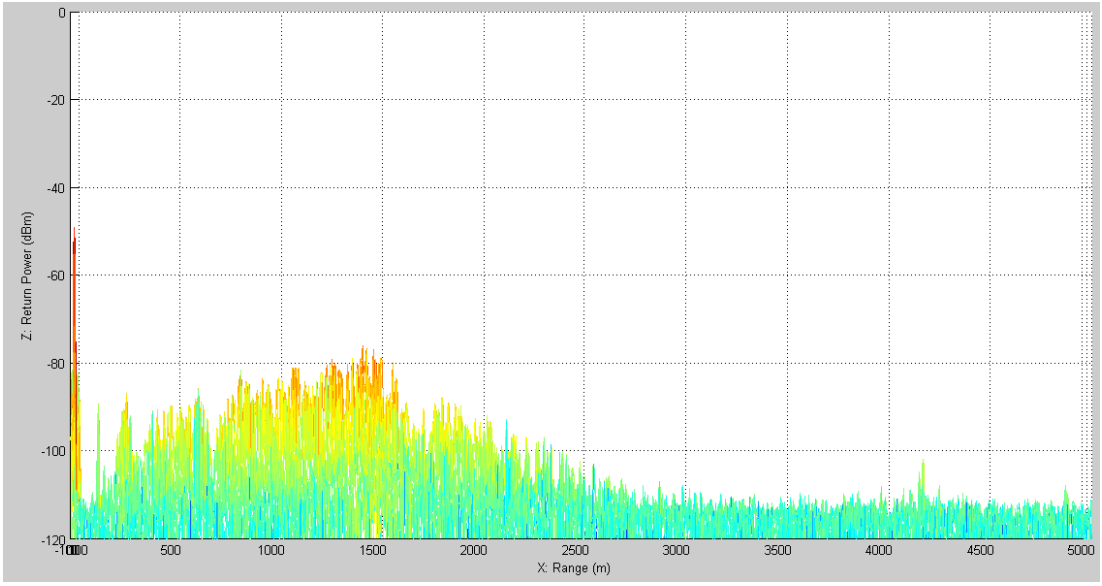

Figure 77: Cloud Detection-2

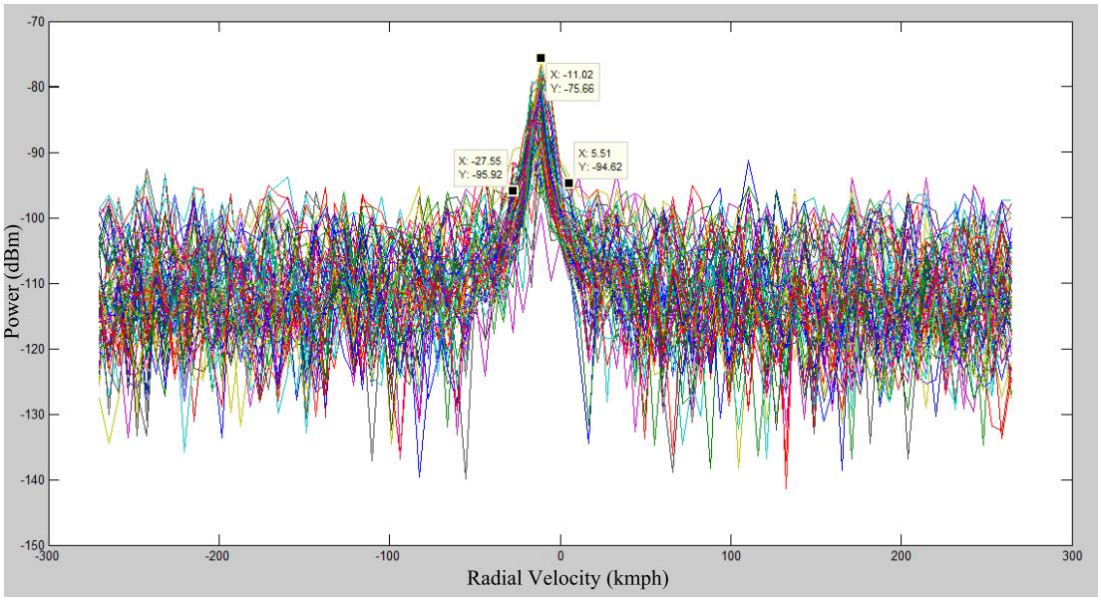

Figure 78: Slow Time Analysis of Cloud-2

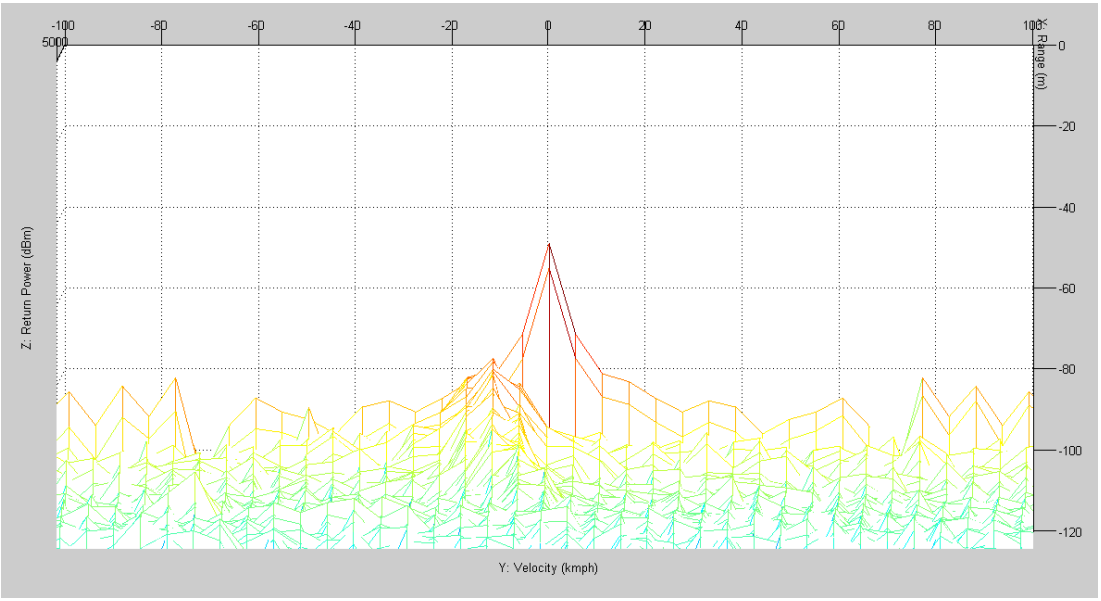

Figure 79: Mesh Plot of Cloud-2

This time, the velocity of particles is changing from 0 to -22 kmph. To understand the difference between a moving cloud and a motionless target Figure 80 should also be analyzed. The bandwidth of stationary target is narrower than the cloud's. Since the velocity resolution is adjusted as 5.4 kmph by (28) the next bins on the left and right dramatically drop out for the stationary targets. However in the case of cloud this drop waits until the velocity measurement reaches higher values such as -22 kmph in the case of Figure 78.

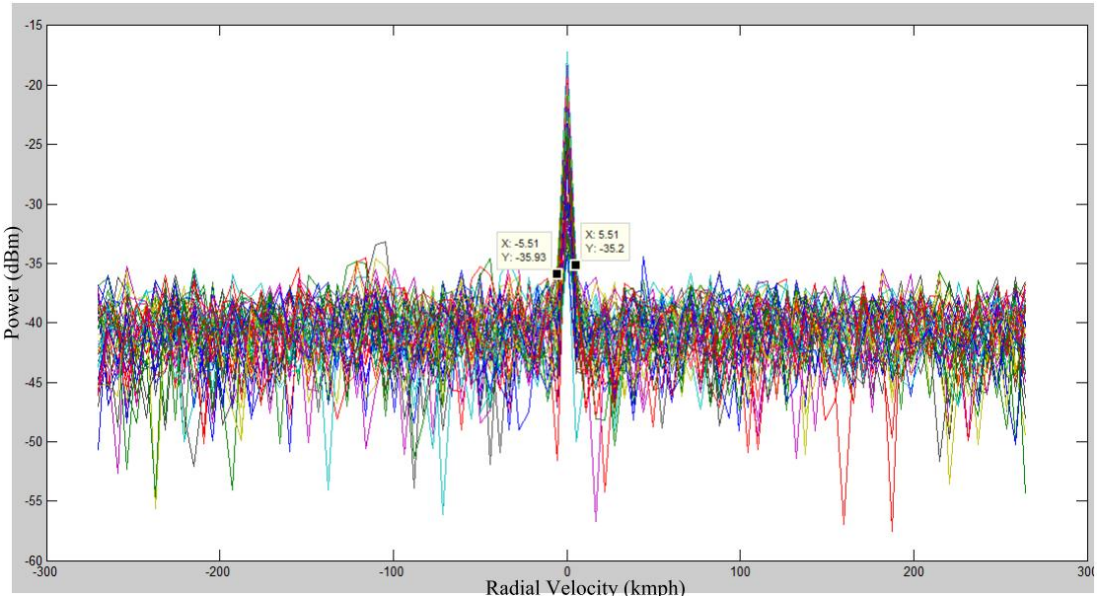

Figure 80: Slow Time Analysis of Stationary Targets

5.7 Rain and Speed of Wind Measurements

Radar system is also tested while it is raining. The test is performed under light rain and strong wind conditions. Fast time signal analysis of the rain differs from detection of the clouds. The range of a cloud region starts from a point and increases until the signal cannot scatter and turn back to receiver. However the rain droplets are distributed to every range bin starting from the very front of the antennas. Therefore the result of the rain is seen on radar screen as an increase on the power level starting from the very close region. Since transmitted wave cannot reach to the water particles located away from the radar they cannot be detected. Hence return power level start to decreases after a point.

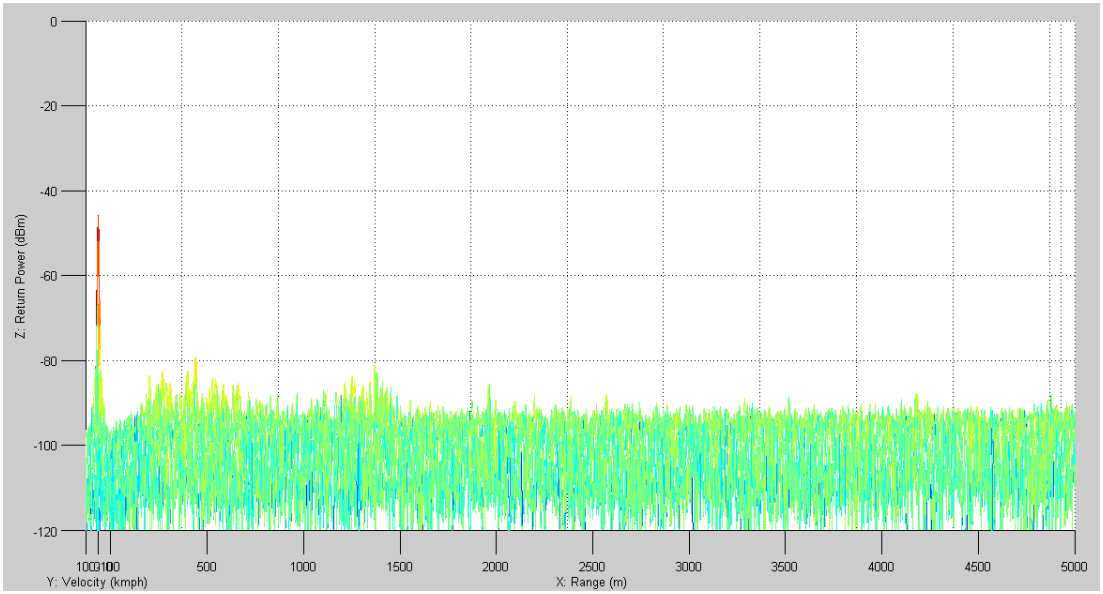

Figure 81: Rain Range Analysis-1

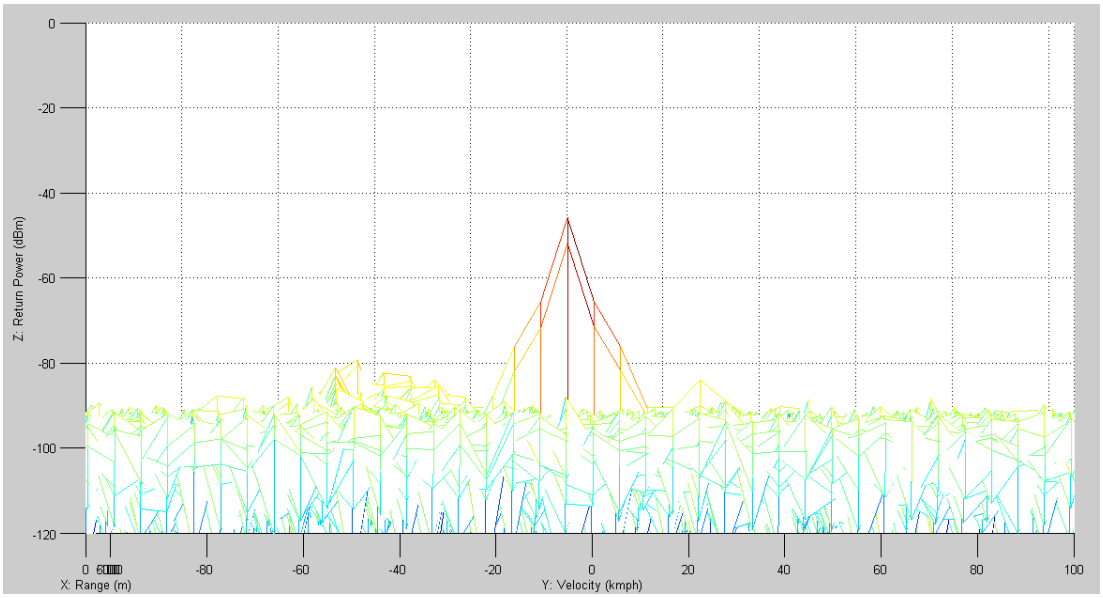

Figure 82: Rain Speed Analysis-1

Figure 81 and Figure 82 shows mesh plots of Doppler analysis from range and velocity axis. This figures show an analysis of a thin rain. Since the rain was not strong it is possible to see far regions up to the clouds. Signal can return to radar from a range of 1.5 km which is a distance of a cloud.

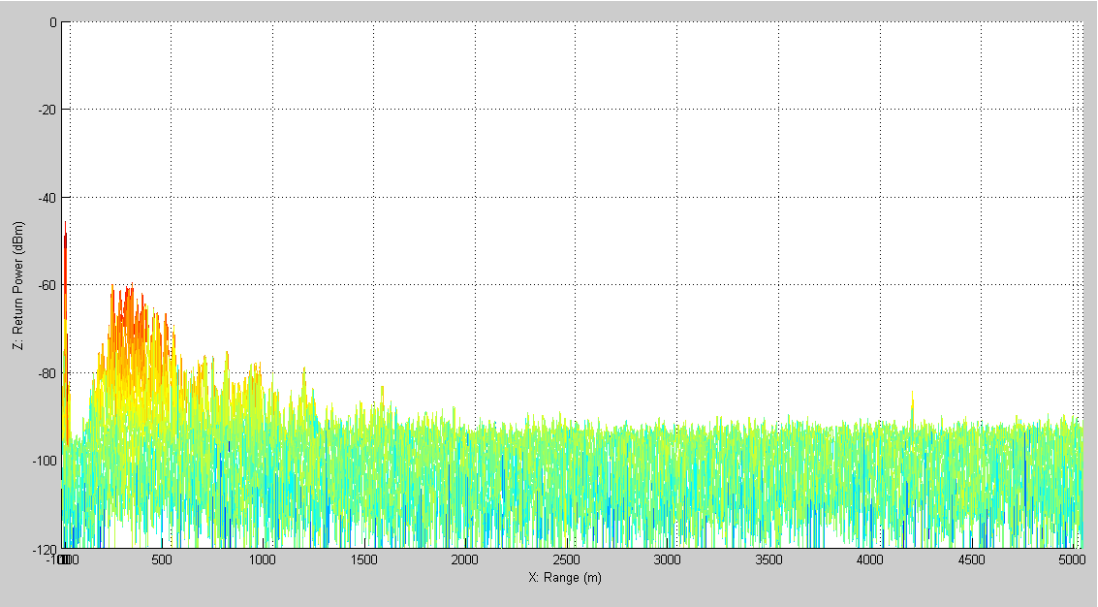

Figure 83: Rain Range Analysis-2

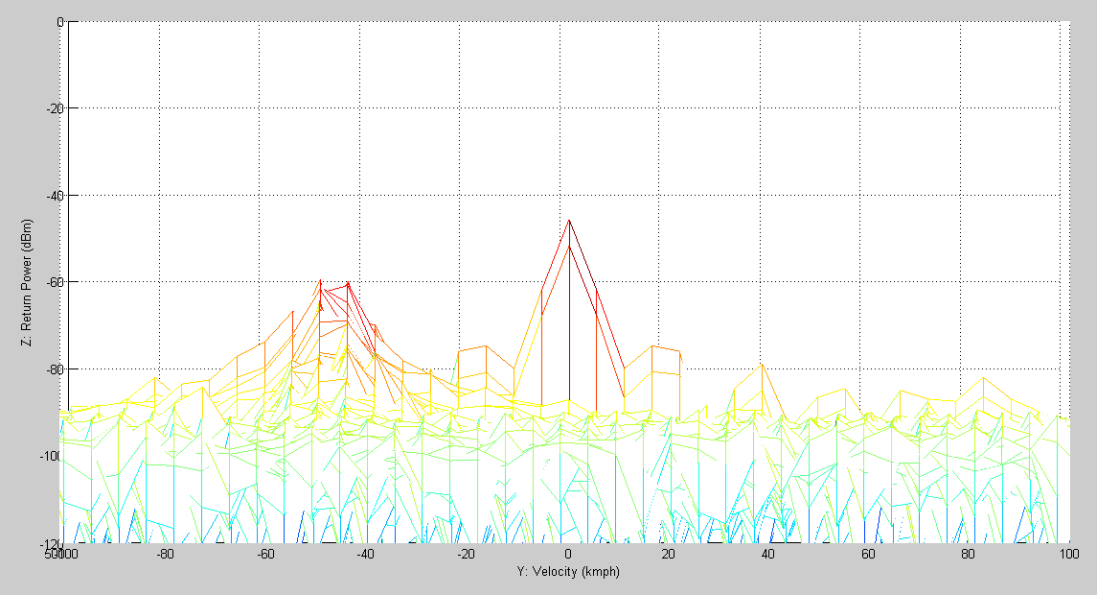

Figure 84: Rain Speed Analysis-2

Figure 83 and Figure 84 represent a stronger rainfall. Since there are more water particles on the air, the return power for the close region is higher. High density of close region particles prevent signal to reach far region water particles. Therefore there is no return signal behind 500 meters. Additionally, the speed of wind was also high while taking the measurements. Therefore speed analysis of the measurement indicates a speed measurement of -45 kmph. This speed matches to Beaufort number

of 6 which corresponds to a strong breeze. In this condition, large branches of trees are in motion. Whistling heard in overhead wires. Umbrella use becomes difficult and empty plastic bins tip over [26]. While doing this experiment it was hard for us to open and close the door of the room at the tower.

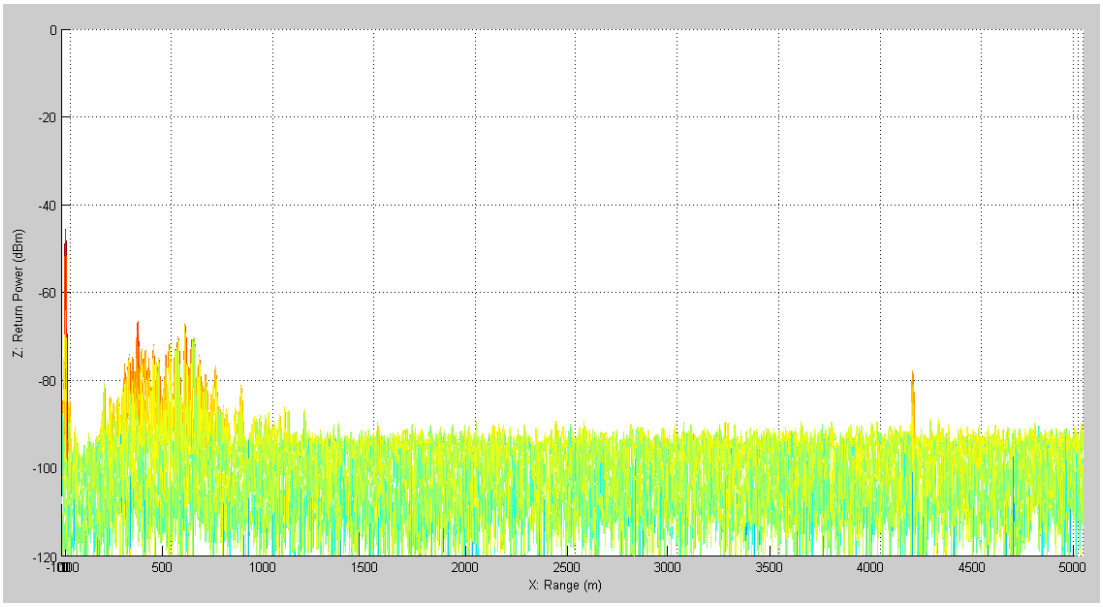

Figure 85: Rain Range Analysis-3

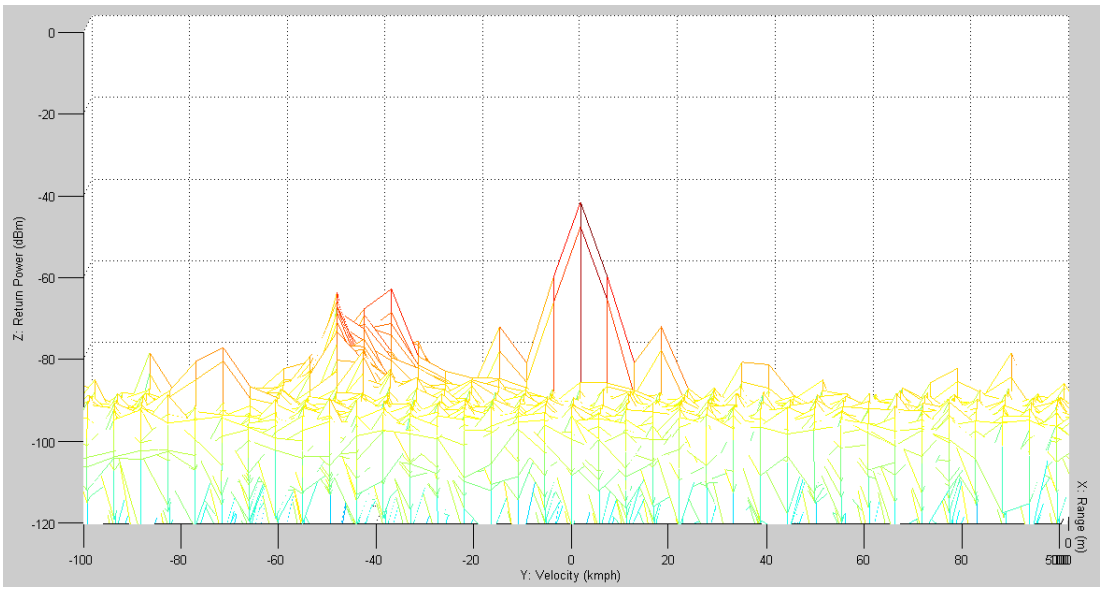

Figure 86: Rain Speed Analysis-3

Figure 85 and Figure 86 indicates a bit weaker rain with almost the same wind speed. Since rain is weaker from the previous one, signal can reach water particles located

about 750 meters away. Speed of wind is similar with the previous test. It blows about 40 kmph.

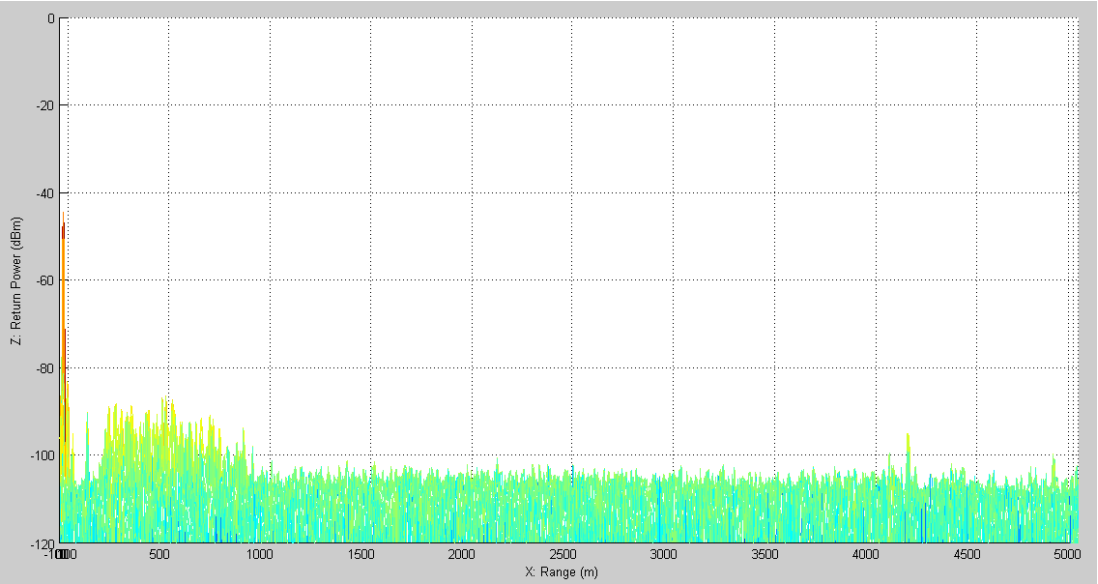

Figure 87: Rain Range Analysis-4

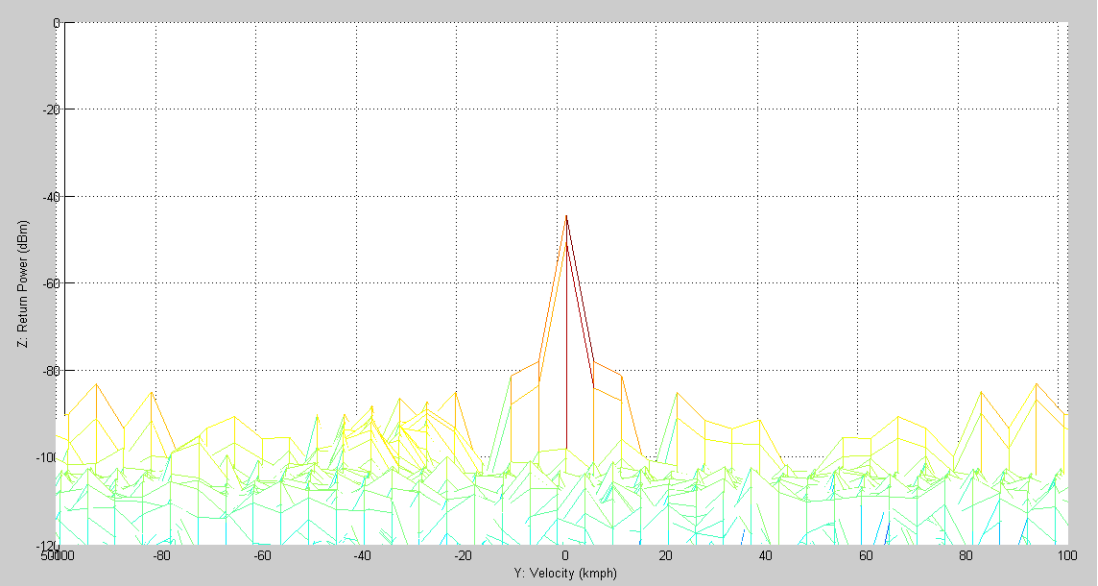

Figure 88: Rain Speed Analysis-4

Figure 87 and Figure 88 depicts also a weak rain. Echo can be received from a range of 900 meters. The speed of wind is also weak and there is not any speed component on the velocity axis.

CHAPTER 6

CONCLUSION

FMCW radars transmit signals continuously and they can reach high signal to power ratio values with low power devices. This property gives the opportunity to design radar system with low power and cheap devices.

In this thesis, an experimental FMCW radar is established specifically to detect the range and velocity of hydrometeors. The main advantage of the system is being power efficient by radiating a maximum power of 0.8 Watts with device in hand. The setup works at a carrier frequency of 10 GHz. This carrier signal is modulated by a positive ramp sawtooth signal with a 30 MHz frequency deviation and 100 microseconds of sweep interval. An observation is made during 10 milliseconds to be able to collect 100 sweeps in slow time. By this arrangement the range resolution of the radar becomes 5 meters, and the maximum unambiguous range becomes 15 kilometers. The system can perform Doppler analysis by implementing signal processing in slow time. The resolution of speed measurement is adjusted as 5.4 kmph and the maximum measurable speed is 270 kmph. All of the parameters are chosen to be able to make appropriate measurements for meteorological targets as the limitations of the devices allow.

Special signal processing algorithms such as clipping, windowing, and integration is applied to increase signal-to-noise ratio and prevent confusion of different targets. Clipping prevents multiple targets to be observed at the same frequencies. Windowing operation is performed to avoid spectral leakage. Coherent integration of cascaded fast time signals is performed to increase SNR about 20 dB. This operation becomes useful to detect signals under noise level for individual sweeps.

As a communication interface between the processing program and the operator, a graphical user interface is generated in Matlab. This interface takes the radar parameters and the starting commands from the operator. Operator can analyze both fast time and slow time result of the process also from this interface.

Established hardware and generated software verified in three steps. Firstly, the software and instrumental devices excluding antennas are confirmed by testing known length cables. In the second step, the antennas in the system are verified. After that the main verification is performed by measuring the range of buildings far away from the radar tower. The ranges of buildings are calculated and compared with the actual ranges calculated by Google Maps.

Last confirmation of the system is performed for slow time analysis. For this purpose, velocity measurement of the radar is confirmed by measuring the speed of a test car which is driven at several constant speeds. Calculated velocity measurements including the direction of propagation are compared by the predetermined speed values at which driver tried to stay.

After verification of the system with known length cables, known range buildings and known speed vehicles, range calculation of clouds and radial velocity calculation of rain droplets are performed. Since echo can be also received from the particles which stay inside of a cloud, it differs from the single point targets on the radar screen. Clouds are seen as volume regions on the screen since they have also a depth.

Dual polarimetric radars that are able to transmit radio waves on both horizontal and vertical polarizations can obtain further information about the size and shape of water particles. By transmitting and receiving radar signals with different combination of the polarization and then analyzing their correlation gives much more information about the amount of precipitation and its type [27]. As a future work, polarimetry can be added to the system for a better estimation of the type of precipitation

REFERENCES

[1] M. A. Richards, *Fundamentals of Radar Signal Processing*. New York: McGraw-Hill, 2005, p. 513.

[2] C. Wolf, "Continuous Wave Radar." [Online]. Available: http://www.radartutorial.eu/02.basics/Continuous Wave Radar.en.html. [Accessed: 30-Mar-2015].

[3] T. Ince, "FMCW radar performance for atmospheric measurements," *Radioengineering*, vol. 19, pp. 129–135, 2010.

[4] J. Figueras I Ventura, "Design of a High Resolution X-band Doppler Polarimetric Weather Radar," Universitat Politecnica de Catalunya, 2009.

[5] T. Schur, "Polarimetric Radar Research," *National Severe Storms Laboratory*, 2003. [Online]. Available: http://cimms.ou.edu/~schuur/radar.html. [Accessed: 09-Apr-2014].

[6] C. J. Baker, "FMCW Radar," Columbus, Ohio, 2014.

[7] I. V. Komarov and S. M. Smolskiy, *Fundamentals of Short-Range FM Radar*. Boston: Artech House, 2003, p. 303.

[8] J. W. Brennan, "The Proximity Fuze Whose Brainchild?," *United States Nav. Inst. Proc.*, vol. 94/9/787.

[9] H. Rohling and M. M. Meinecke, "Waveform design principles for automotive radar systems," *2001 CIE Int. Conf. Radar Proc. Cat No01TH8559*, vol. 1, pp. 1–4, 2001.

[10] D. Atlas, *Radar in Meteorology*. Boston, Mass: American Meteorological Society, 1990, pp. 1–806.

[11] K. Aydin and V. Giridhar, "C-Band Dual-Polarization Radar Observables in Rain," *Journal of Atmospheric and Oceanic Technology*, vol. 9. pp. 383–390, 1992.

[12] C. Wolf, "Maximum Unambiguous Range." [Online]. Available: http://www.radartutorial.eu/01.basics/Maximum Unambiguous Range.en.html. [Accessed: 20-Aug-2014].

[13] Maxim Integrated, “Glossary Term: Frequency-Bin,” 2014. [Online]. Available: http://www.maximintegrated.com/en/glossary/definitions.mvp/term/Frequency-Bin/gpk/136. [Accessed: 20-Aug-2014].

[14] C. Wolf, “Radar Range Equation for Weather Radar.” [Online]. Available: http://www.radartutorial.eu/15.weather/wx05.en.html. [Accessed: 08-Mar-2015].

[15] Agilent Technologies, “‘InfiniiVision 6000 Series Oscilloscopes’ DSO6102A datasheet.” p. 28.

[16] D. S. Zrnic and A. V. Ryzhkov, “Polarimetry for Weather Surveillance Radars,” *Bull. Am. Meteorol. Soc.*, vol. 80, pp. 389–406, 1999.

[17] C. Beg, “A System Level FMCW RADAR Optimization For Automotive Powertrain Control Application Requirements,” University of Waterloo, 2013.

[18] N. D. Kahyaoglu, “Spectral and Statistical Analysis of Experimental Radar Clutter Data,” Middle East Technical University, 2010.

[19] B. Akyildiz, “Spectral Leakage | Bugra Akyildiz,” 2012. [Online]. Available: http://bugra.github.io/work/notes/2012-09-15/Spectral-Leakage/. [Accessed: 22-Feb-2015].

[20] L. Dactron, “Understanding FFT Windows,” *Appl. Note, www. ee. iitm. ac. in/~ nitin/_media/ …*, p. 7, 2003.

[21] National Instruments, “Windowing: Optimizing FFTs Using Window Functions,” 2014. [Online]. Available: http://www.ni.com/white-paper/4844/en/. [Accessed: 15-Mar-2015].

[22] C. Wolf, “Radar Basics - Pulse Integration.” [Online]. Available: http://www.radartutorial.eu/10.processing/sp50.en.html. [Accessed: 22-Feb-2015].

[23] R. Noise, “Detection of Signals in Noise,” pp. 283–302, 1971.

[24] S. W. Smith, *The Scientist and Engineer’s Guide to Digital Signal Processing*, vol. 17. San Diego, California: California Technical Publishing, 1999.

[25] B. C. Wadell, *Transmission line design handbook*. Artech House, 1991, p. 513.

[26] Met Office’s National Climate Information Centre, “National Meteorological Library and Archive Fact Sheet 6 — The Beaufort Scale,” *National Portrait Gallery*, London, p. 7, 2010.

[27] T. Schuur, “Polarimetric Radar Research,” *National Severe Storms Laboratory*, 2003. [Online]. Available: http://cimms.ou.edu/~schuur/radar.html. [Accessed: 09-Apr-2014].